Pulsed laser ablation synthesis of silver nanoparticles with rapid ionophore derivatives for antivirus activities

by

Luke Gaza

A thesis submitted in fulfilment of the academic requirements of Master of Science in Physics in the School of Chemistry and Physics

Supervisor: Prof. M. K. Moodley

Physics

College of Agriculture, Engineering and Science

University of KwaZulu-Natal

Westville campus

Durban

South Africa

February 2022

PREFACE

The research contained in this thesis was completed by the candidate while based in the Discipline of Physics, School of Chemistry and Physics, College of Agriculture, Engineering and Science, University of KwaZulu-Natal, Westville Campus, South Africa. The research was financially supported by the University.

The contents of this work have not been submitted in any form to another university and, except where the work of others is acknowledged in the text, the results reported are due to investigations by the candidate.

_____

Signed:

Date:

DECLARATION

I, Luke Gaza, declare that the contents of this thesis represented my own unaided work, and all the sources have been acknowledged by means of references. It is being submitted for the Master of Science at the University of KwaZulu-Natal. It has not been submitted before for any academic examination towards any degree.

Signed: Luke Gaza

Date: February 2022

ABSTRACT

The world woke up to a deadly pandemic SARS Covid-19 that broke out of Wuhan, China in December 2019. Many drugs were proposed to help in treating this disease. However, at the time, few drugs showed potential effectiveness in curing covid-19. This research proposed the Covid-19 use of ionophores conjugated silver nanoparticle as a potential drug that can be effective because of its antiviral activities. Ionophores allow metal ions to enter the selective cell membrane of a cell. Once silver ions enter the cell, they start disrupting the replication of the virus DNA. Hence, silver plays an important role as a potential ingredient in drugs that can stop the spread of viruses. Pulsed laser ablation synthesis of a silver target placed in a solution was the method employed in this research to develop relatively smaller sized, spherical nanoparticles. In general, pulsed laser ablation synthesis in solution is a low environmental impact technique which does not need metal precursors and reductants and produces colloids of a relatively high purity as compared to chemical methods.

The silver nanoparticles were produced by focusing a pulsed laser beam directed on a silver metal target in a liquid medium. As the laser beam hit the silver target a plasma plume is generated, as the evaporated material expands it then cools and condenses, forming nanoparticles. This approach employs the use of a Q-Switched Nd: YAG dual pulsed laser operating at fundamental 1064 nm and second harmonic 532 nm with energy densities in the range of 34.8 $J.cm^{-2}$ to 37.3 $J.cm^{-2}$. The lens focuses the pulsed laser which irradiate a silver target surface that is immersed in deionized water. Silver nanoparticles that were produced had comparable sizes, spherical in shape and similar composition. Their nanoparticle surface chemistry allowed them to be easily grafted with doxycycline. The period of irradiation was varied from 5 minutes to 25 minutes per sample to get different qualities of AgNPs. The average diameter of the silver nanoparticles was 10,6 nm. The AgNPs were prepared and used to synthesise doxycycline silver nanoparticles. The samples of silver nanoparticles formed were characterised using high-resolution transmission electron microscopy (HR-TEM). The identification of the elements in the nano-material composition was done using Energy dispersive X-ray spectroscopy (EDS or EDX), Raman spectroscopy, and UV-VIS was used to confirm the absorption band gap of AgNPs. The silver nanoparticles that were produced was of high quality, free from toxic reagents and could be used for further medical (*in-vivo* tests).

DEDICATION

This thesis is dedicated to my wonderful family, my mother, and my late father N.C.G. Gaza and Gaza Family. For their unconditional love, support, and encouragement

KEYWORDS

Pulsed laser ablation synthesis of silver nanoparticles with rapid ionophore derivatives for antivirus activities.

Silver nanoparticles

Pulsed laser ablation in solution

Doxycycline

Nano-properties

Ionophore

Antivirus

Conjugate

Wavelength

Cavitation

Doxycycline silver nanoparticles

UV -VIS spectroscopy

Raman spectroscopy

Energy dispersive X-ray spectroscopy

High resolution transmission electron microscopy

GLOSSARY OF ABBREVIATIONS / ACRONYMS

AgNPs	:	Silver Nanoparticles
PLASIS	:	Pulsed Laser Ablation Synthesis in Solution
LASIS	:	Laser Ablation Synthesis in Solution
DO-AgNPs	:	Doxycycline-Silver Nanoparticles
LASER	:	Light Amplification by Stimulated Emission of Radiation
LA	:	Laser Ablation
Nd:YAG	:	Neodymium (Nd^{3+})-doped Yttrium Aluminium Garnett, ($Nd:Y_3Al_5O_{12}$)
HRTEM	:	High Resolution Transmission Electron Microscopy
UV-Vis	:	Ultraviolet – Visible light Spectroscopy
EDS / EDX	:	Energy dispersive X-ray spectroscopy
NPs	:	Nanoparticles
E	:	Energy
s	:	seconds
mins	:	minutes
cm	:	centimeters
ml	:	milliliters
M	:	Molar
mJ	:	millijoules
F	:	Laser Fluence
SAED	:	Selected Area Electron Diffraction

LIST OF SYMBOLS

Ag	:	Silver
nm	:	Nanometer
λ	:	Wavelength
ns	:	Nanoseconds
J	:	Joules
DO	:	Doxycycline
°C	:	Degree Celsius
e^-	:	Electron
H_2O	:	Water
τ	:	Tao
Hz	:	Hertz
mol	:	Moles
C	:	Carbon
H	:	Hydrogen
O	:	Oxygen

ACKNOWLEDGMENTS

It has been a long journey and I have many to thank who have assisted me in completing this Masters' research in record time.

I would first thank God for every step he took me through from start to finish. I would also like to thank Prof M.K. Moodley for helping me throughout the course of this research. Finally, I would like to thank my family for their wonderful support in my life.

TABLE OF CONTENTS

LIST OF TABLES

Table **Page**

LIST OF FIGURES

Figure **Page**

1 INTRODUCTION

1.1 Background

The field of nanotechnology has offered new ways to test, explore and apply our scientific knowledge across all research fields. This has brought about insights into the workings of different materials at the nano scale. The accumulation of innovative scientific techniques has improved and propelled us into a better technological era. Studies that have been done on nanomaterials have innumerable applications and they play important roles in electronics, optoelectronics sensing, energy harvesting, photonics and medicine [1]. Materials like metal oxides are of great interest across the field due to their superior chemical and physical properties [2]. The effectiveness of these tiny materials when used as biosensors, bio-labels, and cancer treatment are recognized to be revolutionary [3].

Scientific research reveals the unique nature of nanoparticles like silver oxides in developing novel diagnostic and antimicrobial agents. This has increased the attention of scientists towards the potential applications of these nano-scale materials for medicinal operations [4]. The studies have been extended to silver and gold nanoparticles. These metals have displayed unique properties that have been extensively studied for biological and medical applications. Many methods are available for nanoparticle synthesis, affording a wide broad spectrum of chemical and physical properties to be capitalised. Typically for gold and silver nanoparticles to give specific medical properties that are required, researchers had to employ different physical and chemical methods for preparation [5]. These two techniques have got their advantages and disadvantages. Mostly, the physical methods are less complicated, the nano properties are easy to manipulate, and the processes normally do not require toxics reactants hence they yield high purified nanoparticles. However most of the physical methods requires expensive equipment that may also require high technical skills for their operation [6]. When it comes to chemical methods, they are very cheap and easy to scale however the process requires chemical reductants that utilize excess toxic reactants, which need to be removed for biological purposes [7].

In this study, we report on silver nanoparticles (AgNPs) produced by laser ablation synthesis in solution and discuss the major features of this approach. Laser ablation synthesis is one of the best techniques used to develop nanoparticles of consistent morphology which can be applied to different medical applications. This method allows the preparation of stable silver colloids in pure solvents without using either capping or stabilizing agents that are normally required in wet-chemical methods [8]. Nanoparticles that have been produced in this way are said to be more suitable for medical and food-related applications where it is important to use non-toxic chemicals. In addition, if you want to achieve nanoparticles with different properties, laser ablation allows easy experimental parameters tuning to give the desired physical properties. These properties can influence the antiviral mechanisms of the produced nanoparticles [9]. In particular, the possibility of fragmenting a metal target without making use of capping and reducing agents intrinsically lowers the risk of contamination of the resulting colloid from unknown chemical agents and provides nanoparticles with unique surface characteristics [10]. One of the draw backs of the laser-generated silver nanoparticles is that it is harder to obtain them in higher concentration. Hence, the process is difficult to scale up in industry. To achieve higher concentration, it is necessary to use high-energy lasers, which are mostly very expensive [11].

Silver nanoparticles that are produced by laser ablation synthesis in solution are said to exhibit higher reactivity, antiviral and antimicrobial effects in comparison to their chemically synthesized homologous nanoparticles, due to the absence of ligands and/or stabilizers on the Ag nanoparticle surface [12]. In addition, when producing AgNPs by laser ablation synthesis in solution, it allows *in-situ* conjugation of nanoparticles with biomolecules, which has proven to be more efficient than the *ex-situ* conjugation required for chemically synthetized nanoparticles. As an example, in the quest to eradicate malaria around the globe many solutions have been proposed by researchers, but Ag nanoparticles have demonstrated significant activity against malarial parasite (*P. falciparum*) and vector (*female Anopheles mosquito*) [13]. It is believed that AgNPs will play a pivotal role in controlling malaria.

In addition, reports indicate that silver ions have been employed as an antimicrobial for several millennia [14]. However, with the emergence of nanotechnology, now there is a better understanding of these nanoparticles and their chemical properties. This has revived a greater interest in silver nanoparticles as potential medication for different illnesses [15].

1.2 Justification

At the end of 2019 an outbreak of severe acute respiratory syndrome coronavirus 2 (SARS-CoV-2) started and spread from Wuhan, China followed by Iraq, Italy and Spain, there after it was a pandemic that crippled the whole world. World leaders enforced lock-down restrictions and other drastic measures to control the fast spreading of the deadly virus [16]. Healthcare facilities got overwhelmed by the numbers of patients that fell sick. The rush to find a drug or a vaccine that can help to treat the virus became important. Many drugs were suggested and repurposed but most of them had lower efficacy. Reports of investigated virus inhibition tests of AgNPs on human para-influenza virus type 3 resulted in redaction of the viral infectivity, via blocking interaction of the virus with the target cell, which was narrowed down to size and zeta potential of these nanoparticles [17]. The *in-vitro* and *in-vivo* reports showed the effectiveness of AgNPs was high on the corona virus family. The smaller-sized nanoparticles had better viral inhibition results. They revealed that by tuning the physical properties of the nanoparticles they can inhibit covid-19 virus replication effectively. In this research, we go in-detail on how to produce pristine AgNPs which have relatively small diameter and high antiviral activities. We employed the double pulsed laser ablation in solution to generate AgNp. Then doxycycline conjugated silver nanoparticle was synthesised to increase its antivirus efficacy in biological systems.

1.3 Silver nanoparticles

Nanoparticles with diameters smaller than 100 nm have shown promising features in pharmaceutical applications, for biomedical imaging and targeted drug delivery. Inhibition of bacterial growth was shown to be more effective with silver nanoparticle with an average diameter of less than 15 nm [18]. However, biomedical applications require extensive and detailed research to gain adequate understanding of interactions between nanoparticles and biological systems [19]. The way nanoparticles may interact with biological systems and mechanisms that they will employ upon entering the cell, must depend on their size, type of material and surface characteristics [20]. The pathways of entry and the subsequent intracellular particle distribution influence the biological effects caused by particles. To understand a possible relationship between intracellular distribution and induced effects, it is important to investigate the processes involved in cellular uptake of nanoparticles and their intracellular trafficking [21]. Studies that have been done with different nanoparticles indicate that size, shape, and surface charge affects the amount of cellular particle uptake.

The proposed mechanisms that these nanoparticles employ include direct contact on microbial cells, which disrupts the cell systems operations and the functions of its membrane. This normally leads to structural damage on the protective cell membrane hence rendering it useless. Generation of reactive oxygen species by nanoparticles can also damage the cell membrane [22]. If cell uptake occurs and nanoparticles find their way into the nucleus of the cell, they may interfere with DNA (deoxyribonucleic acid) replication.

DNA is mostly responsible for the replication process that starts in the cell. Any damage done to its structure will cause either mutation or death of the cell or the organism. It was found that silver nanoparticles interact with the exocyclic nitrogen present in the adenine, guanine, and cytosine bases, which leads to DNA mutation. Ag^+ ions and silver nanoparticles possess antiviral and antimicrobial activity [23]. However, studies are still going on to further understand and to precisely discriminate between the effect of ions and those of silver nanoparticles.

Other commonly accepted mechanisms that silver nanoparticles use are silver–amino acid and silver–thiolate group interactions which happens on the proteins and DNA. *In-vitro* lab tests have also given clues for further support of inhibition of enzymes and other proteins. Positive silver ions (Ag+) are expected to show high affinity to the soft base-like thiolate ligands, which are mostly found in bacterial membrane and subcellular structure (for example: sulphur-containing proteins and enzymes) causing, inhibition of crucial biological cellular functions. These multiple, synergic mechanisms of cytotoxic activity reduce the likelihood that the micro-organisms develop resistance against silver compounds [24].

1.4 Anti-viral properties

Recent research has reported on the effectiveness of AgNPs in laboratory tests (*in-vitro* and *in-vivo*) on corona virus family, especially influenza [25]. More rigorous tests are still going on to understand its mechanisms and effectiveness in clinical tests.

The interaction of silver nanoparticles with HIV-1 (human immunodeficiency virus) was investigated as the AgNPs inhibit the virus from binding to host cells which was demonstrated only in *in-vitro* tests. Another research report has claimed that silver nanoparticle showed anti-HIV activities at an early stage of viral replication and somehow it prevents CD4-dependent virion binding, fusion, and infectivity [26]. Hence, inhibiting the post-entry stages of the HIV-1 life cycle. Also, the *in-vitro* and *in-vivo* study for potential application of AgNPs in controlling the infectivity of Rift Valley fever virus (RVFV) and inhibition of monkey-pox virus [27].

Several scientific studies report on the effectiveness and control of influenza by silver nanoparticles [28]. These articles proposed that silver nanoparticles could inhibit swine flu (H1N1 influenza virus strain, a common member of corona family). Thus, claiming that silver nanoparticle have anti-H1N1 influenza A-virus activities [29]. The reports also stated that inhibitory effects of silver nanoparticles on influenza A-virus could be a new way for the prevention of influenza virus infection [30]. Due to these studies, the scientific community was encouraged to try silver nanoparticles on covid-19 to test its effectiveness.

1.5 Ionophores

Ionophores are chemical compounds that binds to ions forming lipid-soluble complexes that act as vehicles for transporting ions across biological cell membranes. The ionophore is a Greek name that directly translates to “ion carrier”. Structurally, an ionophore contains a hydrophilic center and a hydrophobic portion that interacts with the lipid bilayers found in living cell membranes [31]. These chemical species could be synthetic or biological. Selecting between cation and anion ionophores have found applications where ions are to be delivered into the cell. These methods have improved the drug delivery techniques.

A virus depends on its DNA replication inside a host cell for it to multiply. Ionophores are one of the best ways to transport ions or proteins through the membrane to disrupt the virus replication [32]. As shown in the ***Figure 1.1*** below. Reducing the rate of virus replication inside the cell using AgNPs has been reported to be effective across different types of viruses.
The anti-viral action of AgNPs in general is linked to at least known four distinct mechanisms. Silver nanoparticles may act via four main routes:

- penetration inside the cell leading to organelle (ribosomes, DNA, RNA) dysfunction.
- oxidation of proteins, lipids, and DNA bases through oxidative stress.
- inducing cellular toxicity through the oxidative stress caused by the generation of reactive oxygen species and free radicals
- alteration of cell signalling.

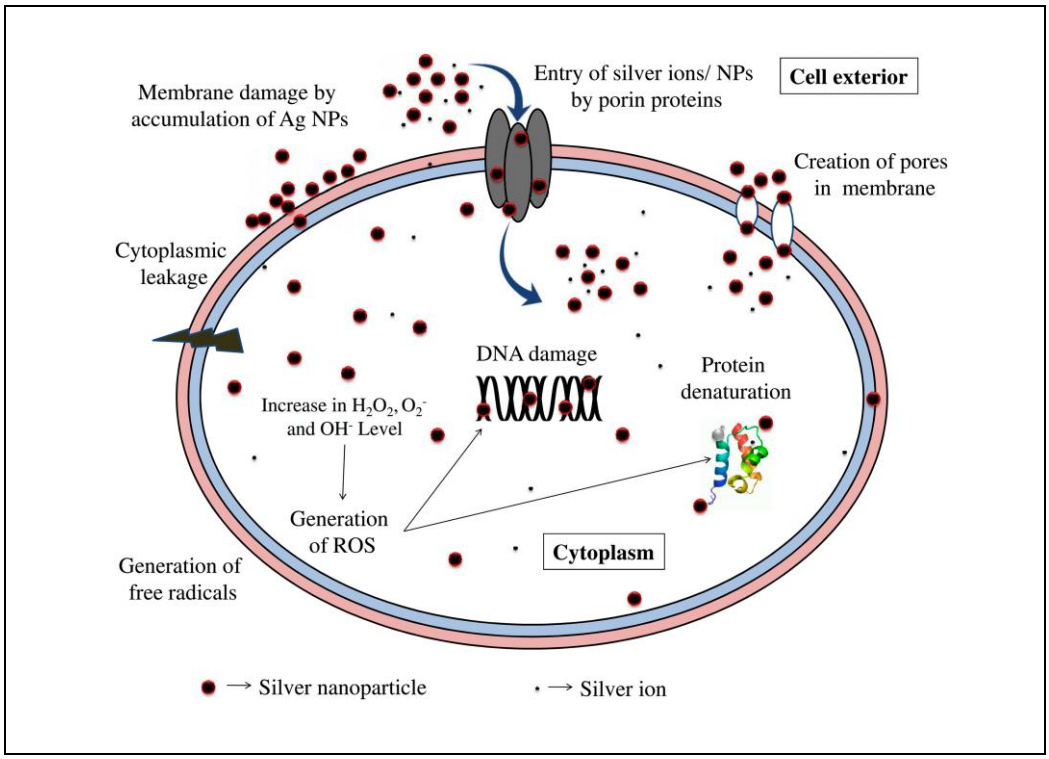

Figure 1.1 Schematic representation of the known mechanisms of anti-virial action of silver nanoparticles and silver ions. With permission from Elsevier [31].

Different chemical ionophores can be chosen to efficiently increase the number of ions inside the cell [32]. Doxycycline, hydroxychloroquine, and quercetin can be used as chemical ionophores. These three drugs have been reported to have anti-viral activities [37]. Hence, combining their virus inhibition properties and those of silver nanoparticles would produce a better drug for corona virus diseases.

1.5.1 Coupled silver ionophores

Conjugating silver nanoparticles with other chemical species enhances its physical and chemical properties. AgNPs can easily attach to other chemical compounds to make transition complex molecules. Doxycycline is considered a broad-spectrum tetracycline class antibiotic. Normally the drag is used to treat infections caused by bacteria and certain parasites [35]. It functionally treats bacterial pneumonia, chlamydia infections, Lyme disease, cholera and prevent malaria in combination with quinine. Quinine has derivatives drugs like chloroquine and hydroxychloroquine [36].

These drugs have been used to treat malaria and auto immune diseases. Chloroquine was first synthesized in 1934, but its toxicity prompts the later introduction of hydroxychloroquine, and it quickly became favoured because of its superior safety profile. Hydroxychloroquine is soluble and less toxic compared to chloroquine, because it is more refined therefore it causes fewer side effects, thus it is considered a safer drug [37]. The mechanism of action of these drugs against plasmodium parasites is believed to be partly related to its interaction with DNA and through inhibition of the polymerization of its proteins. Both drugs are affordable, widely available internationally and are generally considered safe for their present US Food and Drug (FDA)-approved indications. Quercetin is a plant flavonoid and known to be an antioxidant and anti-inflammatory drug that is found in several plants and foods such as onions, red wine, and apples. Quercetin is commonly used for heart conditions, blood vessels, controlling blood sugar and to prevent cancer [38].

All these drugs can be re-purposed as ionophores if they are coupled with silver nanoparticles. Their organic groups allow them to permeate through the selective cell membrane to deliver the AgNPs inside the biological cell [39]. Doxycycline silver nanoparticles (Do-AgNPs) have been reported to be more effective in inhibiting virus replication, growth of E.coli bacteria and can be used in the treatment of cancer [40]. The Do-AgNPs employ a mechanism action of interference in the binding of the tRNA (transfer ribonucleic acid) by blocking the adhesion of aminoacyl-t-RNA, to the mRNA-ribosome complex, that means a portion of the ribosome is impaired to preform protein synthesis. In a similar way, hydroxychloroquine inhibits the multiplication of the SARS-CoV-2 virus by invading the endosome within which the virus replicates and accumulate in lysosomes, where it may interrupt the usual process of lysosome–endosome fusion, thereby inhibiting release of the viral contents [41]. Hydroxychloroquine also blocks the generation of interleukin-6 and other pro-inflammatory cytokines, which are main causes of acute respiratory distress syndrome (ARDS).

1.6 Aims and Objectives

The main objective was to study the mechanism of pulsed laser ablation of a silver target in a liquid and investigate ways of optimising the synthesis of silver nanoparticles in solution by:

1. designing a portable liquid sealed laser ablation chamber.
2. producing pristine Ag NPs in suspension in pure distilled water by laser ablation.
3. studying and characterising silver nanoparticles.
4. grafting Ag ionophores in solution to produce doxycycline silver nanoparticle.

This research was set out to develop pristine silver nanoparticles in water, which means water was used as the medium to develop the nanoparticles. The sizes and shapes of AgNps produced was controlled to better suit its virus inhibiting properties. An optimized procedure of pulsed laser ablation synthesis in solution was used to develop silver nanoparticles. Doxycycline was used as an ionophore. Silver nanoparticles were conjugated with doxycycline to form a complex of doxycycline-silver nanoparticles in solution. The shapes and sizes of AgNps generated were analysed using HRTEM and UV-vis spectroscopy.

1.7 Hypotheses

The proposed technique of producing pristine silver nanoparticles will yield highly effective, non-toxic particles of specific required sizes and shapes for virus redaction. Pulse laser ablation synthesis in solution produces the best quality silver nanoparticle for biological system uptake.

1.8 Outline of dissertation / thesis structure

In Chapter 1, the background to the nature of the dissertation is provided and includes an introduction and justification for this research.

In Chapter 2, pulsed laser ablation of silver nanoparticles is discussed in detail, including growth mechanisms, physical properties, and potential applications e.g; its antivirus activities when conjugated with doxycycline. Background information on laser and laser-material interaction are discussed and the importance for this research is presented.

In Chapter 3, discussions of the experimental setup used to synthesize silver nanoparticles and methods of characterisation are presented. While there are many analytical methods employed to investigate silver nanoparticles properties, in this dissertation, high resolution transmission electron microscope, UV-VIS spectroscopy and energy dispersive x-ray spectroscopy were used to analyse the silver nanoparticles samples.

In Chapter 4, results and discussions of the data obtained from the silver nanoparticles experimental samples are presented.

In Chapter 5, we conclude the research undertaken and propose future research that could extend the scope of the present study.

2 AN OVERVIEW OF LASER ABLATED SILVER NANOPARTICLE IONOPHORES SYNTHESIS.

2.1 Introduction

Silver nanoparticles synthesised by physical means results in superior properties when compared to other processes like chemical, photochemical, or biological approaches. The latter methods may require toxic reagents, caping agent, or unstable catalysts and it is more difficulty to tune the physical properties of the nanoparticles [42]. The biological ineffectiveness, high cost, and negative environmental impact they pose, have been shown to be not sustainable. Physical methods of producing metal nanoparticles generally relying on evaporation and condensation, which could use tube furnaces or laser ablation chambers at chosen atmospheric pressures. However, there are a few drawbacks such as sizeable laboratory space occupation, high energy consumption, vacuum condition that mighty be costly. On the other hand, physical synthesis facilitates producing AgNPs with narrow size distribution and controlled quantities of particles in one single process. Pulsed laser ablation provides a simple, environmentally friendly way to develop tuned nanoparticles [43]. Employing a top to bottom synthesis approach, pulsed laser ablation enables size control by varying the incident laser beam properties and the medium inside the ablation chamber.

Nanoparticles have shown to have several unique optical, photo catalytic and electronic properties. The physical and chemical properties of AgNPs are dependent on the thickness of the shell layer. Varying the ratio of core diameter and shell thickness, large shift in the optical emission and absorption has been reported [34]. By conjugating the AgNPs with an ionophore, enhances antiviral activity which is a better way to treat virus and other drug resistant bacteria and parasites. Furthermore, studies have reported hopeful results of treating cancer using doxycycline silver nanoparticles [44].

2.2 Laser

Laser is an acronym which stands for Light Amplification by Stimulated Emission of Radiation. The name was first coined by Gordon Gould in his famous notebook when he was a student of Professor Charles Hard of Columbia University in November 1957. Albert Einstein suggested that under proper conditions, atoms stimulated by light could spontaneously release excess light energy. Laser exhibit some unique characteristics, for example, they are monochromatic and they can be used as reliable coherent sources of photon energy. [45].

2.3 Laser applications.

In 1960, Maiman built-up the first functional red laser pulses from excited chromium atoms in a synthetic ruby rod. Lasers immediately caught the public imagination, because of their similarity to science fiction “heat rays” from fictional books and cinema. In no time lasers proved to be versatile and robust as they were starting to be used in all fields with great success in ground-breaking applications [46]. Helium-neon lasers were the first to be utilised in commercial use with numerous applications. They could be easily tuned so that they can give off a distinct red light. They quickly started to find use in projecting straight lines for alignment in manufacturing, surveying, and construction. Their large-scale application was as laser scanning for automated checkout in supermarkets. Few years later they were being used in compact disc audio players.

Laser ablation has been used in the production of nano materials and thin film deposition. This technology has been favoured in fabrication of third generation solar cells and micromachining of micro-electromechanical systems (MEMS), because laser ablation enables an easy way to tune the particle sizes and surface area [47]. The thin film layers can be determined precisely by the duration of deposition. Generally, this procedure is used to develop devices that are small, inexpensive, and efficient when it comes to energy use.

Laser ablation has also been used in chemical analysis. When a beam is focused on the sample, the energy from the laser is absorbed by the atoms and they get to be excited as they acquire enough energy to break free from the bonds on the sample surface, this produces a bright plasma as the particles expand [48]. The light emitted from this plasma can be analysed to determine the atomic elements presence and concentration levels of chemical compounds that are found in that sample. Sample optical properties and Laser parameters (energy, wavelength, pulse duration) are also used in these analytical techniques, hence a proper selection of appropriate laser parameters based on the sound understanding of laser ablation fundamentals is a critical prerequisite for achieving precise and accurate measurements [49].

Laser ablation is also used in a variety of medical specialties including ophthalmology, general surgery, neurosurgery, dentistry and veterinary. Several types of lasers, like argon, carbon dioxide, dye, erbium, excimer, Nd:YAG and others are employed depending on the requirement of the surgery or treatment at hand. It has been used to ablate tumours to cure prostate cancer, killing unwanted cells as the embryo grows and skull-base surgery in neurosurgery. The use of lasers has revolutionised the medical fraternity, providing safe surgery practice and allowing integration of new technology.

2.4 Operating principles of a laser

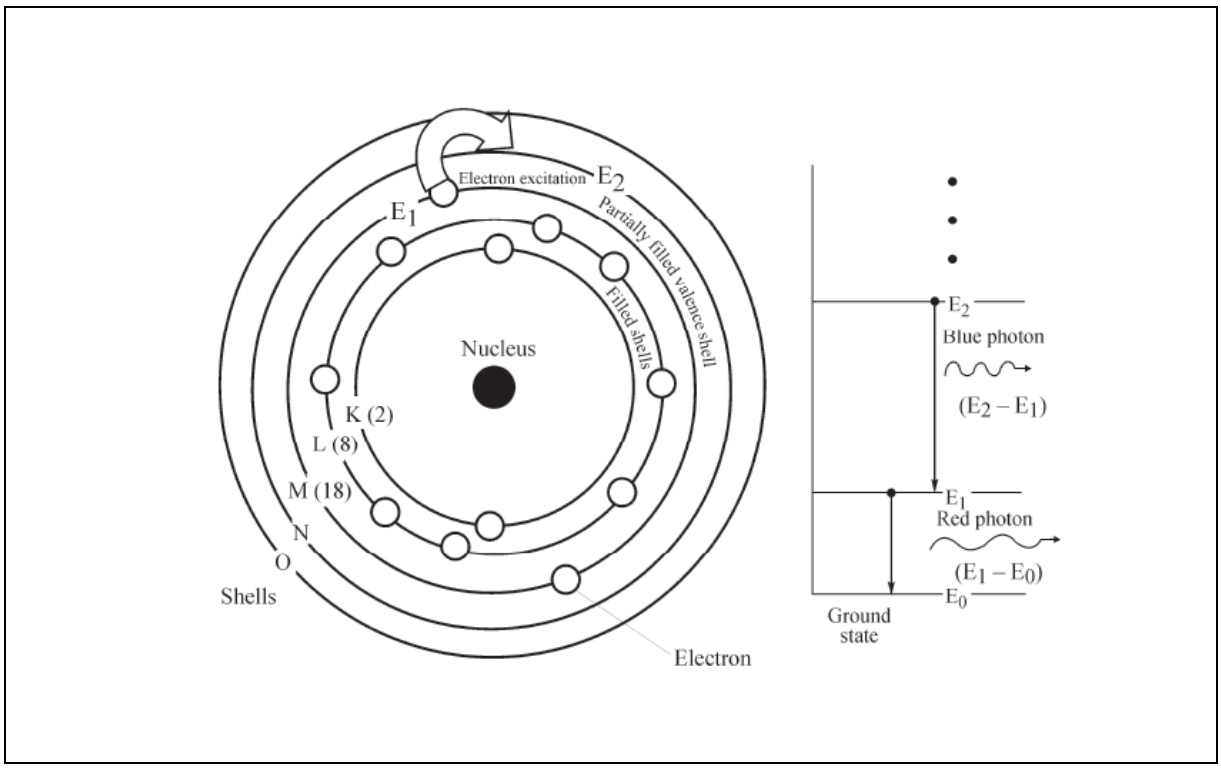

Figure 2.1 A schematic diagram to show a simple Bohr model of the atom [50].

The simple Bohr model of the atom, proposed by Niels Bohr in 1913 consists of a positive nucleus surrounded by negative electrons arranged in distinct energy shells. In ***Figure 2.1*** the shells are designated from K to O as shown. The notation K(2) indicates that the K-shell is complete when it has 2 electrons. Similarly, L(8) indicates that 8 electrons complete the L-shell, and M(18) indicates that 18 electrons complete the M-shell [50]. This simple structure shows electrons orbit the nucleus of an atom and they can move from ground state having lowest energy to a higher (excited) state. Then electrons can decay from a higher state to a lower state, but it cannot be found between these states. The allowed energy states are called quantum states. The atom must absorb energy from an external source, for an electron to jump to a higher quantum state. This can happen through absorption of energy in the form of electromagnetic radiation (e.g., light). Light is made up of packets of energy called photons. Each photon has an intrinsic energy determined by the equation.

$$Energy:\ E = \frac{hc}{\lambda} \qquad [2.4.1]$$

Where the energy (E) of each photon is be given by the product of the Planck constant (h), the constant speed of light (c) and the wavelength (λ). Since the absorb energy is quantised and no electron can be found between two quantum states, the energy of a single photon received must equal, the energy difference between the two states.

$$\Delta E = E_m - E_n \qquad [2.4.2]$$

Where (ΔE) is the released photon energy, (m and n) are energy levels. When an electron decays from a higher energy state the photon of light given off by the atom must have an energy equal to the energy difference between the two states.

2.4.1 Population Inversion and light amplification by stimulated emission of radiation

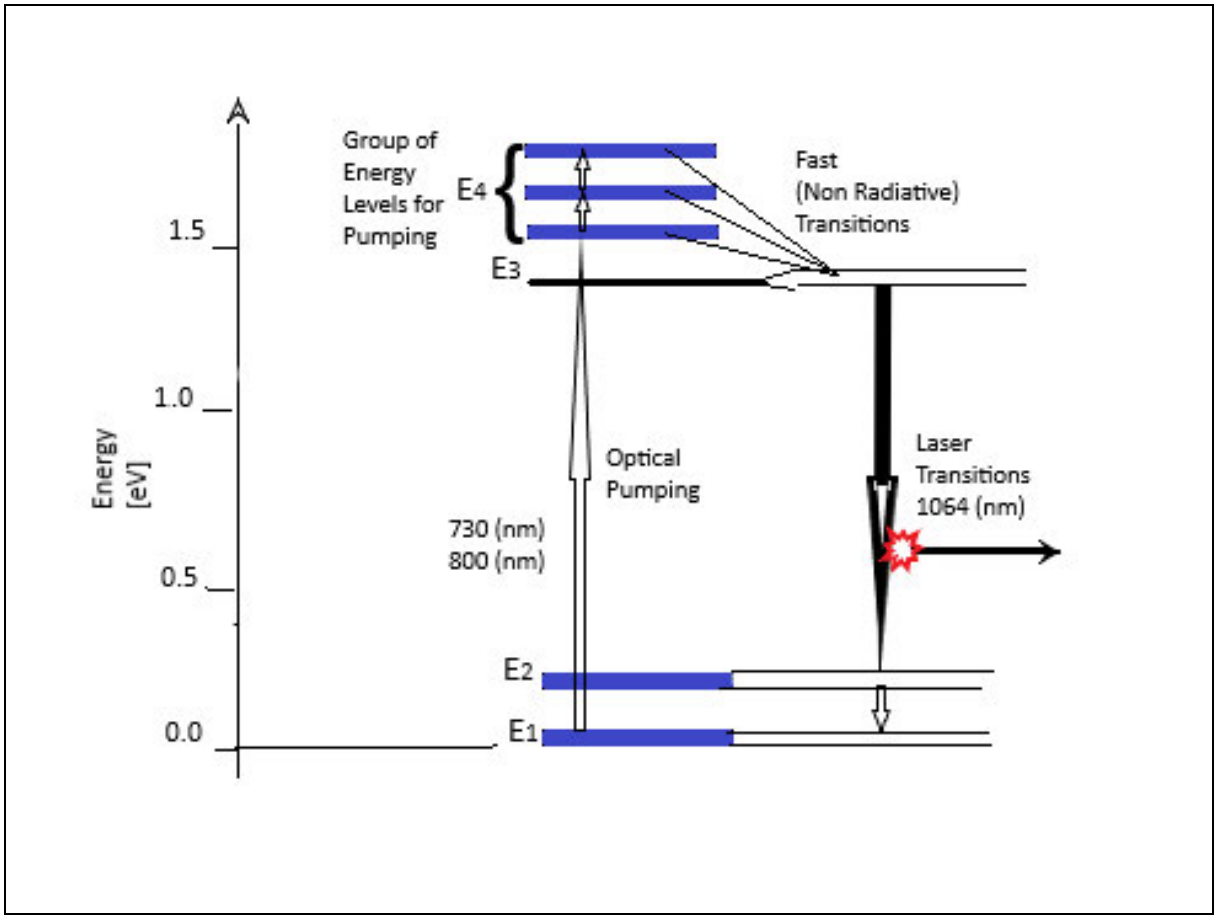

Figure 2.2 diagram showing the excited electron transition.

After an atom gets excited, it must eventually decay to its normal state where its electrons are in their lowest possible energy states. Since electrons are fermions, they will occupy all possible states while obeying the Pauli's exclusion principle. As the electron transitions to the ground state, it releases energy in the form of a photon. The de-excited energy of the electron is equal to the photon energy that it gives off. In the case of a Nd:YAG laser the atoms give off photon energy that corresponds to 1064 nm wavelength. This is its fundamental wavelength which can be doubled to its first harmonic, 532 nm wavelength.

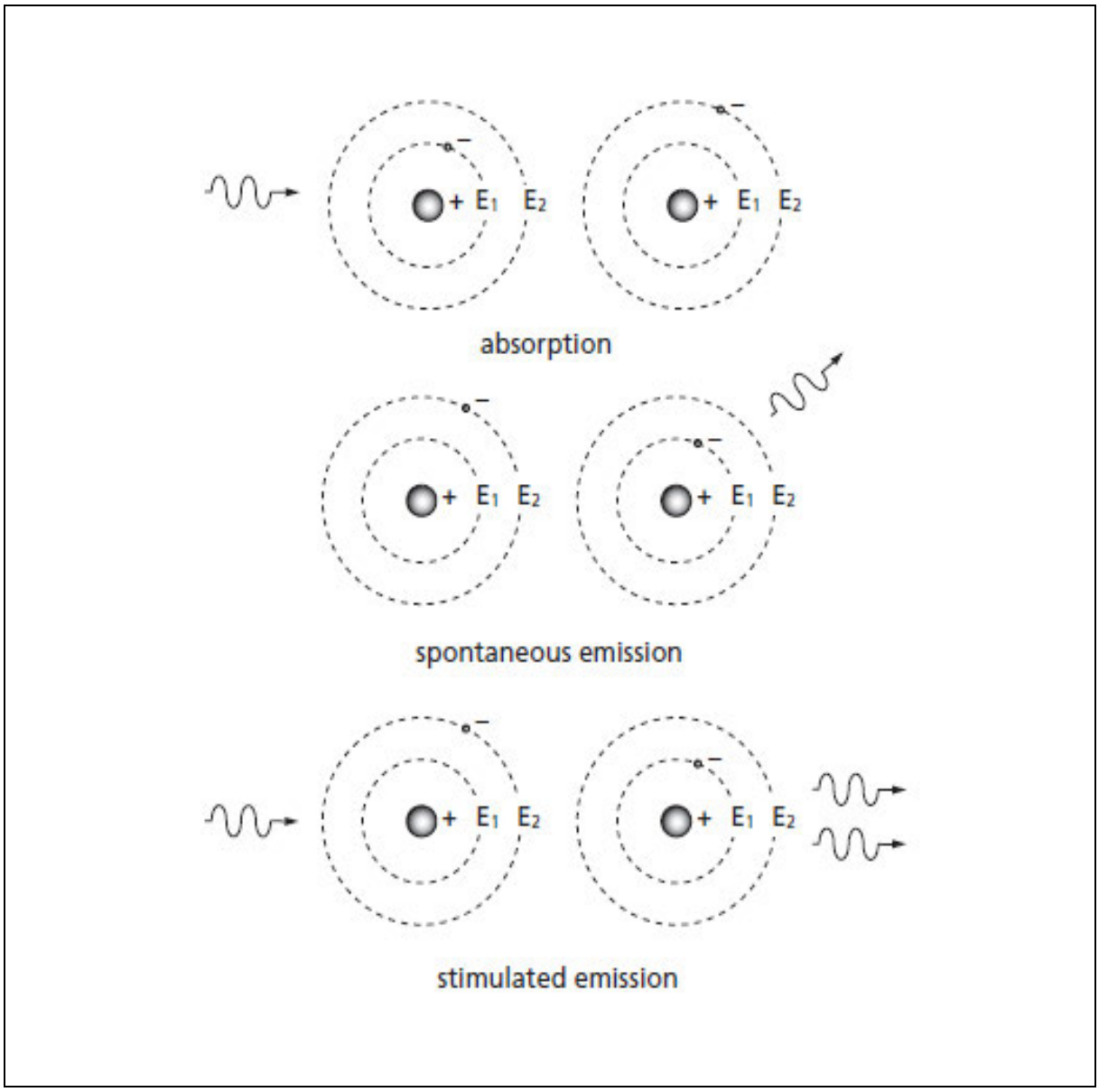

Figure 2.3 A schematic showing the processes involved in a lasing medium when excited by an external source [51].

When all excited atoms release photons in all directions, the event is called spontaneous emission. However, there is a chance that before spontaneously decay of an electron, a passing photon stimulates the electron to decay in such a manner that a photon is emitted at the same wavelength. The second emitted photon will also have the same direction and the same phase as the prior passing photon. This process is called stimulated emission. It is this stimulated emission that lies at the heart of the amplification of light by laser action.

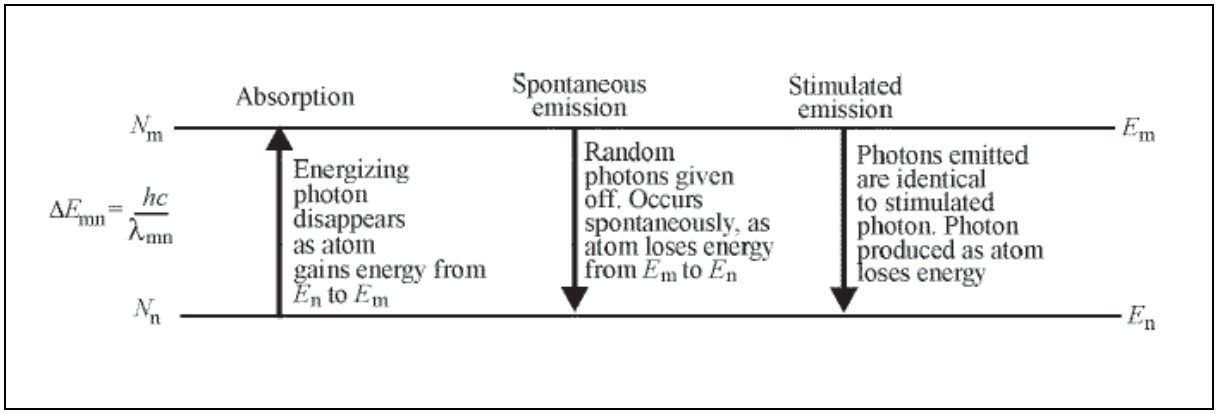

Figure 2.4 Three radiative processes that involve photons and atoms [50].

Now consider a group of atoms within the stimulation range of a passing photon. The probability for stimulated emission is quite small for the whole population of atoms [52]. Thus, to say not all the atoms are usually in an excited state, Boltzmann's principle states that, when a collection of atoms is at thermal equilibrium, the relative population of any two energy levels is given by:

$$\frac{N_2}{N_1} = exp\left[\frac{\Delta E}{kT}\right] \qquad [2.4.3]$$

Where N_2 and N_1 are the populations of the upper and lower energy states, respectively, T, is the equilibrium temperature, and, k, is Boltzmann's constant.

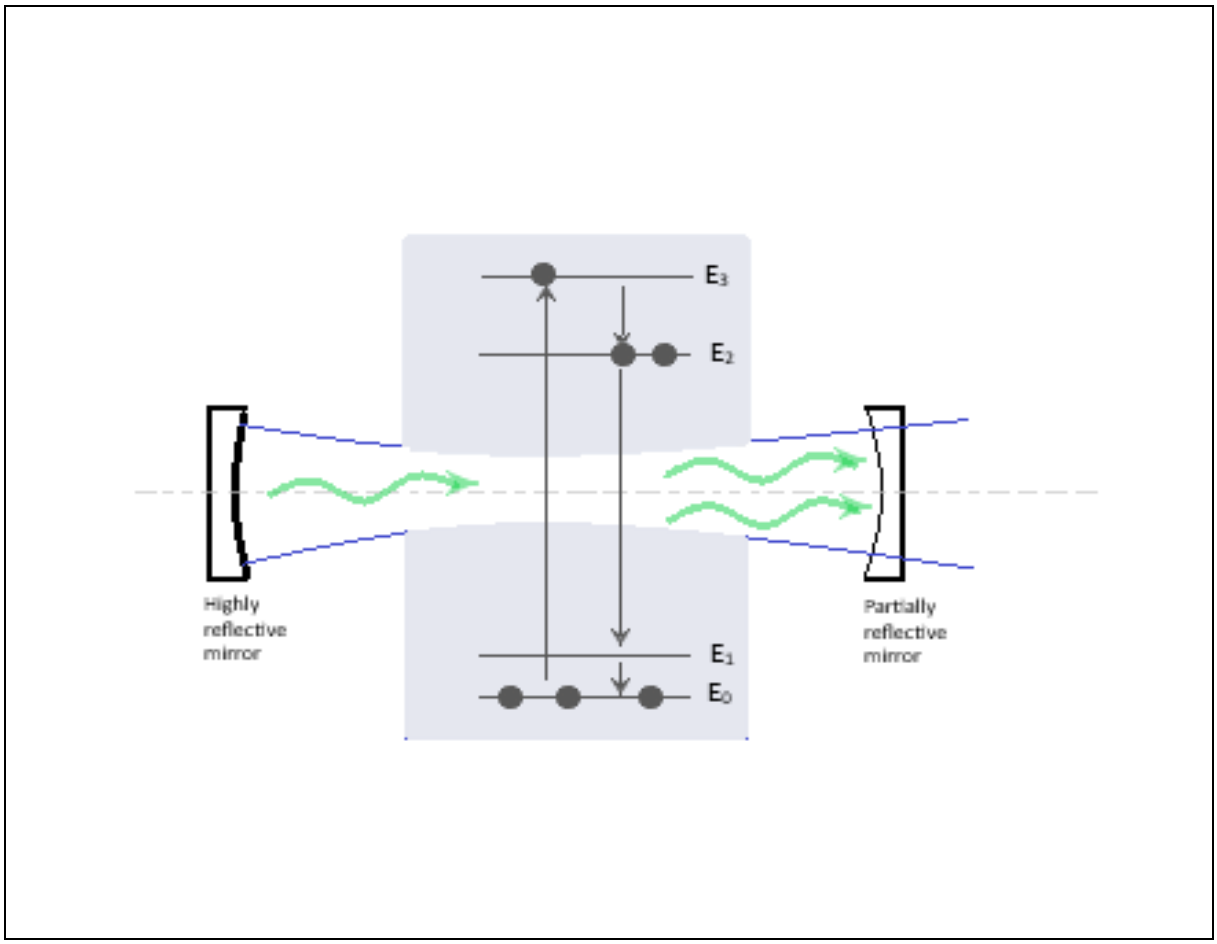

Figure 2.5 stimulated excitation of atoms between the optical cavities.

Although with a population inversion we can amplify a signal via stimulated emission, the overall single-pass gain is quite small, and most of the excited atoms in the population emit spontaneously and do not contribute to the overall output. To turn this system into a laser, we need a positive feedback mechanism that will cause most of the atoms in the population to contribute to the coherent output. This is the resonator, a system of mirrors that reflects undesirable (off-axis) photons out of the system and reflects the desirable (on-axis) photons back into the excited population where they can continue to be amplified [52].

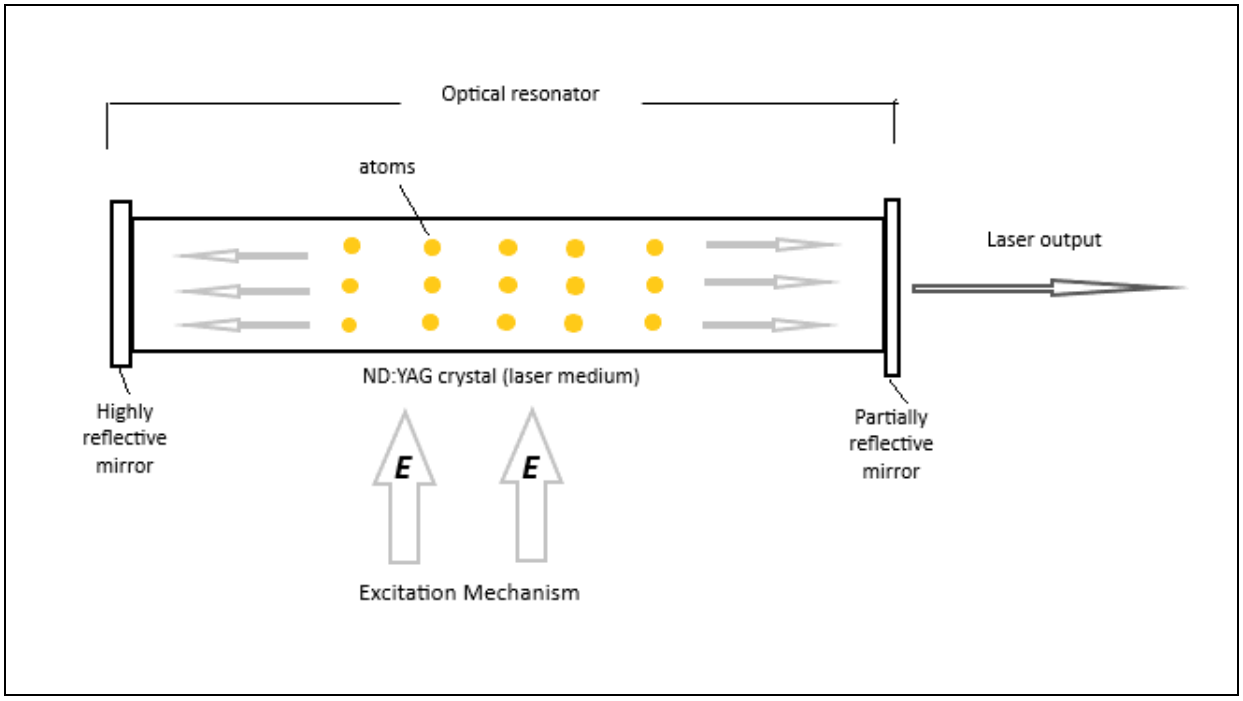

Figure 2.6 diagram showing the Laser mechanism.

In lasers the population inversion is achieved with the optical cavity resonator when photons bounce back between mirrors and a cascading emission is induce and amplification will be possible. Then output coupler being partially reflective permits the laser to exit the cavity [53].

Nano thin-film materials can be made by pulsed laser deposition (PLD) using excimer lasers. This process produces materials that have high quality and superior properties than those obtainable with conventional manufacturing techniques [54]. The synthesis technology that uses pulsed laser ablation in solution/liquid is gradually becoming an attractive approach because it is a chemically simple and a clean method with high product quality.

2.5 Laser Ablation

Laser ablation is a physical process of removing materials from the irradiated zone by focusing the laser beam on the target surface. At low laser flux, the material gains heat energy by absorbing the energy from the laser [55]. The material will then sublimate and condense on the surface of a substrate as a thin film. At high laser flux, the material is normally converted to a plasma then as it cools down nucleation takes place to produce nanoparticles [56].

When a laser is irradiated on to a sample the ablation depth corresponds to the material used. The absorption of the material is directly depended on its ability to absorb the laser energy [57]. The energy absorbed may cause a phase transformation as the material vaporises or it will simple heat up and melt. The depth of ablation on a material is a function of beam energy density, the repetition rate of the pulse (frequency), the laser pulse duration, and the laser wavelength. Laser energy per unit area is the energy fluence and it is very important when developing nanoparticles [50].

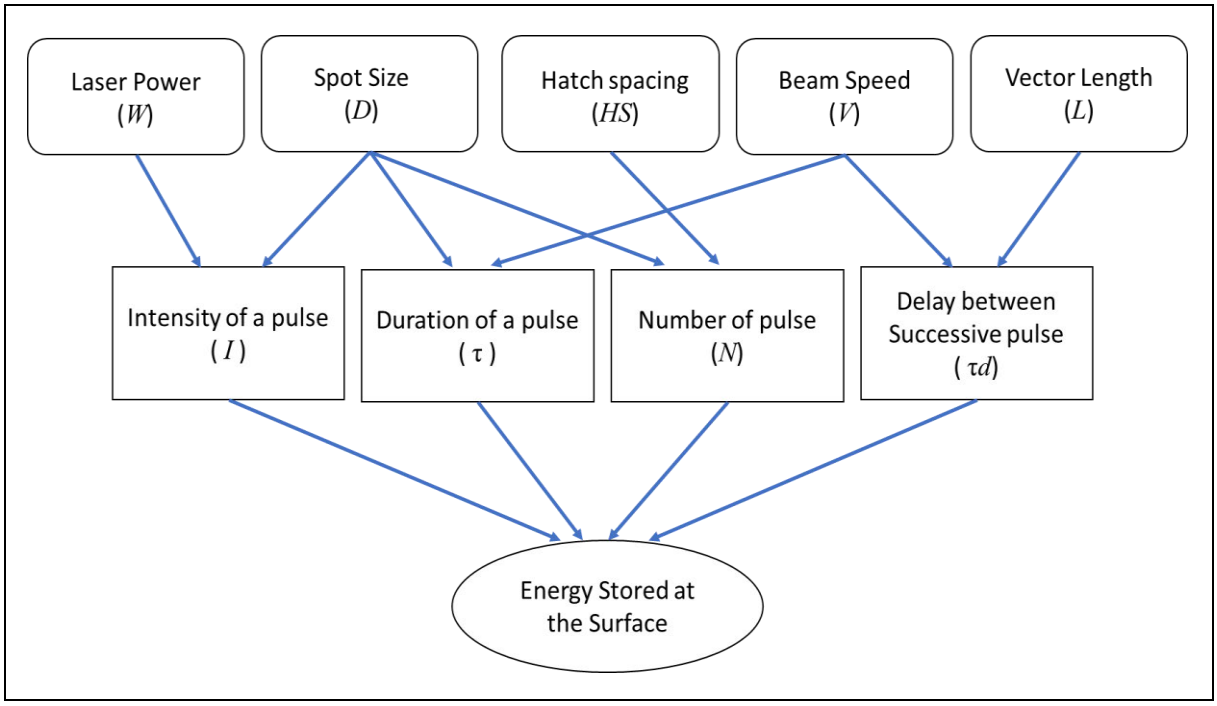

Figure 2.7 Influence of process parameters on the energy delivered onto the substrate surface [58].

Several key parameters are important when considering laser ablation in micromachining or nanoparticle synthesis. To understand how pulse duration and fluence play a role. The concept of thermal and optical penetration depths should be understood. When a laser pulse is irradiated on a target, the electromagnetic energy penetrates to a depth of, $l_\alpha = 1/\alpha$, where, α, is the attenuation coefficient and the thermal depth penetration is given by, $l_T = \sqrt{D_T \tau_L}$, where, D_T, is the thermal diffusivity, τ_L, is the duration of the pulse, *k*, is the electron thermal conductivity, ρ, is density, H_v , heat of vaporization and, c_p, is the heat capacity of the material [59].

$$D_T = \frac{k}{\rho c_p} \qquad [2.5.1]$$

Threshold fluence is the energy needed to be deposited per unit volume onto the material to achieve ablation. Where the characteristic time scales are, τ_p, is lattice heating time and, τ_e , electron cooling time.

Table 2.1 Threshold fluence of different pulse duration:

Time scale	Pulse duration	Threshold fluence
$\tau_L \gg \tau_e$	$\tau_L \lesssim 10^{-11}\ s$	$F_{th} = \frac{\rho H_v}{\alpha}$
$\tau_p \ll \tau_L$	$\tau_L \gtrsim 10^{-11}\ s$	$F_{th} = \rho H_v l_T$

When a nanosecond pulse laser is used to irradiate a metal target its pulse duration is longer enough to allow heat energy to be absorbed around the atoms near the contact area. The lattice heating time is then exceeded and this allows lattice Temperature, T, and electron temperature, T_e, to reach a thermodynamic equilibrium. Hence the thermal governing equation is:

$$C\frac{\partial T}{\partial t} = \frac{\partial}{\partial z}\left(k\frac{\partial T}{\partial z}\right) + I_\alpha e^{-\alpha z} \qquad [2.5.2]$$

Where, C, is lattice volumetric heat capacity, I, is the laser intensity. Melting and vaporization will occur in the heat-affected zone and the thermal penetration depth will be given by *equation 2.5.2*.

Normally, pulsed excimer lasers that have very short pulse widths are mostly preferred. Even though excimer lasers have lower average power compared to other larger lasers, their peak power can be quite large. The shorter pulse duration does maximize peak power irradiated onto the material and this minimizes the time for thermal conductivity to occur. Thus, high energy is rapidly deposited onto a very small volume and the laser is used for complete ablation. The pulse repetition rate is very important in ablation [60]. The pulse frequency must be kept high because if the rate is too low, energy will be lost to the surrounding by cooling. If the residual heat can be retained, that means the conduction time is kept to the minimum by the pulse repetition rate, making ablation processes to be more efficient [61]. A big attention must go to the quality of the beam which is measured by its size and brightness (energy). This can be achieved by aligning and focusing the laser beam to maintain its homogeneity. Controlling the beam spot size on the sample surface would give a desired sizes and shapes of nanoparticles.

2.5.1 Laser Wavelength

Lasers normally have a particular narrow frequency bandwidth, at which the photon energy it produces will correspond to a particular wavelength and it is given by the equation:

$$\lambda = \frac{hc}{\Delta E} \quad where \quad \Delta E = E_m - E_n \qquad [2.5.3]$$

The energy (E) of each photon will be given by the product of the Planck constant (h), the constant speed of light (c) and the wavelength (λ).

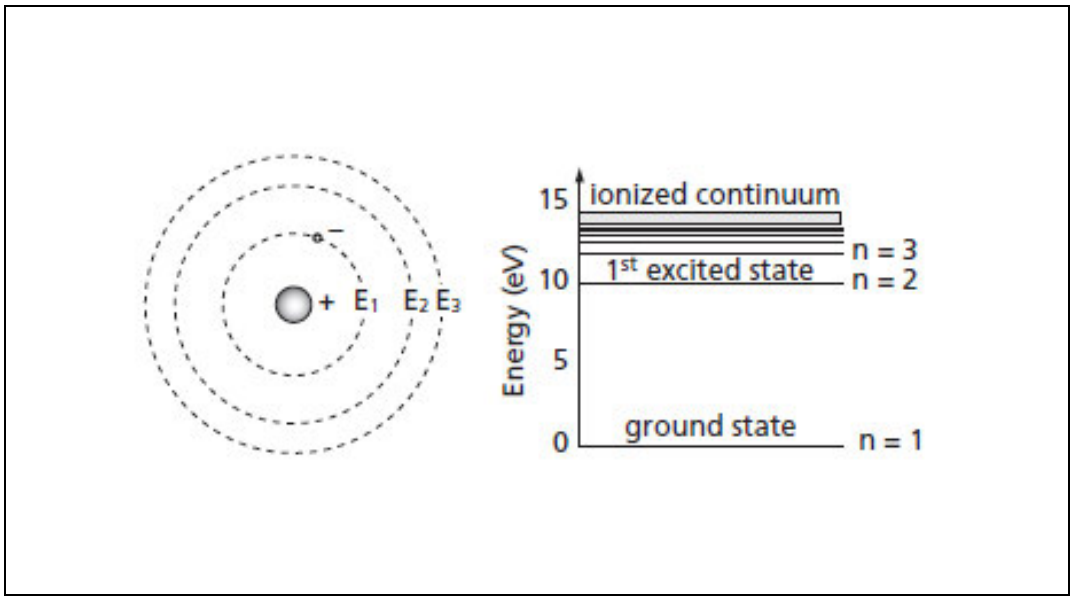

Figure 2.8 A schematic of the Bohr model of the atom to aid in the understanding of excitation and emission of radiation. Figure adapted from Ref [51].

In the electromagnetic spectrum, when the wavelength is shorter it implies that the total photonic energy will be greater and thus long wavelength photons have less energy. For instance, in the visible spectrum band, from the colour blue to red light the energy decreases as the wavelength increases, governed by the *equation 2.5.3*. The green laser pulses have higher photon energy (2.33 eV) at a wavelength of 532 nm. A 1064-nm wavelength in the near-Infrared pulse will produce photonic energy of (1.16 eV). In general, the 532-nm wavelength delivers higher energy per pulse which is more effective at producing smaller silver nanoparticles than the 1064-nm one [62]. This is because less fragmentation takes place with the lower energy of 1064-nm photons, thus resulting in larger nanoparticles with a higher extinction coefficient in the near-infrared region. On the other hand, 532 nm wavelengths have greater photonic energy, that enables the production of nanoparticles with smaller sizes in the colloidal solution.

Table 2.2 Showing types of lasers:

Source	Makeup	Energy input	λ (nm)	Pulse (s)
Excimer	Noble-Reactive Gas: Kr-F, Xe-F, Ar_2, XeCl	Gas discharge or high energy electron beam	126 - 351	10^{-8}
Nd:YAG	Nd^{3+} doped $Y_3Al_2O_{12}$ or other crystal/glass	Xe or Kr arc lamp, or laser diode	$\frac{1064}{n}, n = 1, 2, 3, \ldots$	10^{-8}
Ti-Sapphire	Ti-dopped Al_2O_3	Argon-ion or frequency-doubled Nd:YAG laser	650 - 1100	10^{-14} - 10^{-12}
CO_2	CO_2, N_2, 6He mix	Gas discharge, requires effective cooling	9100 - 10600	10^{-7}

How deep the laser penetrates the metal target is mostly dependent on the wavelength of the incident pulse. The ablation depth on the surface of a target may decrease with the laser wavelength [63]. However, several laser parameters influence the nano-properties of the material that is produced the laser ablation process, e.g., laser wavelength, liquid medium, energy, and pulse duration. It is very important to choose a laser type, considering the work at hand. Different types of lasers are used for different jobs according to their output energy and how easy they are to operate. Nd:YAG laser are stable solid state lasers and they are capable of producing reliable constant pulse laser for micromachining. Nd:YAG lasers can be easily tunned to separately produce higher harmonic wavelengths. Hence, they are preferred lasers in most laboratory settings for experimental purposes.

2.5.2 Nd: YAG lasers

The most common types of solid-state lasers use the crystal rods of neodymium (Nd^{3+})-doped yttrium aluminium garnett, (Nd^{3+} $Y_3Al_5O_{12}$). It is commonly known as Nd: YAG. Its operation was first demonstrated by J.E. Geusic et al. at Bell Laboratories in 1964. The dopant (Nd^{3+}) ions typically substitute a small fraction of the yttrium ions in the crystal. This is possible since they have comparable sizes. The crystal laser medium has excellent thermal conductivity properties suitable for short-pulse laser. Nd: YAG laser are optically pumped using arc lamps, such as krypton or xenon lamps, or diode lasers [64]. The output of the Nd: YAG laser is relatively independent from temperature changes, lending itself to different uses for medium-to high-power applications. Most of the solid-state lasers have several devices such as Q-switches, mode lockers, and frequency doublers in the cavity. These devices enable a better manipulation of the output beam. Solid-state lasers require very little maintenance since the crystals remain unchanged over many years.

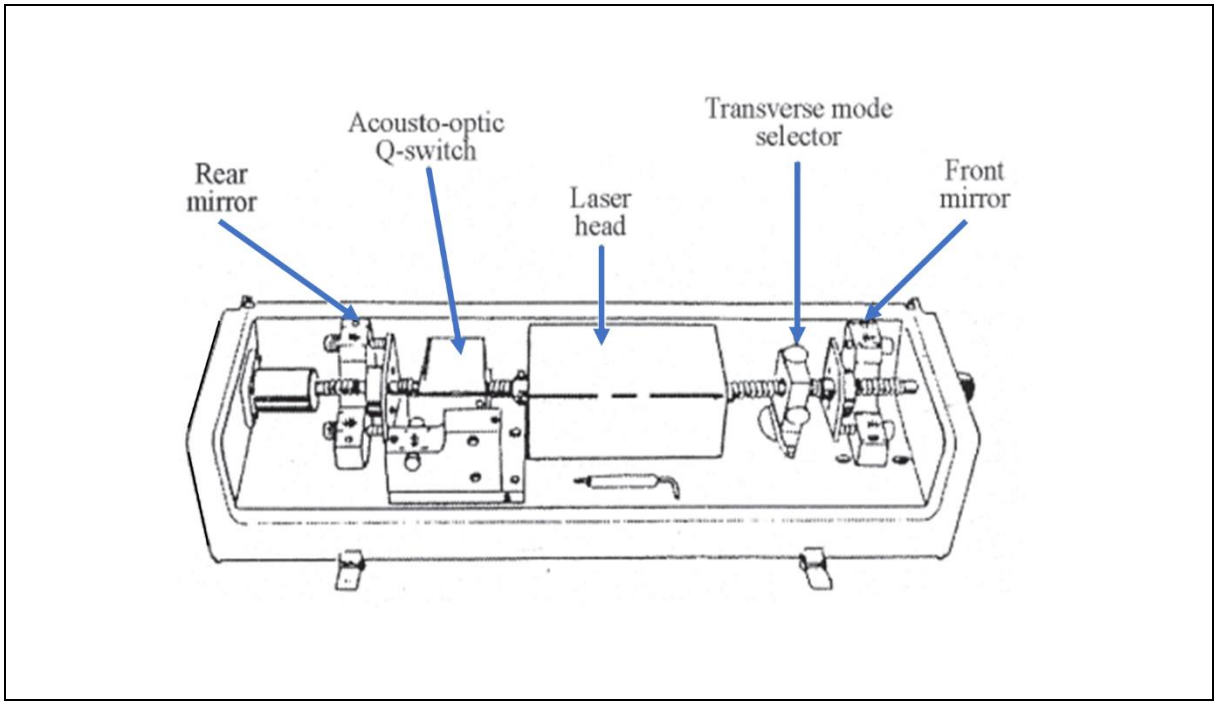

Figure 2.9 Schematic diagram of a Nd:YAG laser [65].

The near-infrared emission is the dominant fundamental frequency produced by a Nd: YAG laser and the photons emitted has a wavelength of 1064 nm and the pulse duration is normally about 7-10 ns with typical mean power that ranges from 10 mJ to about 1 J. First, second and third harmonics can be generated using nonlinear crystals, to produce photons with wavelength of 532 nm, 355 nm, and 266 nm, respectively. However, higher harmonics have less efficiency when it comes to the lasing process, they tend to decrease rapidly. While the pulse-to-pulse stability also deteriorates.

Pulse frequency of 10 Hz is normally recommended for ablation since it can be used when operating at various wavelength. With a fixed duration, the ablation rate normally increases with pulse energy, and this can also increase the concentration of the nanoparticles produced. However, it is necessary to extract the already formed nanoparticles to avoid the attenuation of the incident radiation that may cause a scattering phenomenon.

2.6 Laser Ablation Synthesis in Solution

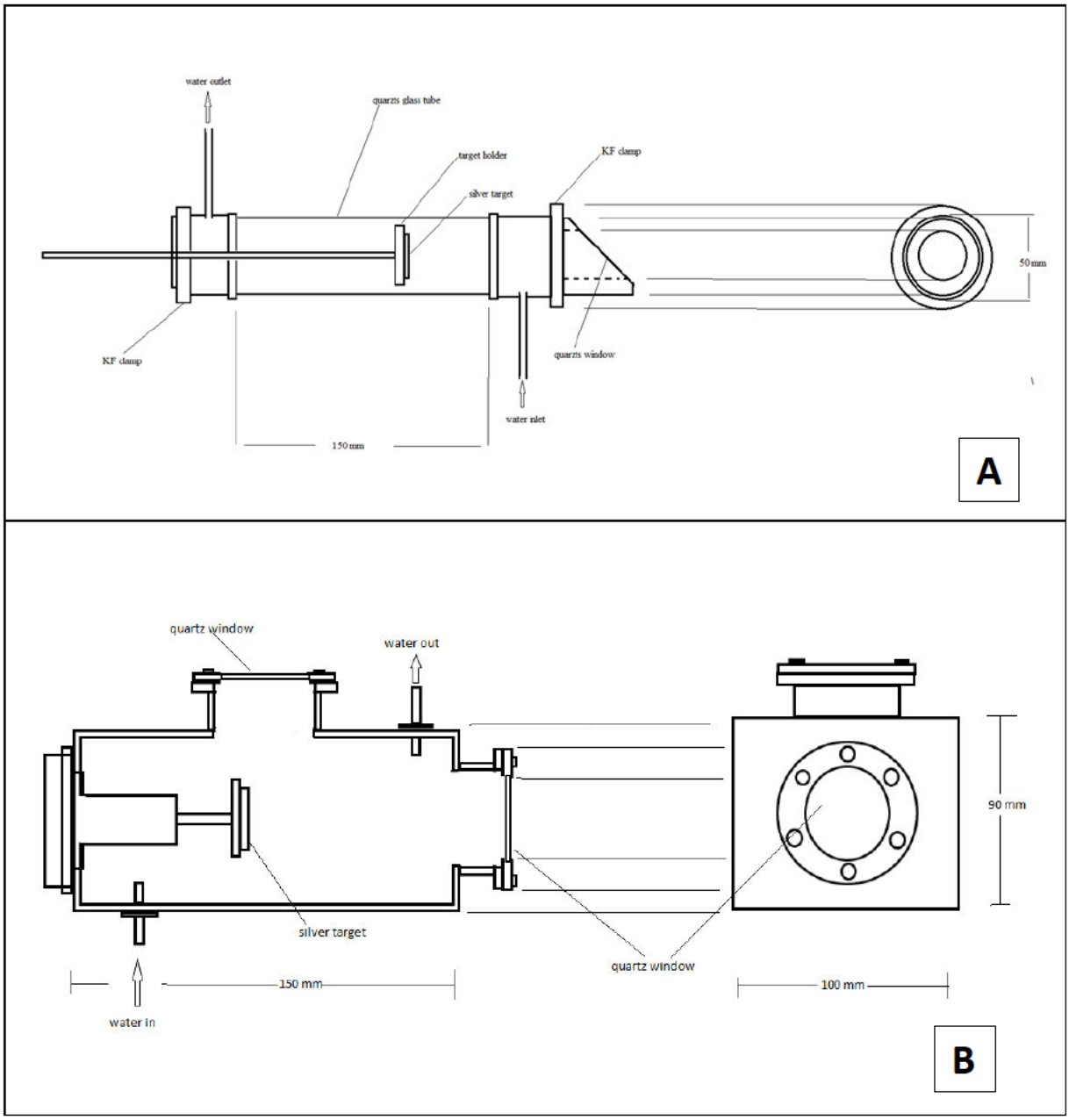

Figure 2.10 (A) Cylindrical ablation chamber design. (B) second stainless steel ablation chamber designed to allow optical spectroscopy to be done through the second quartz window.

Diagrams in ***Figure 2.10*** show two design options for stainless steel ablation chambers. The two chambers must be water and air-tight to avoid liquid leakage. The transparent quartz windows are chosen to allow 1064 nm and 532 nm wavelengths to pass through with minimum attenuation. The quartz window must be strong enough to with-stand the chamber liquid and air pressure during ablation. The cylindrical chamber ***Figure 2.10*** **(A)** was chosen for the experiments conducted in this research.

A pulsed laser focused on a solid target (often metal) immersed in liquid producing nanoparticles with various sizes, shapes, compositions, and surface chemistry is known as the laser ablation synthesis in solution (LASIS) method [66]. The nanoparticles are produced by an incident laser beam directed on a metal target in a liquid medium. As the laser beam hit the metal target a plasma plume is generated as the evaporated materials expand. The plume would start to cool down changing its phase, condensing to form nanoparticles. The higher temperatures, pressure and density in the solution enables the creation of a plume, allows a controlled refinement of smaller nanoparticles. It is considered a ‘’green” approach of developing nanoparticles due to absence of toxic chemical precursors involved in the process.

Beside using water, many different solutions can be used as ablation liquid media to produce colloidal nanoparticles in solution. The produced nanoparticles are found to be highly stable, monodispersed, chemical contamination free particles that can be used for different applications [67]. To have the required nano properties from a colloidal solution a careful selection of the liquid media is important to resizing and reshaping of nanoparticles produced by other conventional routes.

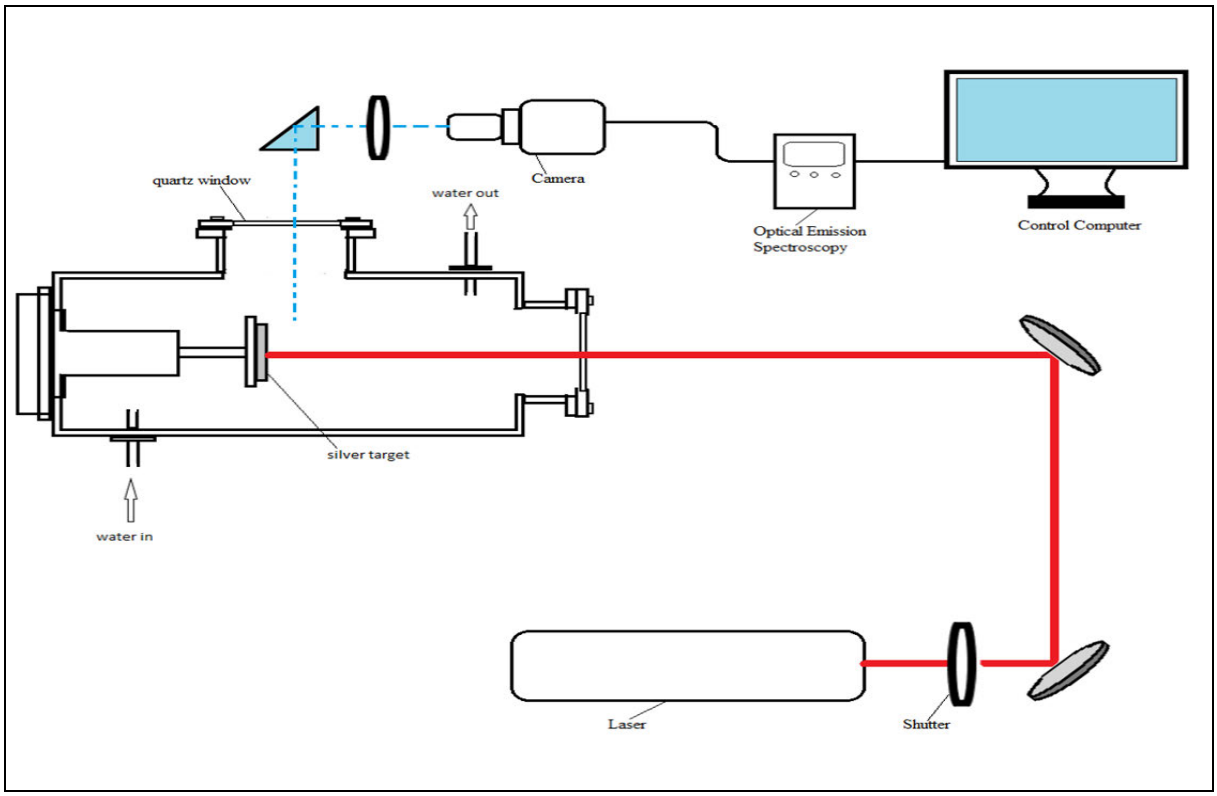

Figure 2.11 A schematic diagram for laser ablation synthesis in solution with optical spectroscopy.

In the laser ablation process, an extremely high energy is concentrated at a specific point on a solid target, to remove the material from a surface. When a laser pulse irradiates the surface of a bulk material, electromagnetic radiation is adsorbed by the target electrons and energy transfers to material vibrational lattice. As a result, the material is ablated from the surface in the form of a plasma plume (in which nanoparticles are formed) [68].

The most relevant parameters that distinguishes between laser ablation of solid in a vacuum and in a liquid medium is the strong confinement of species in the laser produced plasma by the liquid. Therefore, a series of mechanisms including generation, transformation and condensation of plasma plume produced laser ablation of solid in liquid environment takes place in the condition of the liquid confinement [69]. The mechanism of pulsed laser ablation in solution is very complex for it depends also on the width of the pulsed laser and the energy that is delivered by each pulse to ablate the sample. The confinement of plume formed in liquid medium greatly influences the thermodynamic and kinetic properties of the species inside the bubble [70]. The evolution of the plasma plume creates a different environment to allow material phase changes.

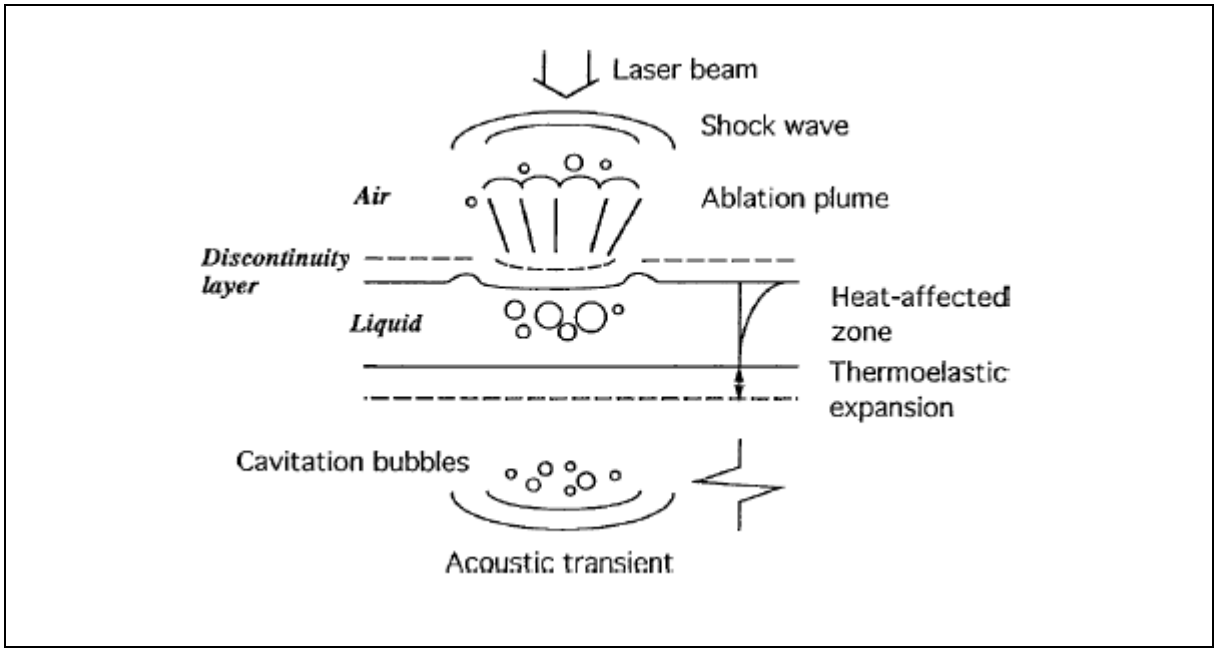

Figure 2.12 A diagram indicating various phenomena involved in the pulsed laser induced ablation of absorbing liquids [71].

The plasma plume is confined, because of the intense pressure exerted by the surrounding liquid inside the chamber. The cavitation bubbles produced by the expanding plasma plume would have to uniformly cool all the species inside it in a very short period. As the cooling takes place, the plasma decays and its energy is transferred to the surrounding liquid medium producing a layer of vapor whose volume would be approximately equal to that of the plasma. The bubbles undergo a periodic evolution of further expansion and shrinkage until they finally collapses [72]. This will allow nucleation to take place before it bursts and releases the nanoparticles into the solution. Thus, the cavitation bubbles play a crucial part in the nanoparticle synthesis as it would be a container for the nanomaterial reaction. Picosecond lasers and femtosecond lasers have shown to produce pulses with better direct photoionization in liquid medium hence the sizes of the nanomaterials are easily tuned to the required shape and diameter.

The ablation rate is generally determined by laser parameters such as: wavelength, fluence, pulse duration and repetition rate, light absorption efficiency of the target material, transmission, and chemical composition of the liquid [73]. Consequently, NP features depend on laser parameters as well as on the liquid medium. Typical requirements for laser ablation are a wavelength from UV-Vis to near infrared (NIR-IR), a laser fluence approximately comprised between 0.1 and 100 J/cm^2, pulse durations from nanosecond (ns) to picosecond (ps) and femtosecond (fs). A significant amount of energy is required to deliver a good ablation efficiency, but it decreases with long ablation time because of significant number of newly developed nanoparticles deflecting the laser beam inside the chamber. This inconvenience can be solved through a careful choice of fluids to be used and by removing the nanoparticles from the optical path by using a flow-through system[74]. Such a technical solution allows to spatially avoid the laser-induced bubbles that prevent higher ablation rates due to the shielding effect. Therefore, pulsed laser synthesis in solution represents a very interesting and versatile way to produce technologically relevant silver nanoparticles [75].

2.6.1 Spherical bubble dynamics

The rapid formation and dynamic collapse of a vapour bubble in a liquid is called cavitation. Cavitation occurs mainly when the static pressure becomes smaller than the liquid vapour pressure. Normally when water boils it forms vapour bubbles. The boiling of water takes place when heat energy increases isothermally while pressure remains relatively constant [76]. Evaporation of water is not only possible when temperature is increased at constant pressure. Reducing the pressure below the vapour pressure isothermally also causes evaporation to occur. Both evaporation and condensation can occur below 100 °C if static pressure is low enough and that’s when cavitation occurs [73]. Cavitation generates mechanical, thermal, and chemical effects, affecting everything from the micro scale to the atomic scale.

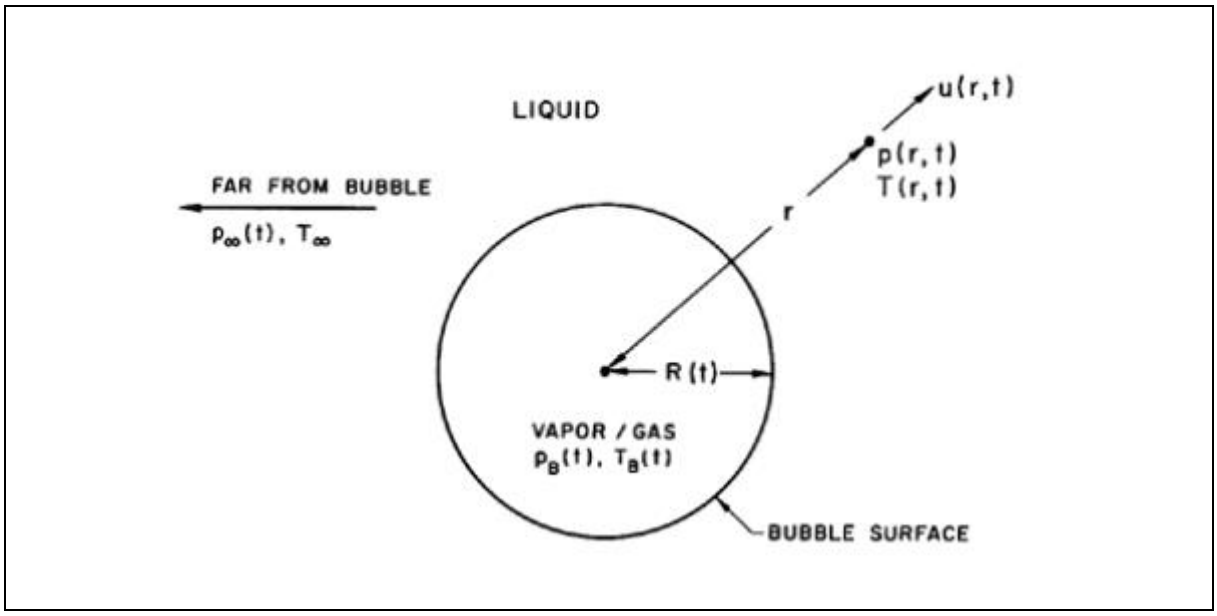

Figure 2.13 Schematic of a spherical bubble in an infinite liquid [79].

The radius of the bubble, *R(t)*, is one of the primary results of the analysis. As indicated in ***Figure 2.10,*** radial position within the liquid will be denoted by the distance, *r*, from the centre of the bubble; the pressure, *p(r, t)*, radial outward velocity, *u(r, t)*, force, *F*, and temperature, *T(r, t)*, within the liquid will be so designated. Conservation of mass requires that:

$$u(r,t) = \frac{F(t)}{r^2} \qquad [2.6.1]$$

where *F(t)* is related to *R(t)* by a kinematic boundary condition at the bubble surface. In the idealized case of zero mass transport across the bubble surface. The velocity of the interface is $u(R,t) = dR/dt$ and hence:

$$F(t) = R^2 \frac{dR}{dt} \qquad [2.6.2]$$

But this is often a good approximation even when evaporation or condensation is occurring on the target surface. The sudden drop below the critical pressure of the liquid, facilitates cavitation to occur. The liquid cavitation parameters can be deduced based on the Rayleigh-Plesset (RP) equation that describes the evolution of the bubble and its physical properties [79]. The equation is an ordinary differential equation which describes the dynamics of a spherical bubble in an incompressible fluid. The general form is usually written as:

$$R\frac{d^2R}{dt^2}+\frac{3}{2}\left(\frac{dR}{dt}\right)^2+\frac{4\nu_L}{R}\frac{dR}{dt}+\frac{2S}{\rho_L R}+\frac{\Delta P(t)}{\rho_L}=0 \qquad [2.6.3]$$

Where, R, is the bubble radius, p, is the surrounding pressure, ρ_L, is the liquid density, ν_L is the viscosity of the liquid and S, is the surface tension of the bubble-liquid interface. Taking, $P_\infty(t)$ to be external pressure surrounding the bubble and $P_B(t)$ is the pressure inside the bubble. Then the pressure difference is given by:

$$\Delta P(t) = P_\infty(t) - P_B(t) \qquad [2.6.4]$$

The Rayleigh-Plesset equation can be used to solve the time-varying bubble radius *R(t)*, for a special case where simple approximation can be done to get a simplified solution.

$$\dot{R} = \sqrt{\frac{2}{3}\frac{P_B - P_\infty}{\rho_L}} \qquad [2.6.5]$$

Where $P_\infty(t)$ and $P_B(t)$ values inside and outside the bubble are known. The surface tension and viscosity would be neglected, together with the second order term in the equation. The over-dot denotes d/dt.

2.6.1 Bubble contents

Cavitation bubbles that contain chemical species or plasma can be governed by the Rayleigh-Plesset equation. To be general, it would be assumed that the bubble contains some quantity of contaminant gas whose partial pressure is P_{Go} at some reference size, R_o, and temperature, T_∞. Then, if there is no mass transfer of gas to or from the liquid across the bubble boundary, it follows that:

$$P_B(t) = P_V(T_B) + P_{Go}\left(\frac{T_B}{T_\infty}\right)\left(\frac{R_o}{R}\right)^3 \qquad [2.6.6]$$

There are circumstances in which the temperature difference, $(T_B(t) - T_\infty)$, is important and the effects caused by this difference dominate the bubble dynamics. Then the temperature difference, $(T_B(t) - T_\infty)$, leads to a different vapor pressure, $P_V(T_B)$, and this alters the growth or collapse rate of the bubble. When cavitation occurs accurate evaluation of the gas or plasma in the bubble requires the solution of the mass, momentum, and energy equations. The bubble contents combined with appropriate thermal boundary conditions at the bubble wall are also required and such an analysis would probably assume spherical symmetry [80]. However, it is appropriate to observe non-spherically symmetric internal motion that tend to mix the contents, producing different chemical species eg: nanoparticles.

2.6.1 Ablation medium

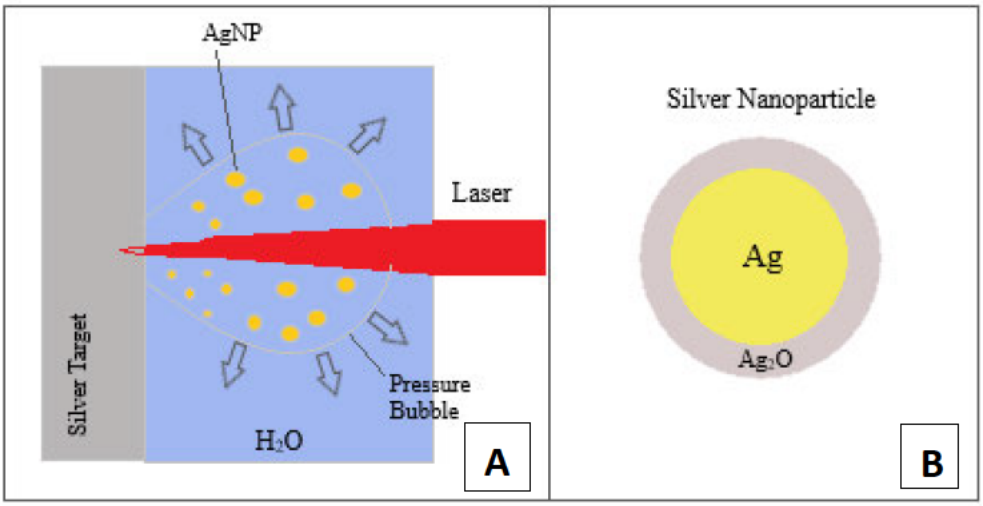

Figure 2.14 Diagram showing the AgNPs formation inside a pressure bubble in water.

When the incident laser pulse interacts with the solid target inside the chamber. The target got to be heated up as the material is ablated. The targeted area would absorb energy till it gets molten. Depending on the temperature inside the ablation zone, the target can be vaporized to a vapor or plasma state [81]. The irradiated energy induces a plasma plume on the surface of the target, which gets supersonically expanded after absorbing the laser pulse and cavitation occurs. The rapid growing bubbles would then explodes after reaching their critical radius, sending shock waves throughout the medium [82].

Normally different chemical reactions and physical processes initiated by the presence of the ablated metal species, solvent molecules, and surfactant molecules in the medium, which induces the formation of several molecular species, that would pose as seeds for the growth of silver nanoparticles. The plasma plume cools and condenses into nanoparticle after losing its energy by expanding against pressure [83]. The plasma plume also gets condensed on the surface of the target and is applicable for surface coating of the material. The structure, morphology, size and hence properties of silver nanoparticles will depend on the temperature, pressure, and composition of plasma plume, which itself is dependent on the laser ablation parameters and nature of liquid media [84].

The best liquid medium in most ablation processes is water because it is cheap, safe, it has a high thermal capacity, and does not absorb laser light. Organic solvents have been considered for quite a while as solvents medium, and the most used ones are methanol, ethanol, isopropanol, acetonitrile, and ethylene glycol [85]. When using organic solvents, the higher dipole moment of the solvent gives a higher ablation efficiency and produces smaller particles. This effect thought to be as a result of electrostatic interactions induced by higher molecular dipolar moment of the solvent, which produces a stronger electric double layer on the metal nanoparticle surface. The dipolar moment of a solvent and its viscosity plays a fundamental role in avoiding nanoparticle agglomeration [86]. When using homologous solvents, such as alcohols with different chain lengths, it has been shown that short-chain alcohols produce unstable silver nanoparticles with different shapes. This is because solvents like ethanol decompose during the ablation process, promoting the formation of permanent gas bubbles. The cavitation transitions in the solvent medium affect the ablated plasma plume and the formed nanoparticles, and with time these may act as obstacles within the laser path, thus reducing the energy reaching the target [87]. Ethanol and acetone solvents can be good stabilizing media to keep metal nanoparticles from precipitation and oxidation; however, organic liquids resulted in very low yields and a larger mean particle size compared to water.

2.7 Silver target ablation in water

Distilled or deionized water is the most used for the laser ablation synthesis in solution of AgNPs. Using water, it is easy for pyrolysis reaction to occur. Free hydrogen and hydroxyl radicals are produced that will facilitate the reaction to produce several oxide or hydroxide species [88]. These reactions will continue to occur between the target material and dissolved oxygen, or oxidizing reactions caused by the plasma-induced decomposition of water. Molecules like hydroxyl groups can go on to attach on the forming silver nanoparticles surface, which can lead to highly charged surfaces that contribute to the electrostatic stabilization of the synthetized nanoparticles [89].

The energy produced by the laser pulse after ablating the silver target will cause a plasma bubble to expand. Inside the bubble containing all the reacting molecules as its temperature cools down in it will break down into smaller pocket bubbles [90]. Inertial confinement occurs in this newly formed small cavitation with a very small volume that tends to heat up to extremely high temperature and pressures. Pyrolysis of water occurs to produce free $^{+}$H and $^{-}$OH radicals that are highly reactive chemically and they are important especially for silver ions reduction [91].

The reported mechanisms for silver nanoparticles formation occurs in the following three steps:

- Generation of high temperature and high-pressure plasma after the interaction of laser beam with matter forming cavitation in the medium.
- Ultrasonic and adiabatic expansion of the plasma plume against the liquid environment, cooling of the plasma and formation of cold clusters.
- With the extinguishment of the plasma, the produced clusters encounter the solvent and surfactant molecules in the solution, which induces some chemical reactions and capping effects.
- There is a competitive mechanism between aqueous oxidation of silver clusters to form Ag(OH) molecules, which can easily dissociate to form Ag_2O molecules and AgNPs.

The depth of ablation cavities on the target gives a measure of nanoparticle productivity [92]. Moreover, the cavity depth increases with the number of laser pulses, but this also causes saturation to occur. Hence, it would be difficult to obtain great improvement of the nanomaterial productivity just by prolonging the laser irradiation times. To avoid this, it is better to change the focus area on the target after an appropriate laser irradiation time by rastering the target.

2.8 Doxycycline conjugated silver nanoparticles

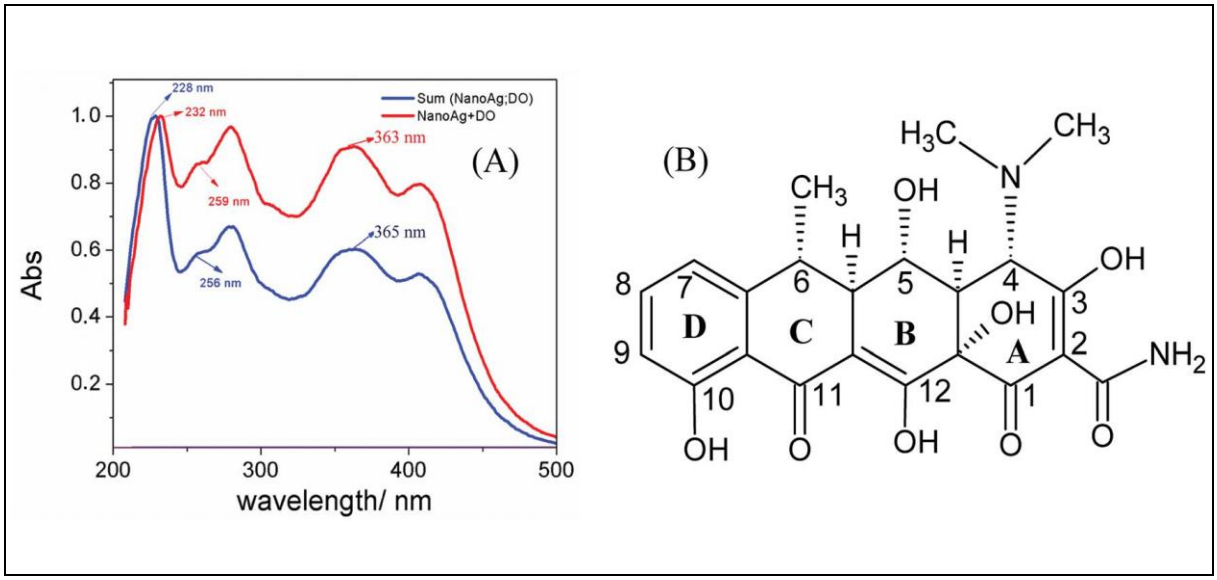

Figure 2.15 (A) UV-VIS spectra of conjugated doxycycline (DO) with AgNPs (red curve) and the mathematical combination of the doxycycline and nano-silver pure spectra. (B) Chemical structure of doxycycline. [32] printed with permission of the Royal Society of Chemistry.

The conjugation of doxycycline silver nanoparticles yields quite a potent agent for the inhibition of several virus replication and their combination culminated in an increased in bactericidal activity [93]. Doxycycline silver nanoparticle also prohibits matrix metalloproteinase (MMP) activation and cellular proliferation. Thus interfering with protein synthesis in cancer cells [94]. Biological membranes have selective permeability and doxycycline-AgNPs assist the transportation of the nanoparticle across the cell barrier. Thus, it works as a better efficient ionophore with less side effects [95]. The coupled doxycycline silver nanoparticle is affordable, accessible and has been applied in clinical tests of cases with advanced cancer. However, every technology has benefits and its own drawbacks, the use of doxycycline AgNPs is not the exception. Reports have pointed out towards the toxicity associated with the use of AgNPs which is said to depends upon the shape, size, and concentration of the nanoparticles. Studies have proved that spherical nanoparticles are non-toxic compared to nanomaterials of other shapes, like nanorods [96]. All these were reasons chosen for this research to employ the use of pulsed laser synthesis in water solution, to have the ability to produce spherical AgNPs with required nano-size. Moreover, the approach allows: to avoid using toxic capping agents, inedible solvents and to easily control the concentration by varying the laser parameters [97].

2.9 Importance of the Research

This research was caried out to investigate the method of developing ionophore silver nanoparticles. The procedure allows a careful optimisation of this process and finding a better way of tuning the sizes of the silver nanoparticles by using a combination of the fundamental and first harmonic pulsed laser beams. The use of the Q-switched pulsed laser enables a controlled, physical top to bottom approach of creating nanoparticles without the use of any toxic capping agents [98]. The relatively small diameter of the AgNPs that are produced by the combination of the fundamental and first harmonic wavelengths of a Nd:YAG pulsed laser were collected and used to make doxycycline silver nanoparticles. With further tests this could prove to be the much-needed drug to be used in the fight against the covid-19 virus. Several research has been done focusing on ways to treat and prevent the disease. Despite that most of the countries in the world were caught un-aware at first. A good number of promising outcomes have emerged out of these drug and vaccines research.

2.10 Research Limitations

This research was limited to the production of the conjugated silver nanoparticles. The conditions and parameters followed were based on previously experiments [78]. However, most of these were not conclusive and they also required further investigations to come up with the best product. The process of knowing the effectiveness of the ionophore silver nanoparticles in the cell of a human being is long and it requires a lot of contributions from different fields. Clinical tests that give quicky positive feedback are necessary for rapid changes to take effect as soon as possible, tailoring the product to the fore known requirements to reduce serious side effects. This research requires a large group of dedicated experts and a big budget to fund it through. Long periods of time are also required after clinical tests to assess how the whole body is responding with time.

3 METHODOLOGY AND ANALYTICAL TECHNIQUES

3.1 Introduction

In this chapter we are introduced to various analytical techniques that were employed in the study and synthesis of silver nanoparticles. The data and results obtained are discussed in the next chapter.

3.2 Experimental layout

The laser that was used for this research was a Q-switched pulsed laser operated at a pulse repetition frequency of 5.2 Hz. The laser unit model was a Nd: YAG: Spectra-Physics Quanta-Ray Laser GCR series. The laser unit produced two different wavelength pulses: an ultra-violet, 1064 nm pulse and a 532 nm green laser pulse. The fundamental wavelength was 1064 nm. The frequency is doubled to produce 532 nm pulses separated temporarily by about 50 ns from the fundamental operating wavelength.

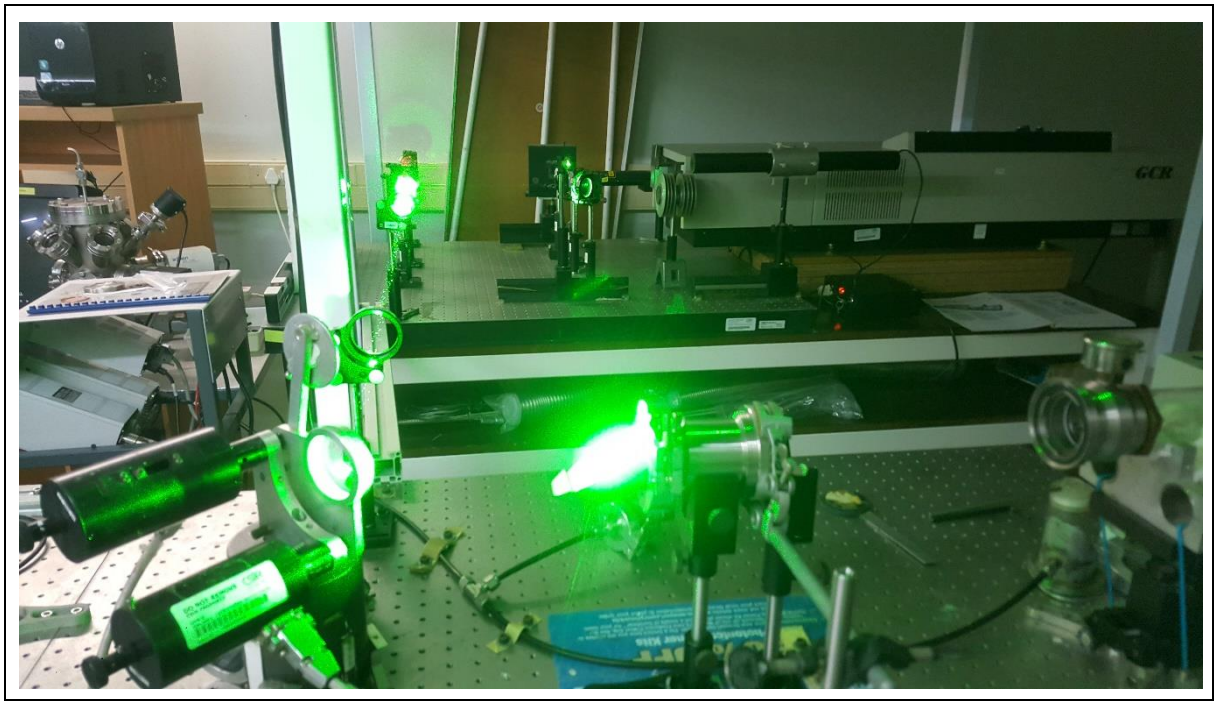

Figure 3.1 The pulsed laser ablation in solution experimental setup.

Laser mirrors with dielectric coatings were used to combine 532 nm and 1064 nm beams from different optical paths. The mirrors coating was designed to optimally reflect 1064 nm or 532 nm wavelength at 45° angle [99]. This made the alignment of the beam easier over the optical breadboard. After the two beams were aligned a lens was placed 0.5 m away to focus the laser onto the silver target that was placed inside the ablation chamber.

3.2.1 Ablation chamber

A stainless-steel chamber was used. It was made to be air and liquid tight. After it was filled with water, the chamber was positioned parallel and adjacent to the laser unit. This was done to align the laser beam with the silver target inside the chamber. The ablation chamber was rotated slightly to reduce energy loss by laser refraction as the beam passes through different refractive index mediums.

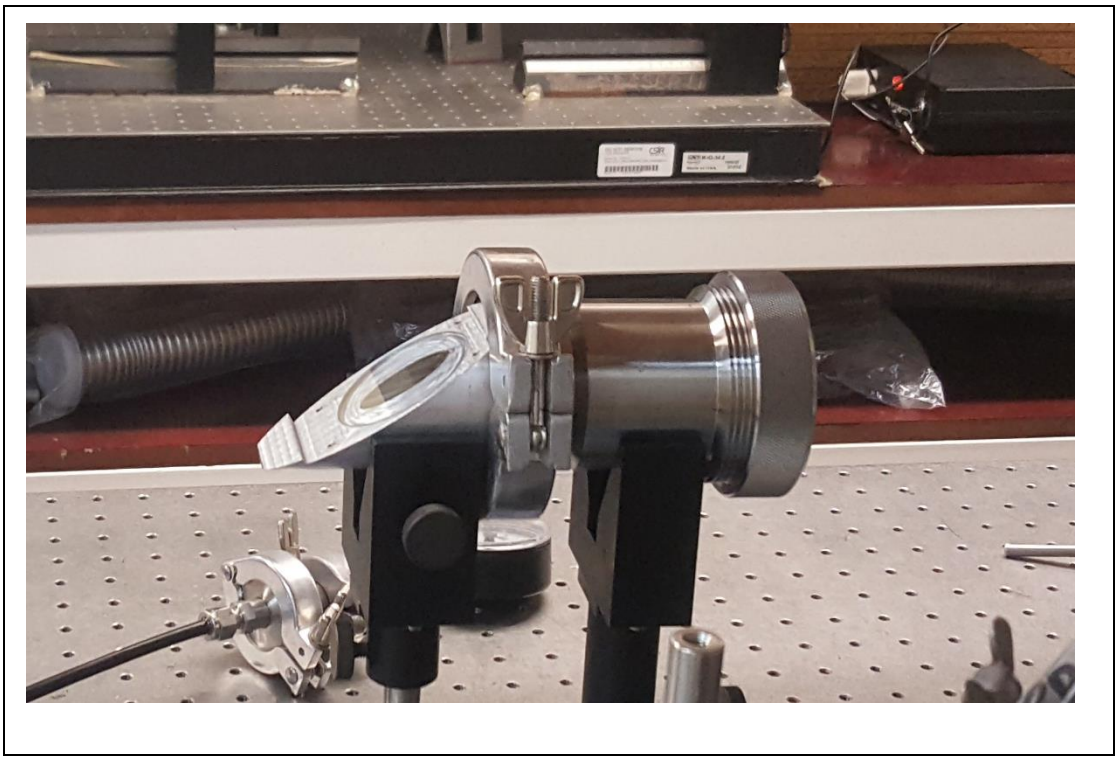

Figure 3.2 The stainless-steel ablation chamber.

3.3 Experimental arrangement for the synthesis of silver nanoparticles in solution using pulsed laser ablation.

The experimental setup employed for pulsed laser ablation is shown in ***Figure 3.3***. The Q-switch pulsed laser was used to irradiate a 25 mm diameter silver target placed inside the ablation chamber. The chamber was filled with 120 ml of pure distilled water and the silver target was completely submerged in the solution.

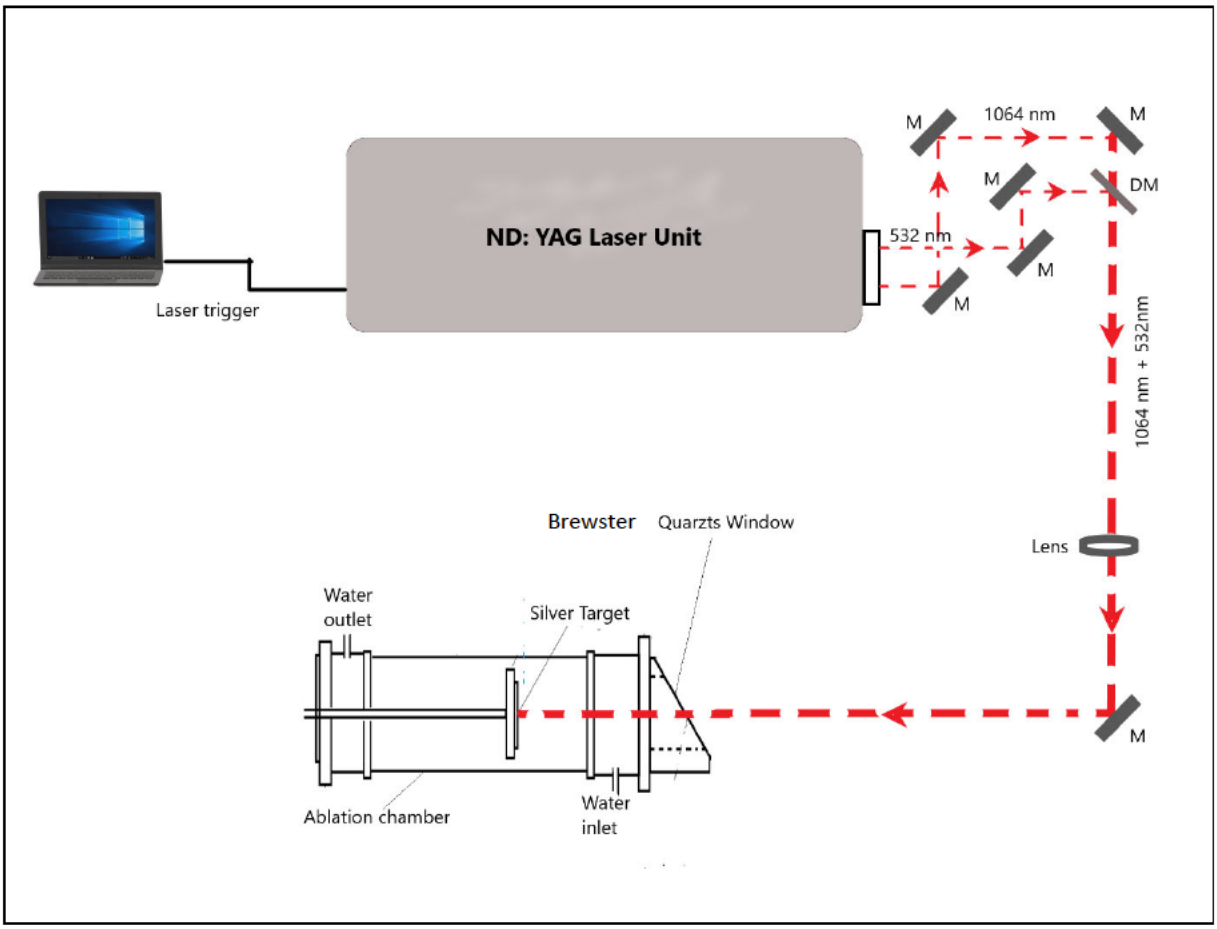

Figure 3.3 diagram to show the experimental setup for the pulsed laser synthesis of AgNPs in solution. M = mirror, DM = dichroic mirror.

The experimental layout employed to synthesize silver nanoparticles is shown in ***Figure 3.1***. The laser was installed on purpose-built tables to accommodate an optical breadboard. The optical tables used were firm enough to minimize vibrations. This is an important feature in any laser-optical experiment. These breadboards were supplied with holes threaded for M6 bolts and which were spaced 25 mm apart. This made it easier to bolt down opto-mechanical components to ensure that the laser optical beam path was kept always aligned and focused on the surface of the silver target [99].

Note: A slight vertical adjustment was done on the mirrors to avoid secondary laser reflection directed back into the laser unit that may cause saturation into the optical gain medium and this may break the laser unit.

3.4 Experimental procedure

The laser was switched on, with only the flash lamps being fired. It was left to run in free mode for 30 minutes. This was to get the lamps and Nd:YAG laser rods warmed up to operating temperature. Once the system was ready to start ablating the target, the alignment of the laser entering the ablation chamber was double-checked by operating the laser at reduced energy. Then these steps were followed to synthesize silver nanoparticles:

1. A clean silver target was placed inside the ablation chamber.
2. The ablation chamber was filled with 120 ml of distilled water.
3. The pulse repetition frequency was kept at 5.2 Hz and the laser was switched on.
4. The silver target was ablated for 5 minutes. Ablation time was changed for every sample that was produced.
5. The samples were collected and were clearly labelled e.g: sample A1, B1, C1, …

The collected samples were characterized using a high-resolution transmission electron microscope (HR-TEM, model: Japanese electro-optic laboratory JEM-2100). The identification of the elements inside the solution was done using energy dispersive x-ray spectroscopy (EDS or EDX), and the ultraviolet-visible (UV-VIS) spectroscopy was used to confirm the optical band gap of silver nanoparticles. After characterization was done, the results obtained were used to choose the right wavelength and the ablation time that produced high quality AgNPs.

3.5 Measurement of laser parameters

Before the synthesis experiments started, the laser parameters which play an important role in the laser ablation process were measured and are shown in **Table 3.4.**

- Average power (W) was measured with a Newport 818E-20-50F power head coupled to a Fieldmax 2 laser power / energy meter.

- Pulse width (ns) for the 532 nm and the 1064 nm pulsed beams, were measured with a New Focus model 1621 VIS and model 1623 IR photodetectors respectively and was connected to a Hewlett Packard 54502A 400 MHz oscilloscope.

- Pulse laser energy (mJ) was measured with a Newport 818E-20-50F energy head coupled to a Fieldmax 2 laser power / energy meter.

3.6 Laser Pulse duration measurement

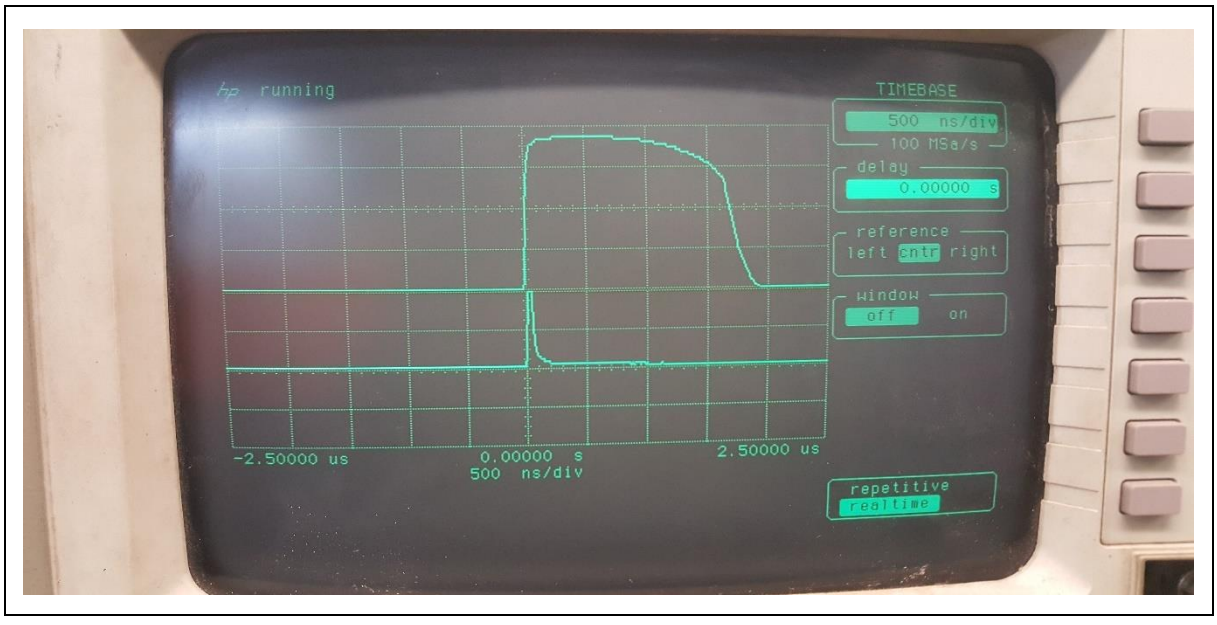

Figure 3.4 The diagram shows the image of the Hewlett Packard model 54502A oscilloscope used for the Nd:YAG pulse width measurement.

The pulse duration for the two-pulse laser 1064 nm and 532 nm wavelength was measured using the energy photodetector and an oscilloscope in ***Figure 3.4***. The energy of a laser pulse is typically measured using an energy meter. This quantity is expressed as total energy per pulse. The laser beam spot was 1 mm in diameter.

Table 3.1 Showing energy and pulse duration measurements:

Wavelength (λ) (nm)	**Energy (E) (m J)**	**Pulse Duration (*ns*)**
1064	273	0.95
532	285	0.1
1064 + 532	293	-

3.6.1 The intensity of a laser irradiation

The intensity of a laser irradiation can be described in many ways: The power provided by the laser is the energy of the pulse irradiated over a certain period. Thus, the power highlights the rate at which the energy is delivered by the laser. The standard unit of measurement is called a watt (W).

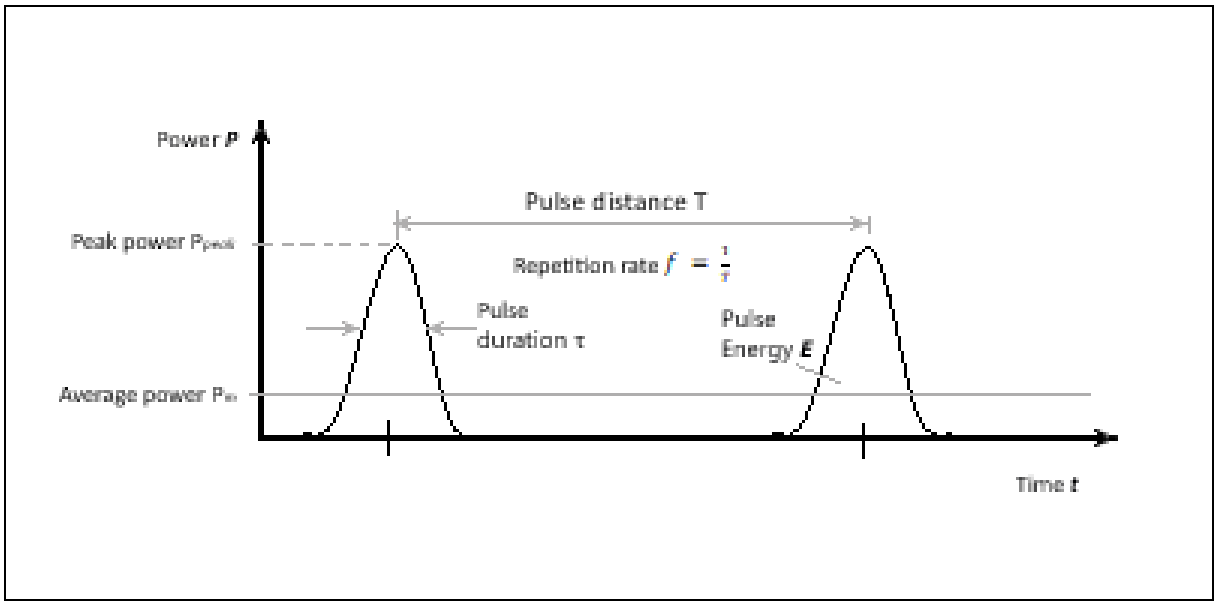

Figure 3.5 Shows the diagrams laser pulse profile

$$Power: \ P = \frac{Energy\ (E)}{Area} \qquad [3.6.1]$$

The average power will be the total energy of all pulses emitted in 1 second, thus: average Power = Energy per pulse × pulses rate. The pulse rate is the repetition rate of the laser pulse which can be referred to as the laser Frequency (f). The pulse rate was kept at 5.2 Hz.

$$average\ Power\ = \ Energy\ \times \ Frequency \qquad [3.6.2]$$

The fluence of a laser is the energy of a laser pulse incident onto a given area. This quantity is typically measured in $J.m^{-2}$ or $J.cm^{-2}$ which is more commonly used.

$$Fluence\ = \frac{Energy\ (E)}{Area} \qquad [3.6.3]$$

Table 3.2 Showing energy and mean power produced by the laser per pulse:

Wavelength (λ) (nm)	Energy (E) (m J)	Mean Power (P_m) (W)	Fluence ($J.cm^{-2}$)
1064	273	1.42	34.8
532	285	1.48	36.3
1064 + 532	293	1.52	37.3

$$Irradiance = \frac{Power\ (P)}{Area} \qquad [3.6.4]$$

Irradiance is the power delivered onto a given area. This distribution power per area is a very important property of a laser, since it describes the total energy of the pulse, as well as how it is distributed in both space and time. This can then be used to determine how a certain material responds to the laser light.

Table 3.3 Showing the laser pulse parameters:

Wavelength (λ) (nm)	Power (P) (MW)	Irradiance ($MW.m^{-2}$)
1064	2.87	3.66×10^6
532	2.85	3.63×10^6

The laser parameters shown in the **Table 3.3** above were used to calibrate and set the laser unit to the desirable power. The laser unit was turned on and left to run for 30 minutes before use as a precaution to achieve a constant power delivery.

Table 3.4 Showing the process parameters:

Process Parameters		
Fluence	F	37.3 (J. cm^{-2})
Beam Spot Size	r_b	1.0 mm
Ambient Medium	liquid	H_2O
Pulse Duration: (s)	1064 nm	0.95 ns
	532 nm	0.1 ns

Table 3.5 Experimental conditions for pulsed laser ablation of a silver target.

	Sample	Wavelength (nm)	Ablation time (minutes)	Energy (m J)	Fluence (J. cm^{-2})	mean Power (W)	beam Spot size (mm)	liquid	volume (ml)
	A1	1064 + 532	5	293	37.3	1.52	1.0	H_2O	120
	B1	1064 + 532	10	293	37.3	1.52	1.0	H_2O	120
Test 1	C1	1064 + 532	15	293	37.3	1.52	1.0	H_2O	120
	D1	1064 + 532	20	293	37.3	1.52	1.0	H_2O	120
	E1	1064 + 532	25	293	37.3	1.52	1.0	H_2O	120
	A2	1064	5	273	34.8	1.42	1.0	H_2O	120
Test 2	B2	1064	15	273	34.8	1.42	1.0	H_2O	120
	C2	1064	25	273	34.8	1.42	1.0	H_2O	120
	A3	532	5	285	36.3	1.48	1.0	H_2O	120
Test 3	B3	532	15	285	36.3	1.48	1.0	H_2O	120
	C3	532	25	285	36.3	1.48	1.0	H_2O	120
	A4	1064 + 532	5	293	37.3	1.52	1.0	H_2O	120
Test 4	B4	1064 + 532	15	293	37.3	1.52	1.0	H_2O	120
	C4	1064 + 532	25	293	37.3	1.52	1.0	H_2O	120
	A2A	1064	5	273	34.8	1.42	1.0	H_2O	120
Test 5	B2A	532	5	285	36.3	1.48	1.0	H_2O	120
	C2A	1064 + 532	5	293	37.3	1.52	1.0	H_2O	120
	A2B	1064	15	273	34.8	1.42	1.0	H_2O	120
Test 6	B2B	532	15	285	36.3	1.48	1.0	H_2O	120
	C2B	1064 + 532	15	293	37.3	1.52	1.0	H_2O	120
	A2C	1064	25	273	34.8	1.42	1.0	H_2O	120
Test 7	B2C	532	25	285	36.3	1.48	1.0	H_2O	120
	C2C	1064 + 532	25	293	37.3	1.52	1.0	H_2O	120
Test A	E	1064 + 532	25	293	37.3	1.52	1.0	H_2O	120

All the other parameters used in this experiment are shown in the **Table 3.5.** above. *Test 1* was done following all the fore-mentioned steps and method. Five samples were collected, and a distinct colour change was noticed among these samples. A dual pulsed laser of 1064 nm and 532 nm laser pulses were used for first tests. The second tests were caried out allowing only the 1064 nm wavelength pulse to pass through. The silver target was irradiated for *Test 2* experiment samples, then *Test 3* samples were synthesised using the 532 nm wavelength pulse. The silver nanoparticles were synthesised inside the chamber filled with distilled water by following the previously stated procedure while varying the target ablation time as the table above illustrate.

Doxycycline-Silver nanoparticles synthesis procedure.

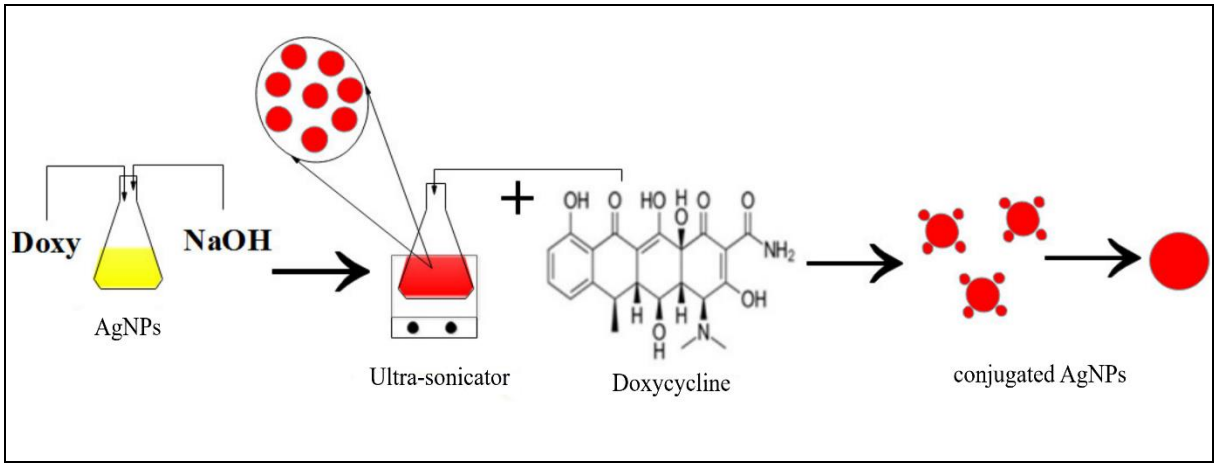

Figure 3.6 A schematic diagram to show the reaction procedure of doxycycline silver nanoparticles[40].

The preparation of doxycycline silver nanoparticles was done using monohydrate doxycycline. A powder form of doxycycline was required because of its large surface area makes it easy to dissolve. *Sample E* that was synthesised using a dual pulse laser for 25 mins ablation duration was used to synthesise DO-AgNPs. These were the steps used to prepare a sample of DO-AgNPs:

1. A well-prepared sample of silver nanoparticles was used eg: we used the *Sample E*.
2. A measuring balance was used to measure 0.182 g of doxycycline and then it was dissolved in a 250 ml volumetric flask filled with deionised water. A concentration of 0.002 mol. L^{-1} was obtained.
3. A 0.01 M of NaOH solution was also prepared.
4. Using a measuring cylinder 20ml of doxycycline and 30 ml of AgNPs solution was measured and mixed in a conical flask. 5 drops of NaOH were placed into the conical flash.
5. The flask was placed into a water bath in an ultra-sonicator bath.
6. The reagents were sonicated for 30 mins whereafter the solution turns to a yellowish colour.

Table 3.6 Showing the stoichiometric measures for DO-AgNPs synthesis:

	Mass (g)	Molarity ($mol.L^{-1}$)	Volume (ml)
Silver nanoparticles	0.0004	0.0037	1.0
Doxycycline	0.182	0.002	250
NaOH	0.04	0.01	100

The mass, concentration and volume stated in the above **Table 3.6** were used to prepare reagents used for silver-doxycycline conjugation. The stochiometric calculations were used for the sample preparations: refer to the Appendix A.

3.7 UV-Vis Spectroscopy

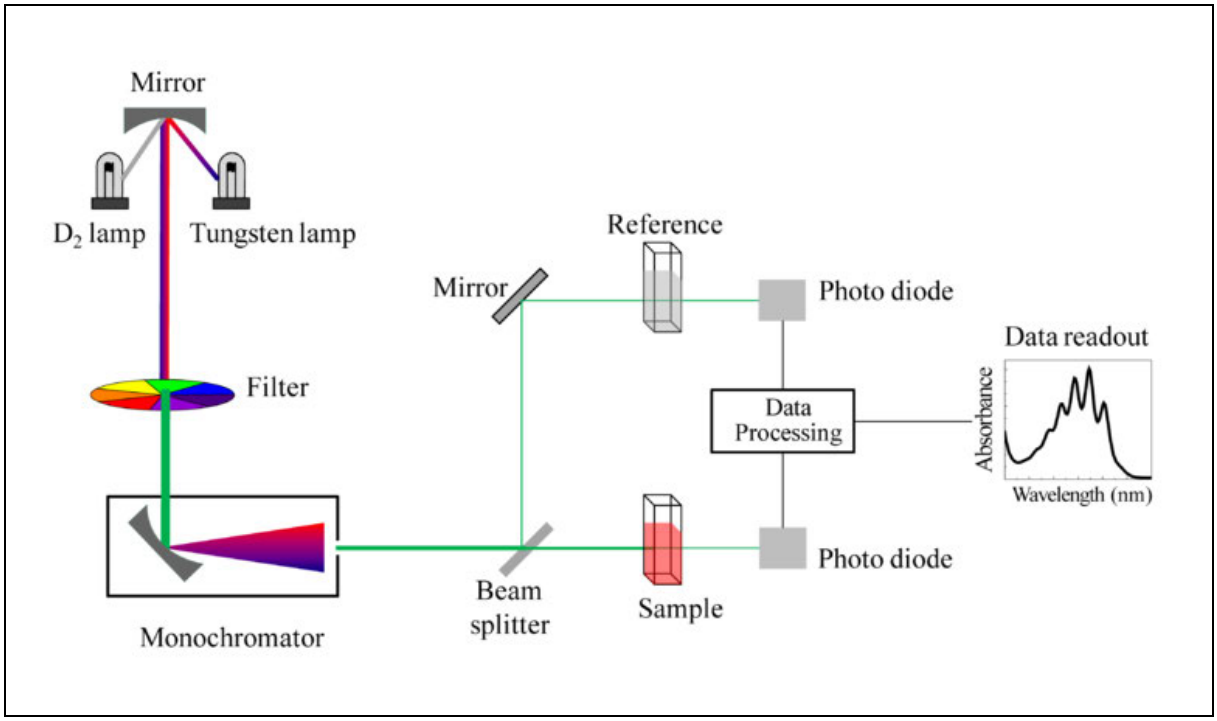

Figure 3.7 A schematic diagram of a UV-VIS spectrometry [100].

UV-visible (UV-vis) absorption spectrometry is an analytical technique that uses the interaction of ultraviolet and visible light to determine the absorbance characteristics of a material. It can be used to determine both chemical composition as well as the physical properties of mater. It typically utilises the measure of the electromagnetic radiation intensity as a function of the wavelength of the radiation [101]. The Beer-Lambert law is a linear relationship between the absorbance, A, and the concentration, c, molar absorption coefficient, ε, and optical coefficient, l, of a solution:

$$A = \varepsilon c l \qquad [3.7.1]$$

UV-visible spectra explain the radiation absorbance region of a compound. The molar absorption coefficient is a sample dependent property and is a measure of how strong an absorber the sample is at a particular wavelength of light. When UV-visible light strikes the matter, some of the light is absorbed within the molecules of the compound while the rest will be transmitted through it [100]. This technique gives an easy way to characterise silver nanoparticles. Silver nanoparticles absorb at the far UV band and near visible light band. Quantum size effect can cause a shift of the absorption edge towards high energy side. Purely ionic silver may show a contribution in the near UV range of the UV-VIS spectrum close to 300 nm wavelength and the absorption of more than 500 nm wavelength shows the precipitation of silver without the formation of nanoparticles. The concentration can be determined by the absorbance intensity of the sample [102].

UV-VIS absorption spectroscopy is normally preferred for quick tests on synthesized nanoparticles. By analysing the UV-VIS spectra graph you can quickly determine the qualitative and quantitative characteristics of the nanoparticles. Experimental parameters can be adjusted according to the shape and size of the nanoparticles required.

3.8 High Resolution Transmission Electron Microscopy

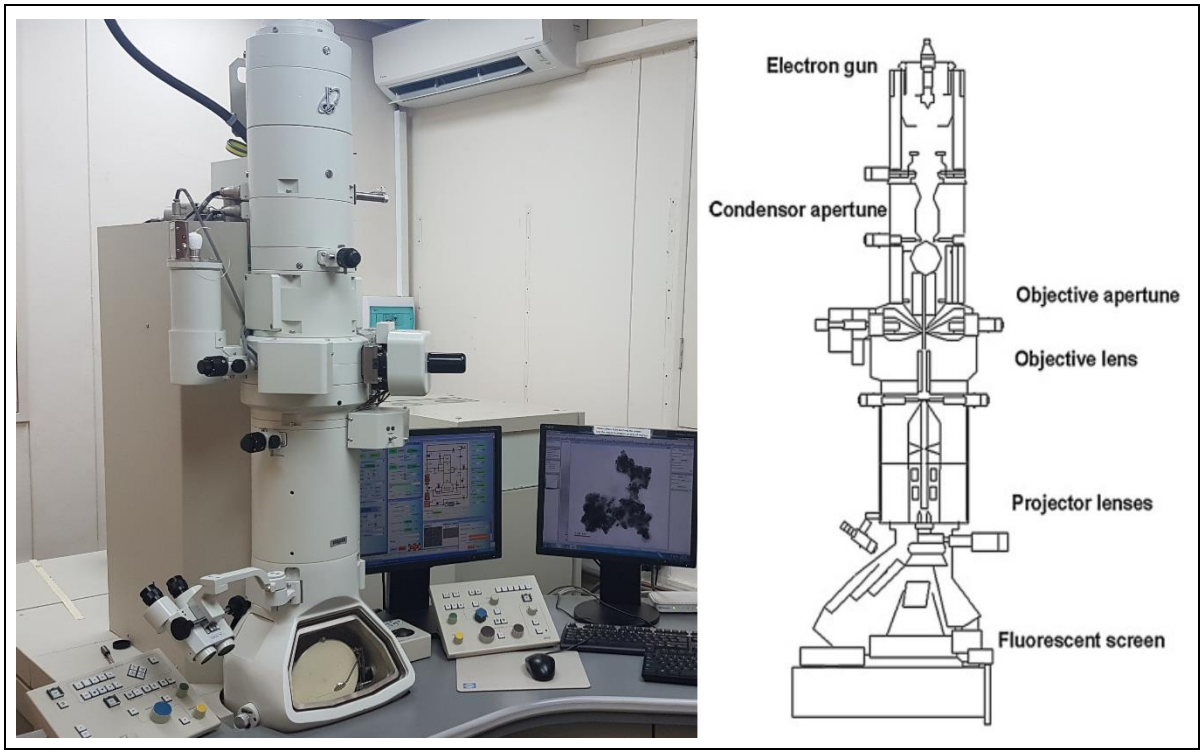

Figure 3.8 diagram showing a high-resolution transmission electron microscope [103] [100].

High-resolution transmission electron microscopy (HRTEM) was used to determine the morphology and distribution of the sizes of the synthesized nanoparticles. Ernst Ruska, a nobel lauruate, invented the TEM in 1933 [104]. The high voltages used in the TEM have to the tunnel through the sample and come out of the other side. The area under review is illuminated by a parallel beam of electrons. The beam is focussed and controlled using condenser lens which depends on, how large is the magnification area scanned [103]. This depends on the amplitudes and phases that form the electron diffraction pattern in the back focal plane of the objective lens. The function is governed by ***equation 3.8.1***

$$T(k) = -\sin\left[\frac{\pi}{2} C_s \lambda^3 k^4 + \pi \Delta f \lambda k^2\right] \quad [3.8.1]$$

where, C_s, is the spherical aberration coefficient, T, is the electron relativistic kinetic energy, λ, the wavelength of the beam, Δf, the defocus value and, k, is the spatial frequency.

The lower magnifications are utilized to determine the distribution of the sizes of the nanoparticles and the higher resolutions is used to determine the morphology and internal structure of the nanoparticles. The most common mode of operation is when the electrons are forward scattered or transmitted when they encounter the sample [105]. The transmitted electrons form the bright field image and the region that are thicker have a higher atomic number, or higher density would appear darker [106]. The image obtained is like a cross sectional 2D projection of the sample.

The nanoparticle samples that that were synthesised were drop-cast on Cu grids for observations on transmission electron microscopy. After ultra-sonicating the sample solution further test was carried out on EDX to identify the elements presences. The data that was collected came in form of numerical values or graphs and the findings were discussed in the following chapter.

3.9 Raman spectroscopy

Raman spectroscopy was discovered by two physicists, C.V. Raman, and K.S. Krishnan in the year 1928. The instrument has been widely used to characterize material composition, sample temperature and strain from the material phonon mode analysis. Characterization is done using two different processes which are Raleigh scattering and Raman scattering, of which the Raman scattering is the most useful. When a visible light laser beam is incident through a translucent substance and a small amount of radiation would be scattered and its output signature is recorded [107].

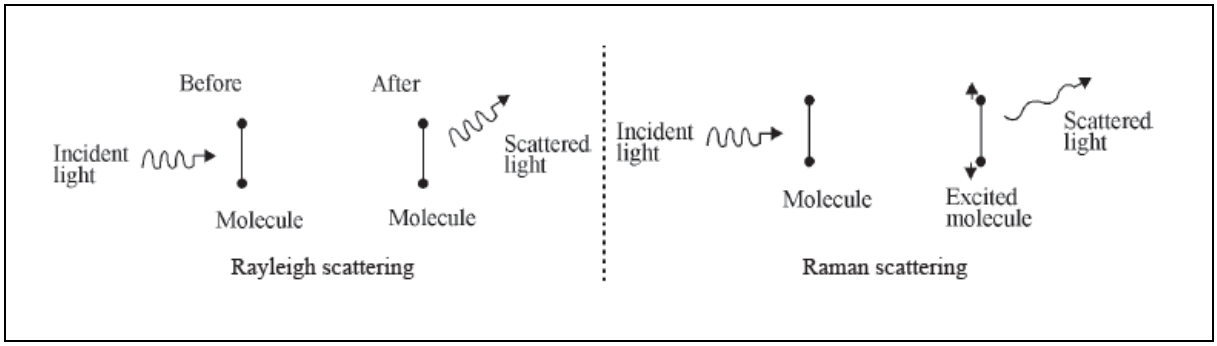

Figure 3.9 Figure Rayleigh and Raman scattering [50].

Raleigh scattering is obtained when a narrow frequency range radiation is used, and the scattered energy signature returned is the same as the incident frequency. But when the beam energy scatter certain discrete frequencies above and below that of the incident, then the process is referred as Raman scattering [108]. Raman scattering is an example of inelastic scattering because of the energy transfer between the photons and the molecules during their interaction. These transitions are depicted graphically in Jablonski energy diagram in

Figure *3.10*. of The Raman scattering depends on the chemical properties of a particular molecule; hence it gets to be used for both qualitative and quantitative analysis.

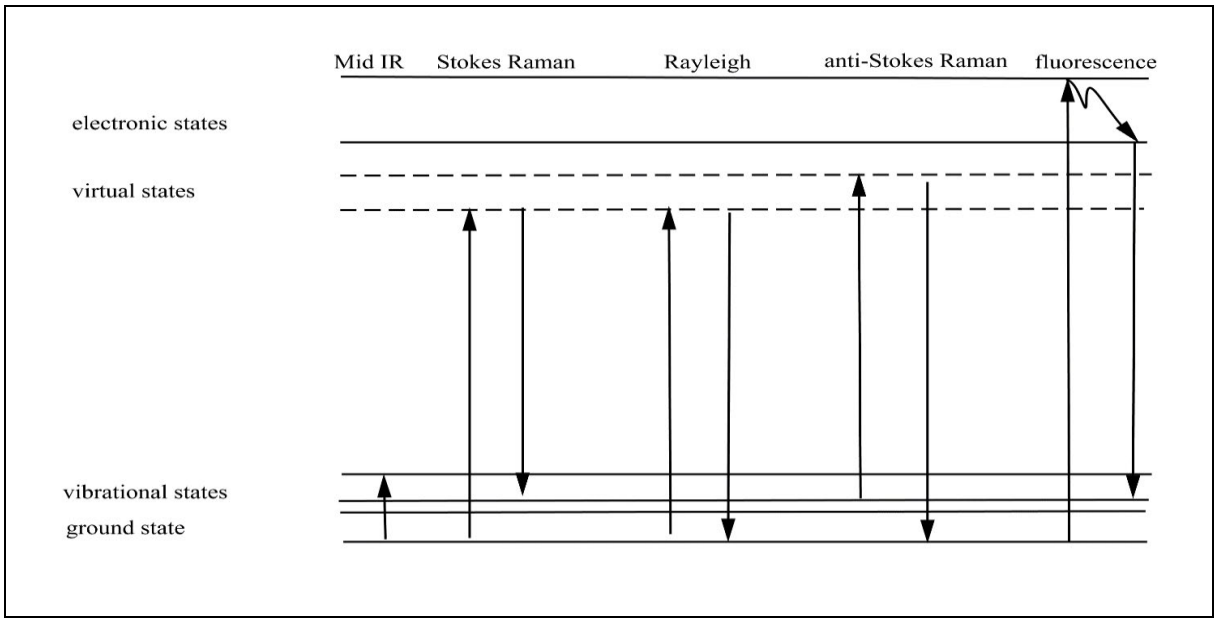

Figure 3.10 Jablonkski energy diagram depicting electronic transitions of several processes in an excited atom resulting in the emission of photons of deferent energies [99].

A change in the molecular polarization potential or amount of deformation of the electron cloud with respect to the vibrational coordinate is required for a molecule to exhibit a Raman effect. The amount of the polarizability change will determine the Raman scattering intensity. The pattern of shifted frequencies is determined by the rotational and vibrational states of the sample [99].

3.10 Precautions

Safety when operating the laser was of paramount importance for caution need to be taken from dangers of electric shocks, fires outbreaks, and high energy laser beam radiation. It is important to use a well-equipped laboratory, with safety requirements in place such as fire extinguishers, protective clothes. Ultra-violet (UV) certified laser protection goggles were worn as your eye protection whenever the laser machine was in use.

3.11 Cleaning and preparation

The cleaning was done thoroughly to ensure that all micro and nanoparticles that might be in the pulsed laser ablation chamber was removed. All the experimental equipment that was to be used had to be cleaned first using ethanol, followed by 5 mins ultrasonication bath at 60ºC. The water bath was replaced by distilled water and placed back for another 5 minutes ultrasonication procedure. Lastly, the wet apparatus would have to be placed in a 60ºC temperature oven for a quick dry. The optical lens and mirrors used had to be cleaned regularly using ethanol alcohol, then wiped them using a soft lens cleaning tissue.

4 RESULTS AND ANALYSIS

4.1 Introduction

The experimental setup and procedures described in chapter three were used to obtain results according to the stipulated parameters that were chosen. After data acquisition the results were recorded for further analysis to understand the physical and chemical properties of the nanoparticles that were produced. The results obtained were used to optimise and improve the quality of the product we had synthesised. The samples characterization was done on the HRTEM, Raman and UV-VIS spectroscopy.

4.2 Silver nanoparticles data analysis.

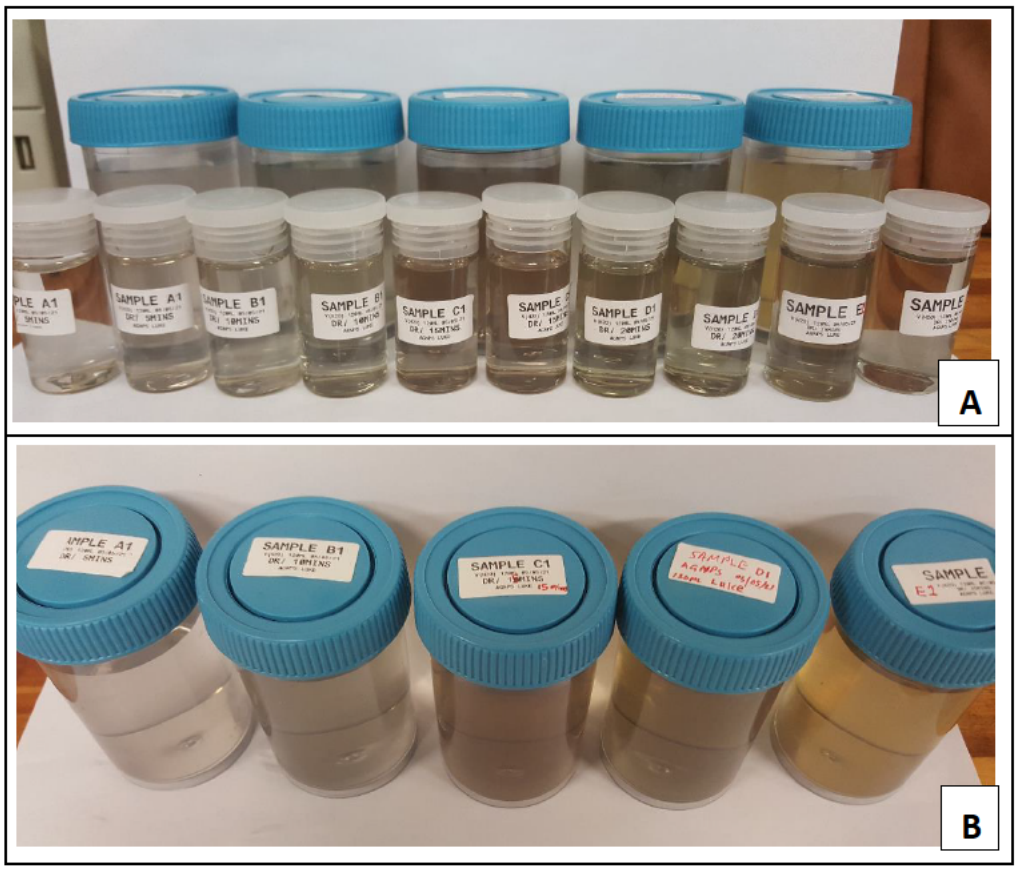

Figure 4.1 **(A)** and **(B)** Labelled samples of synthesised silver nanoparticles.

The synthesised AgNPs in ***Figure 4.1*** **(A)** image showing different colours as particles sizes changes from *sample A1* to *sample E1*. Ablation time was increased at intervals of 5 mins per sample.

4.2.1 UV-VIS absorption spectroscopic analysis of AgNPs

Silver nanoparticles that have diameter less than 100 nm normally absorb wavelengths in the range of 380-470 nm. Smaller wavelengths are absorbed by smaller sized particles. Spherical silver nanoparticles with diameter of 10 nm absorb wavelength between 400-410 nm. Lager particles would show a red-shift while smaller AgNPs shows a blue-shift on the spectra graph. The dominant shape of the nanoparticles can shift the absorbance peak of the spectrum. Agglomeration of the nanoparticles would cause a sensible broadening of the plasmonic band towards larger wavelengths [101].

Table 4.1 ***Test 1*: experimental conditions under which AgNPs samples were synthesised.**

Sample	Wavelength (nm)	Ablation time (minutes)
A1	1064 + 532	5
B1	1064 + 532	10
C1	1064 + 532	15
D1	1064 + 532	20
E1	1064 + 532	25

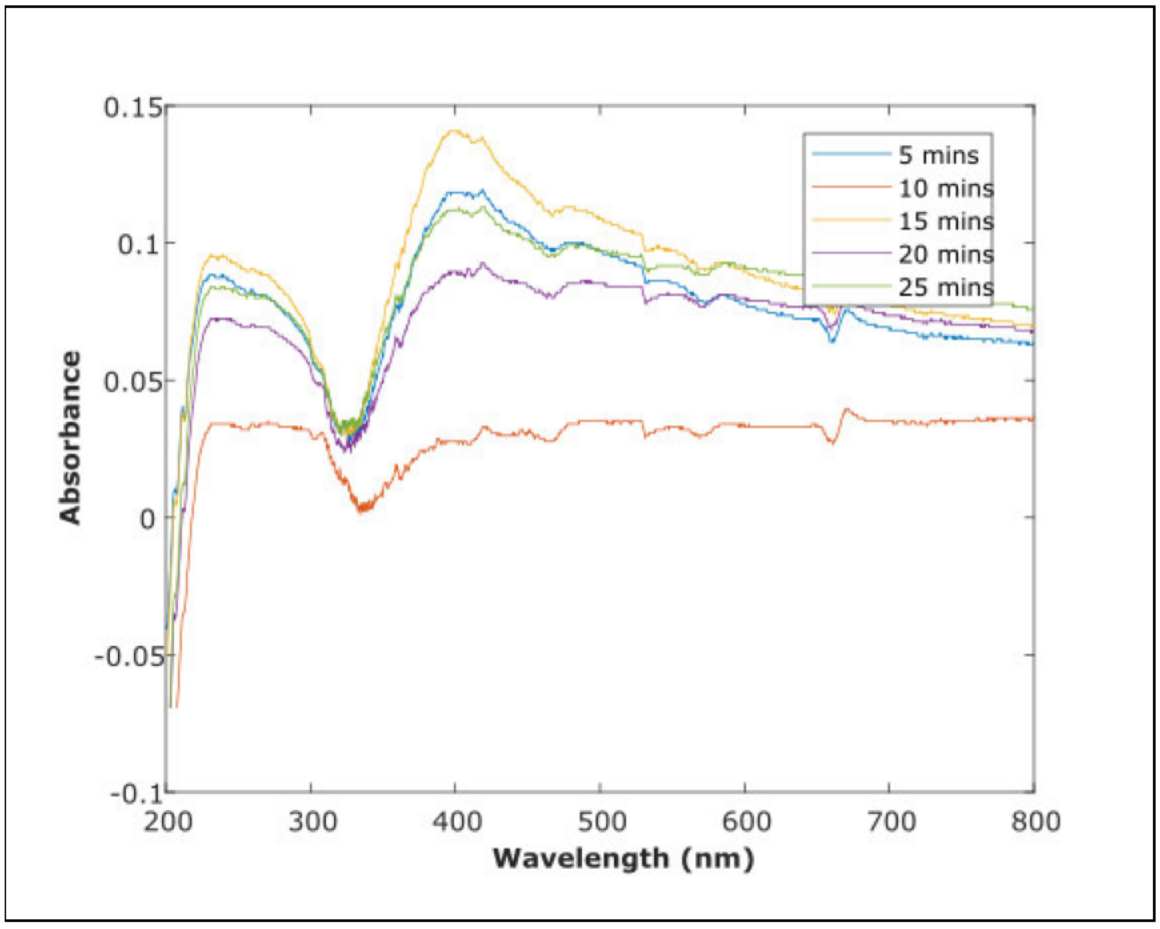

Figure 4.2 Shows *Test 1*: UV-VIS absorption spectra of AgNPs synthesised using 1064 nm and 532 nm wavelength pulse.

Table 4.2 ***Test 2*: experimental conditions under which AgNPs samples were synthesised.**

Sample	Wavelength (nm)	Ablation time (minutes)
A2	1064	5
B2	1064	15
C2	1064	25

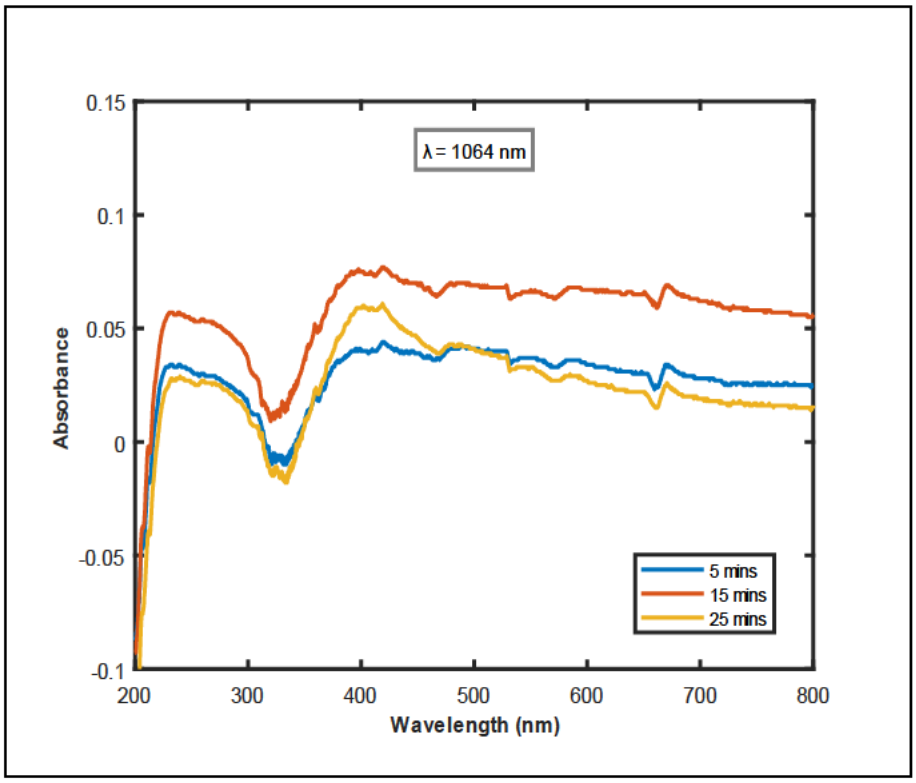

Figure 4.3 Shows *Test 2*: UV-VIS absorption spectra of AgNPs synthesised using 1064 nm wavelength pulse.

Table 4.3 ***Test 3*: experimental conditions under which AgNPs samples were synthesised.**

Sample	Wavelength (nm)	Ablation time (minutes)
A3	532	5
B3	532	15
C3	532	25

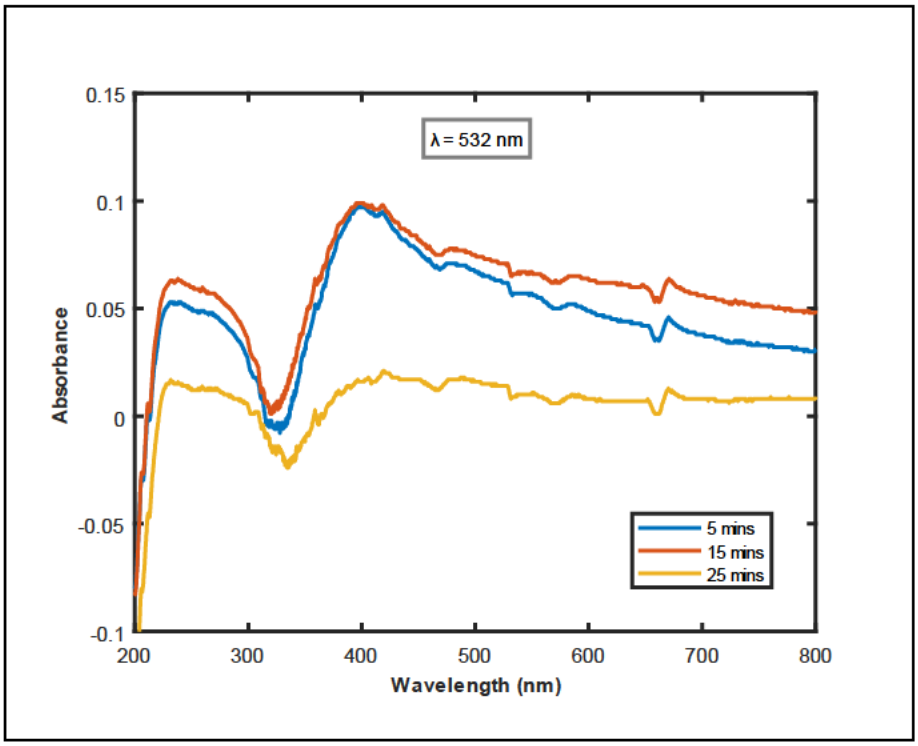

Figure 4.4 Shows *Test 3*: UV-VIS absorption spectra of AgNPs synthesised using 532 nm wavelength pulse.

Table 4.4 *Test 4*: **experimental conditions under which AgNPs samples were synthesised.**

Sample	Wavelength (nm)	Ablation time (minutes)
A4	1064 + 532	5
B4	1064 + 532	15
C4	1064 + 532	25

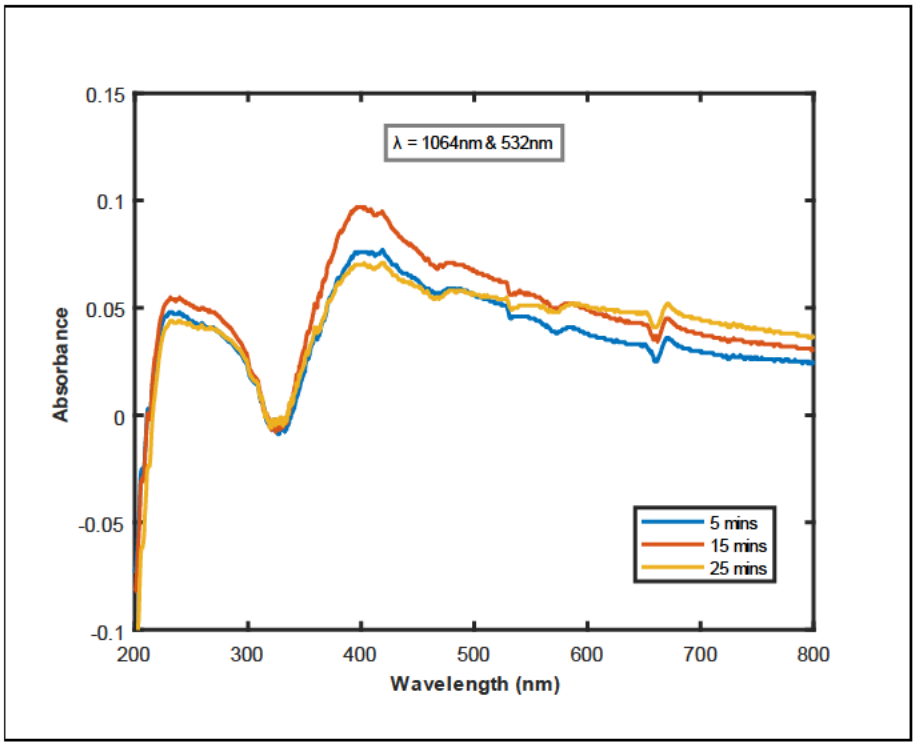

Figure 4.5 Shows *Test 4*: UV-VIS absorption spectra of AgNPs synthesised using 1064 nm and 532 nm wavelength pulse.

Table 4.5 ***Test 5*: experimental conditions under which AgNPs samples were synthesised.**

Sample	Wavelength (nm)	Ablation time (minutes)
A2A	1064	5
B2A	532	5
C2A	1064 + 532	5

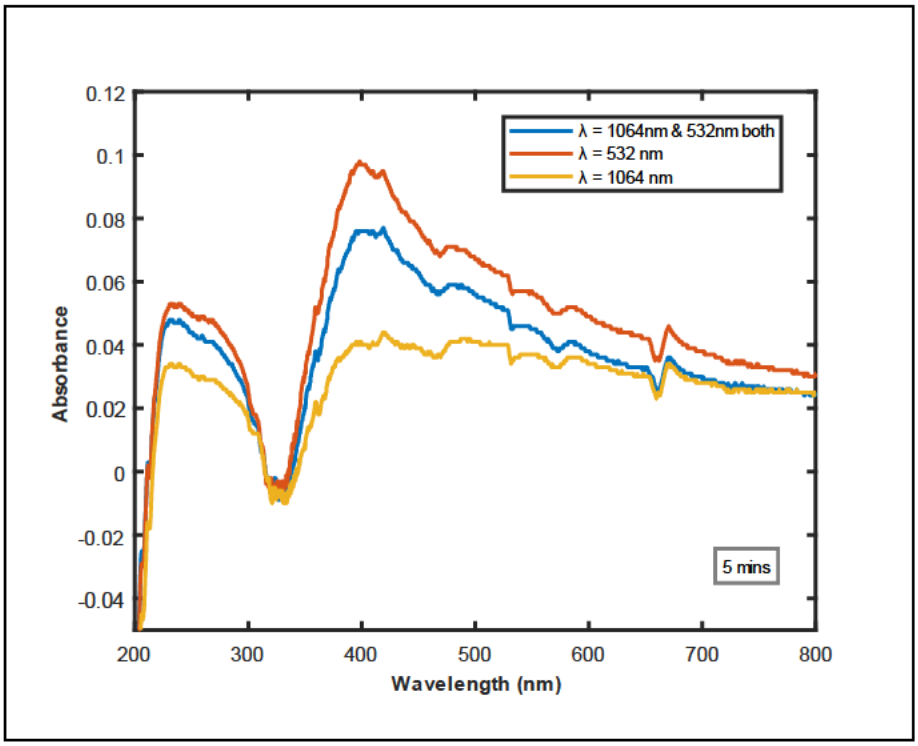

Figure 4.6 Shows *Test 5*: UV-VIS absorption spectra of AgNPs synthesised by ablating the silver target for 5 minutes.

Table 4.6 Test 6: experimental conditions under which AgNPs samples were synthesised.

Sample	Wavelength (nm)	Ablation time (minutes)
A2B	1064	15
B2B	532	15
C2B	1064 + 532	15

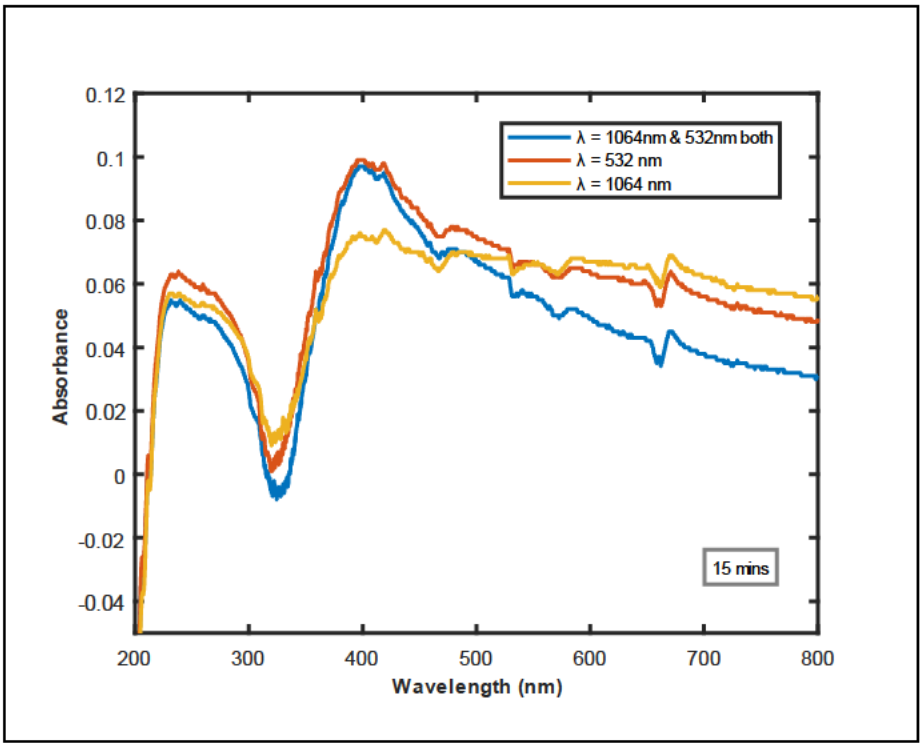

Figure 4.7 Shows *Test 6*: UV-VIS absorption spectra of AgNPs synthesised by ablating the silver target for 15 minutes.

Table 4.7 ***Test 7*: experimental conditions under which AgNPs samples were synthesised.**

Sample	Wavelength (nm)	Ablation time (minutes)
A2C	1064	25
B2C	532	25
C2C	1064 + 532	25

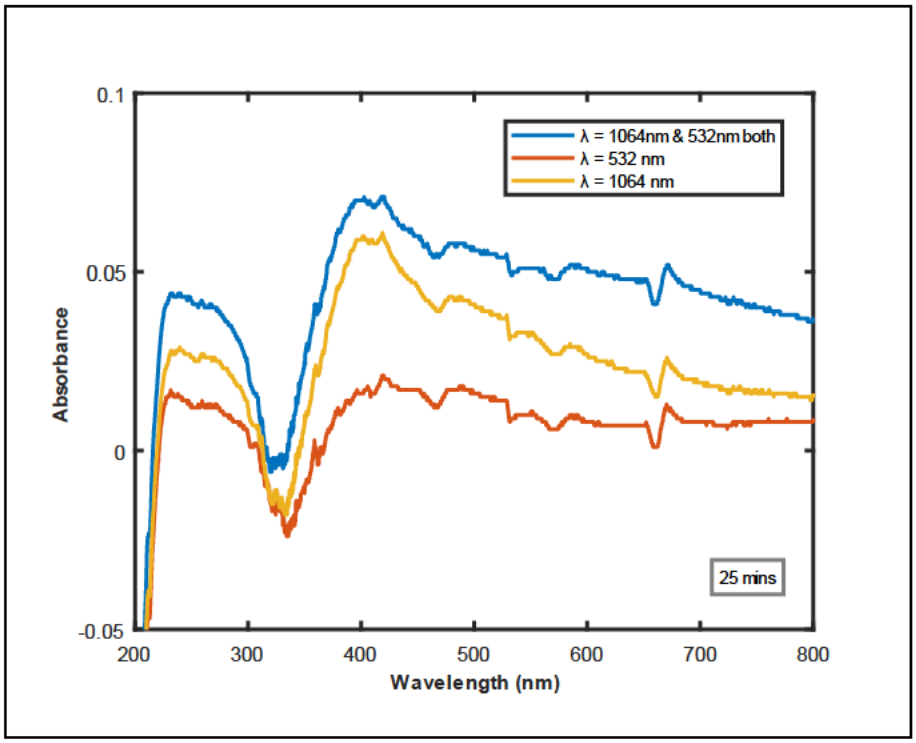

Figure 4.8 Shows *Test 7*: UV-VIS absorption spectra of AgNPs synthesised by ablating the silver target for 25 minutes.

Table 4.8 ***Test A*: experimental conditions under which AgNPs samples were synthesised.**

	Sample E
Wavelength (nm)	1064 nm + 532 nm
Ablation time (minutes)	25 minutes
Pulse rate (Hz)	5.2 Hz

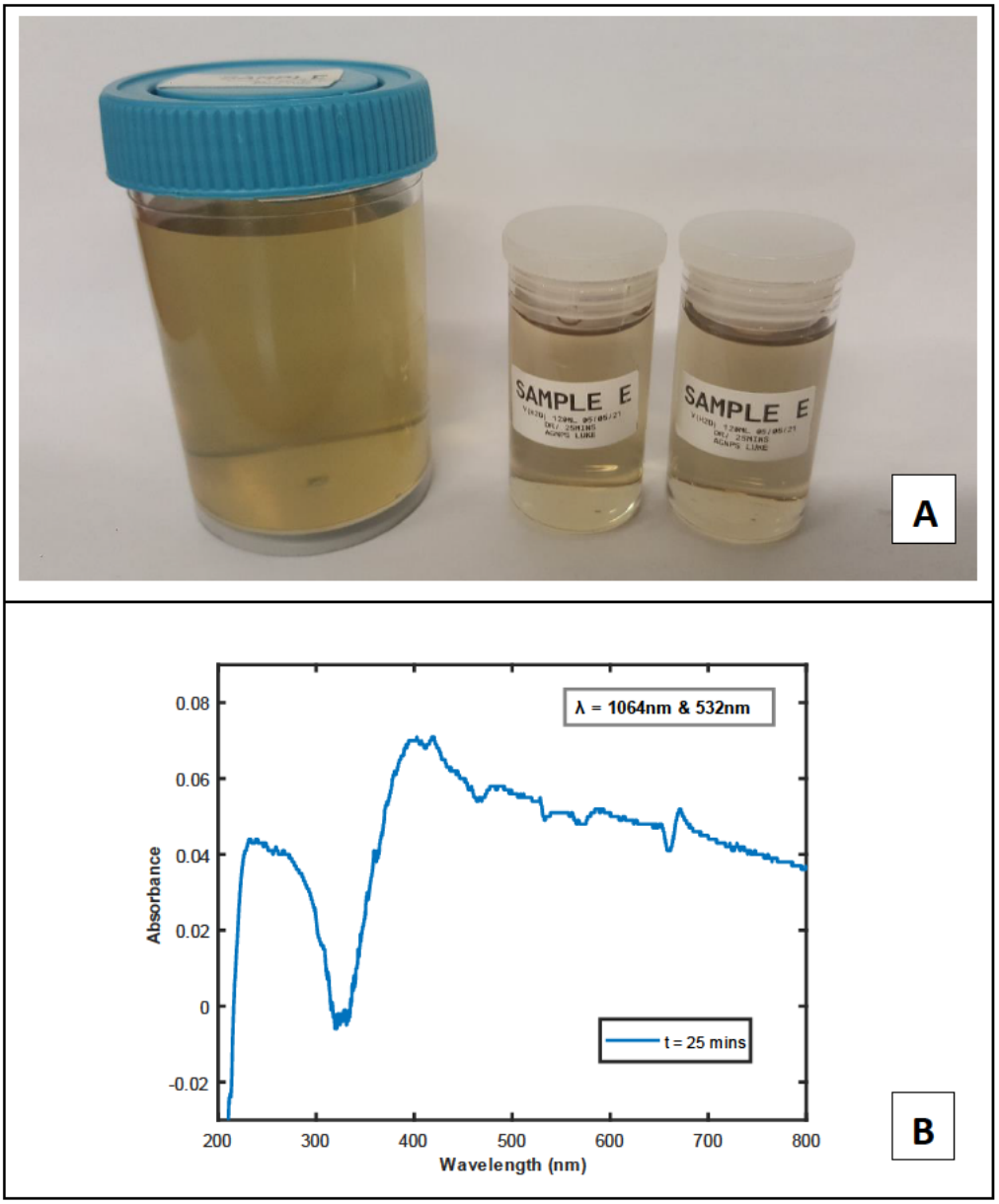

Figure 4.9 Shows *Test A*: Diagram **(A)** shows prepared *sample E* ablated for 25 minutes and **(B)** shows the UV-VIS absorption spectra of AgNPs (*sample E*), synthesised using 1064 nm and 532 nm wavelength pulse.

Pulsed laser wavelength of 1064 nm and 532 nm was used to synthesis silver nanoparticle while varying the ablation time from 5 mins to 25 mins for *Test 1*. The synthesised AgNPs in ***Figure 4.1*** image showing different colours as particles sizes changes from *sample A1* to *sample E1*. Ablation time was increased with a difference of 5 mins per sample. *Test 1* was done to get the optimum duration for ablating a silver target. The absorbance spectrum from the UV-VIS in ***Figure 4.2*** shows absorption plots of AgNPs developed over different ablation duration. From the spectrum it was deduced that all the nanoparticles' samples were resonating at band of 380-430nm wavelength. Thus, they had slightly different nanoparticles sizes cross all the samples. Agglomeration of the nanoparticles started to occur with time as samples had broadened base curves at the higher wavelength e.g *sample C1* that was ablated for 15 mins. The expected diameter was between the range of 9-20 nm and the nanoparticles we produced had an average diameter of 10.6 nm.

The UV-VIS absorbance spectroscopy in ***Figure 4.3*** was collected from three samples from *Test 2*. The silver nanoparticles were synthesised by ablating a silver target in water for three different ablation times using the 1064 nm laser pulse. Wavelength 532 nm was used for samples in *Test 3* and *Test 4* used a combination of both wavelengths. The *sample B4* from *Test 4* had AgNPs that were synthesised using the combination of laser pulse 1064 nm and 532 nm and had a spectrum graph that was slightly blue shifted. Its resonance band was between 385-415 nm. *Sample B4* and *B3* that have silver nanoparticles that had a smaller distribution diameter size. There was prominent evidence of dissociation of the silver nanoparticle across all the chosen best samples as there was a significant absorption in the near ultra-violet wavelength range.

The shapes of the silver nanoparticles produced were generally spherical in shape across all the sample tests. Confirming reports from other research that laser pulse ablation in solution produce one constant structural shape across the board [43]. The same deduction was also backed-up by the results obtained from the UV-Vis absorption spectrometer that showed that for all the spectra were resonating at the 390-420 nm wavelength range.

Agglomeration occurred especially in most of the samples from *Test 5, 6,* and *7*, that were ablated using the 1064 nm and 532 nm wavelength pulses only. The evidence of larger nanoparticles was noticed on the unlikely broadening peaks at far visible light wavelength ranges. This appears to almost flattened spectral peak. This could be due to the presence of high concentration of silver nanoparticles.

Dissociation occurs when the nanoparticles shrink in size with time, and this is due to ionic particles detaching themselves from the surface of the nanoparticle into the solution. This may increase the rate of agglomeration for those shrinking nanoparticles. This can be seen on the broadening of the base curve for all the spectrum at the higher wavelength bands, signifying the increase in size of AgNPs in the solution. To reduce the rate of dissociation a silver oxide outer shell could stabilize the nanoparticles better for longer period.

The UV-VIS absorption spectrum for *Test A* was synthesised using 1064 nm and 532 nm and the silver target was ablated for 25 minutes as shown in **Table 4.8** Test *A:* experimental conditions under which AgNPs samples were synthesised. and ***Figure 4.9*** **(B)**. *Sample E* absorbed light at the 400 nm wavelength band and that was its peak absorbance. Its expected particle size was in the range for 9 nm to 12 nm. To confirm the results further tests were to be done on HRTEM spectroscopy.

4.2.1 High-resolution transmission electron microscopic analysis of AgNPs

Table 4.9 Test 1: Average diameter of AgNPs samples

	sample A1	sample B1	sample C1	sample D1	sample E1
Ablation time (mins)	5	10	15	20	25
Particle mean area (nm^2)	2.235	2.007	1.860	0.823	0.600
Particle mean diameter (nm)	20.102	18.192	16.777	15.290	10.589

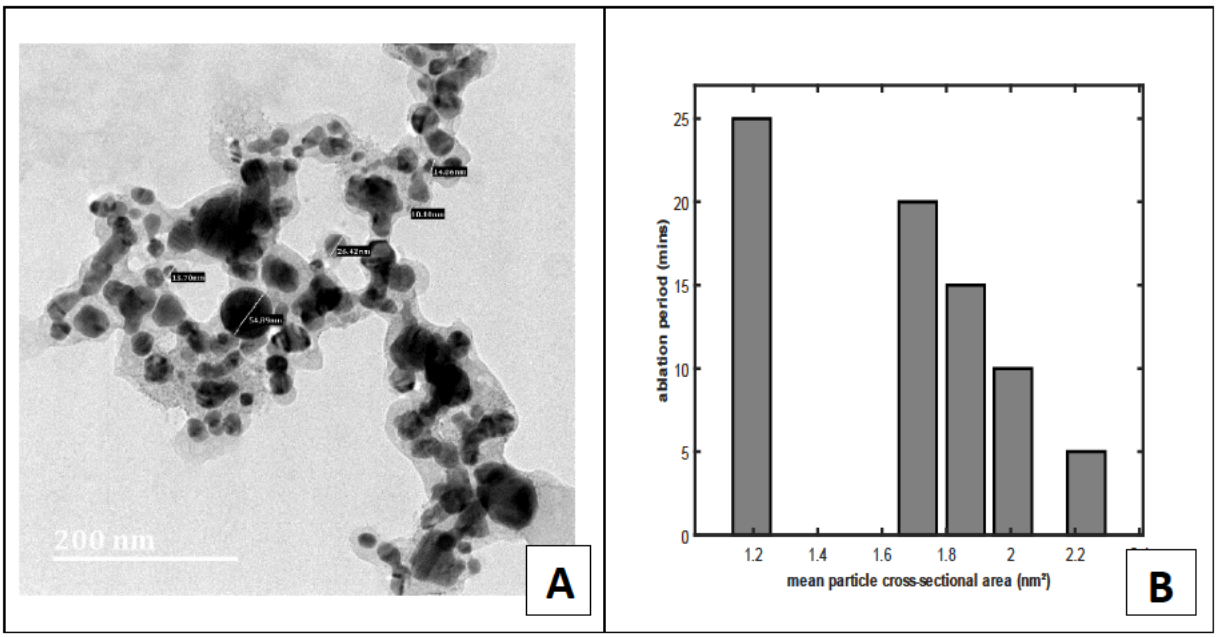

Figure 4.10 The HRTEM image **(A)** showing particle diameter of AgNPs. **(B)** The scale bars for the average cross-sectional area for the synthesised nanoparticles.

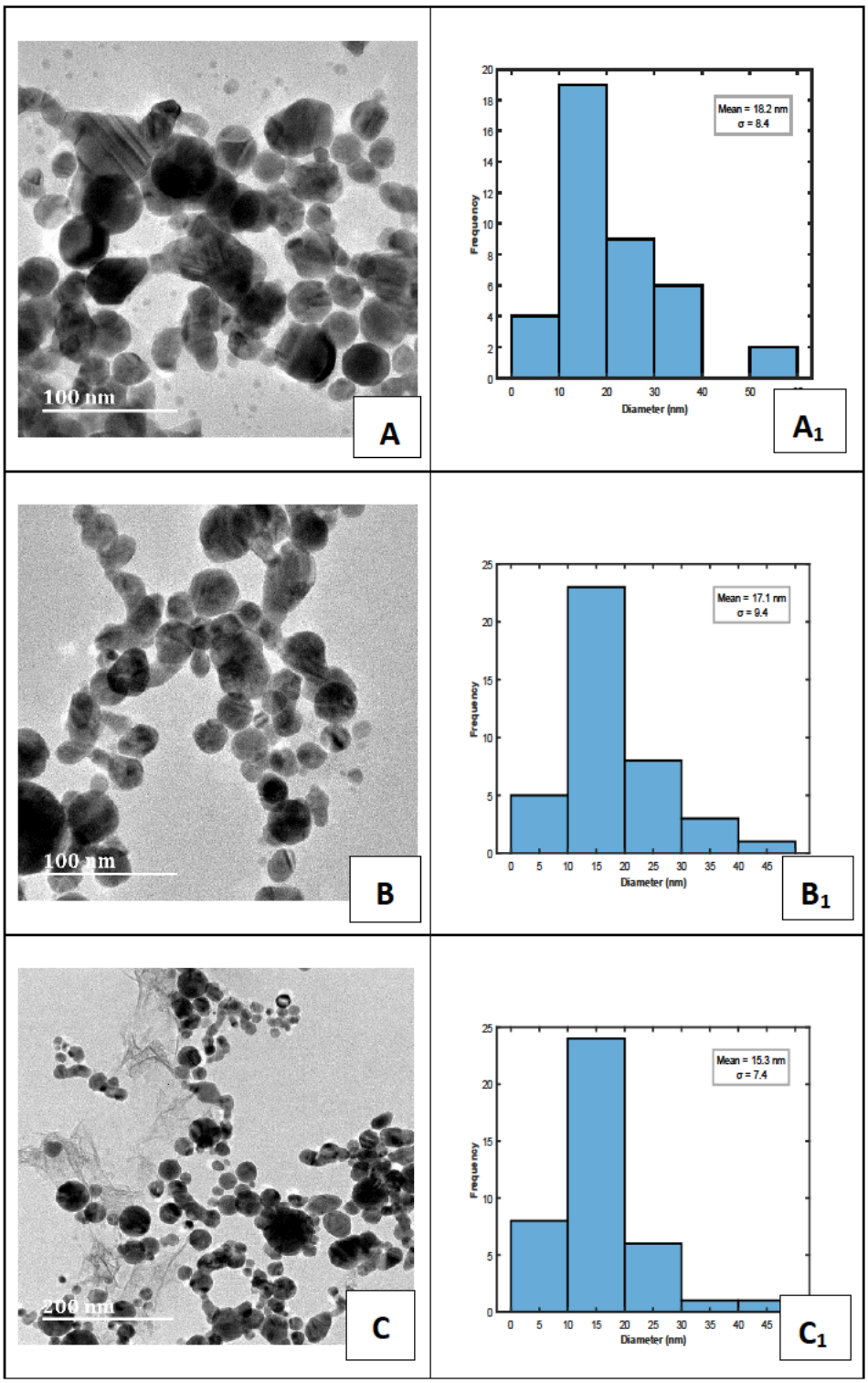

Figure 4.11 shows **(A), (B)** and **(C)** The HRTEM image showing particle diameter for the selected *samples* (*C2, B4*, and *A3*) absorption spectra of AgNPs prepared over 25 mins, 15 mins and 5 mins respectively, **(A_1), (B_1)** and **(C_1)** shows the frequency histograms depicting, particle distribution sizes for the selected AgNPs.

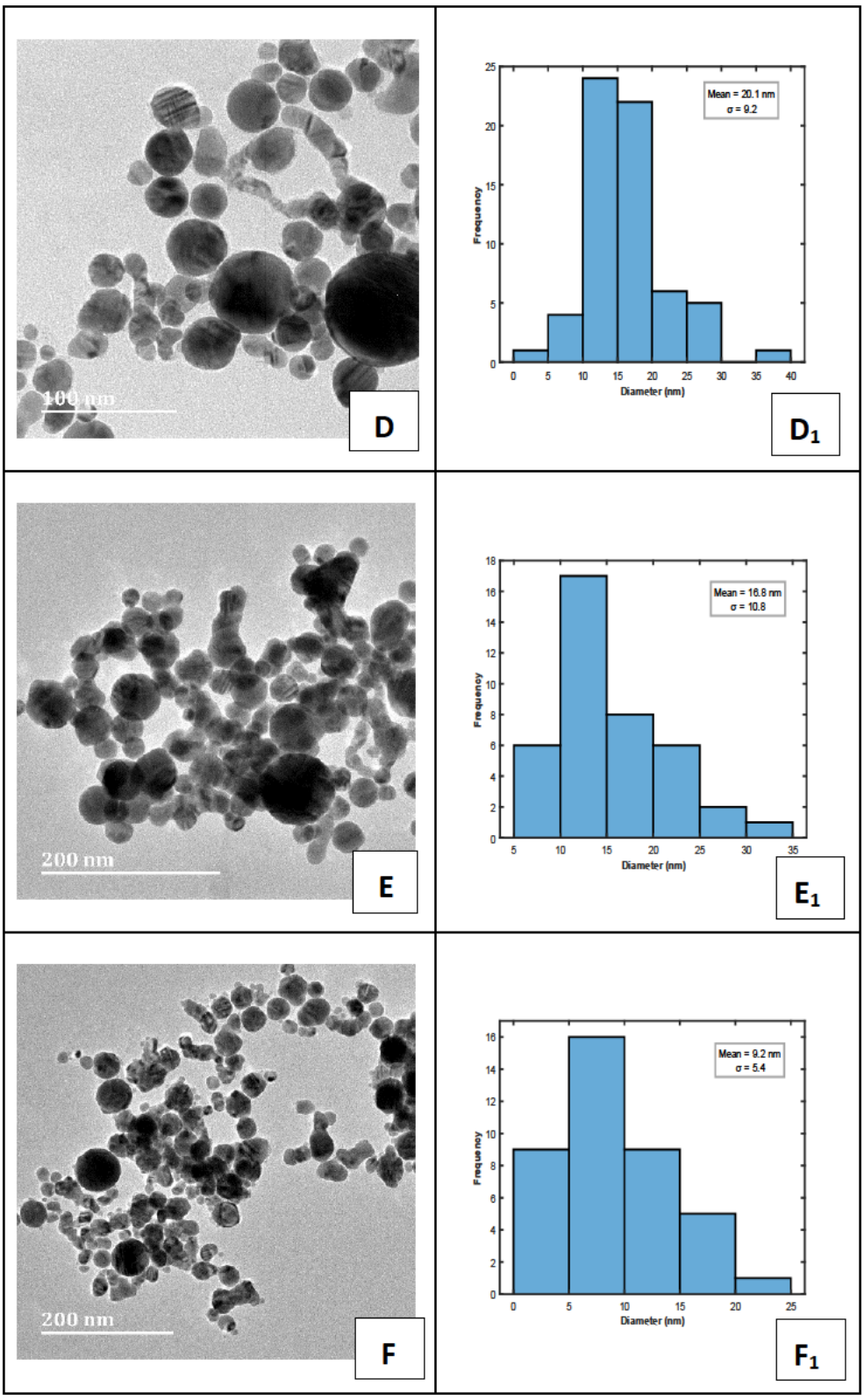

Figure 4.12 shows **(D), (E)** and **(F)** The HRTEM image showing particle diameter for the selected *samples* (*B2C, C2B*, and *C2A*) absorption spectra of AgNPs prepared over 25 minutes, 15 minutes and 5 mins respectively, **(D_1), (E_1)** and **(F_1)** shows the frequency histograms depicting, particle distribution sizes for the selected AgNPs.

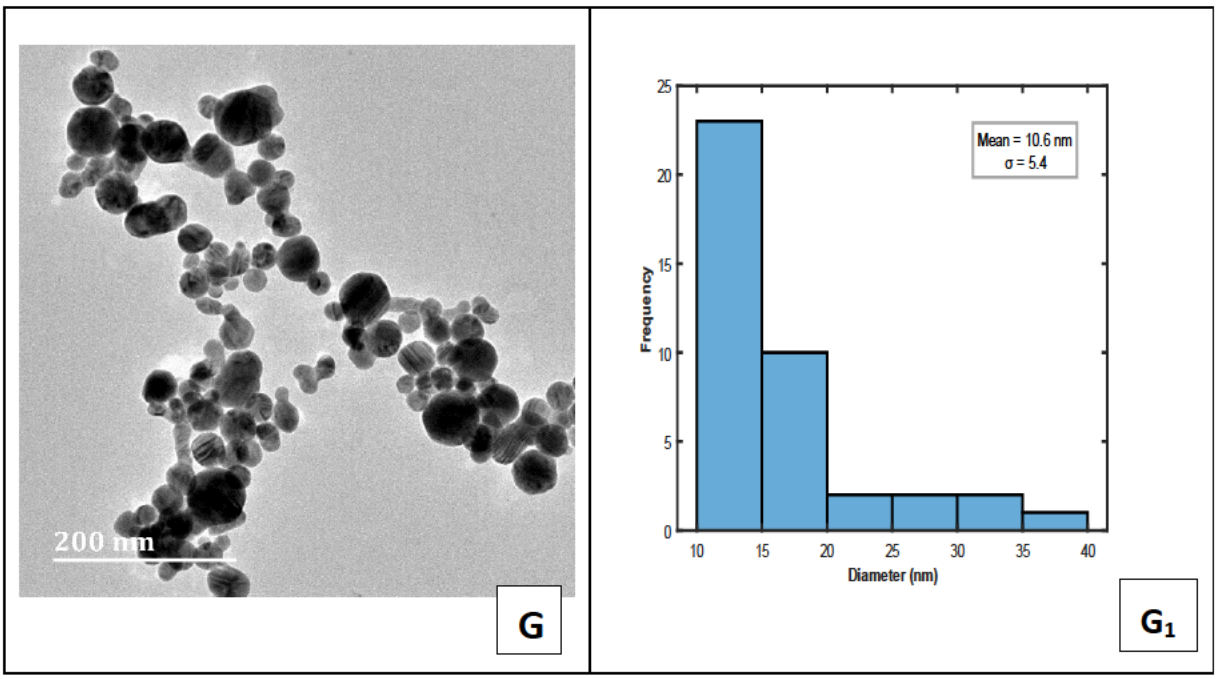

Figure 4.13 *Test A*: shows **(A)**, The HRTEM image showing particle diameter for *sample* (*G*) absorption spectra of AgNPs prepared over 25 minutes, using 1064 nm and 532 nm wavelength, **(G_1),** shows the frequency histogram depicting, particle distribution size.

Figure 4.10 **(A)**, shows the HRTEM image for the synthesised silver nanoparticles that was synthesised from *Test 1* samples using the infrared and the green light pulsed laser combination. The image gave a clear picture of the formed silver nanoparticles. From this image the particle size distribution was determined. The diameter and the cross-sectional area of the AgNPs could be extracted from the HRTEM image. The results obtained was used to plot the area distribution bar graph of the AgNPs. The average area of these nanoparticles was presented as scale plot bar in ***Figure 4.10*** **(B).** Since the spherical shape was the dominant shape in all the developed nanoparticles their diameter was proportional to their particles surface area.

The HRTEM gave clear shapes and structure morphology of the silver nanoparticles on the images that was obtained from ***Figure 4.11*** **(A), (B)** and **(C)**; *samples (A3, B4* and *C2)*. The results were used to plot the frequency histogram bars to clearly show the distribution of AgNPs sizes. With 18.2 nm, 17.1 nm, and 15.3 nm average nanoparticle diameter. Fairly consistent with the narrow band peaks on all the sample absorption spectrum.

The absorption spectrum in ***Figure 4.12*** **(D), (E)** and **(F)** were irradiated using a combination of 1064 and 532 nm. A 1064 nm and a 532 nm wavelength pulses laser respectively. In each wavelength three ablation periods were chosen. Which were 5 minutes, 15 minutes, and 25 minutes. The HRTEM images gave clear structure morphology of silver nanoparticles. All the nanoparticles were spherical in shape. Using the raw image pictures from the HRTEM the cross-sectional area and the diameter of the nanoparticles was easily deduced. The data obtained was used to plot the frequency histogram bar graph to clearly elaborate the size distribution of the AgNPs. The diameter of the ***Figure 4.12*** **(D_1), (E_1)** and **(F_1)** were 20.1 nm, 16.8 nm, and 9.2 nm respectively.

The HRTEM images shows several secondary formed smaller nanoparticles due to dissociation of silver nanoparticles with diameter less than 5 nm in size. This explains the blue shift in the absorption spectrum of some samples, eg *sample C2A* and ***Figure 4.14*** **(F)**.

The results analysis done showed clearly the best samples were those produced by the combination of both 1064 nm and 532 nm wavelength pulse laser. These samples had desirable properties, monodispersed spherical nanoparticles, smaller sized nanoparticle distribution and reduced agglomeration. The frequency histogram in ***Figure 4.13*** **(G_1)** was plotted to show the distribution of the particle size. The diameter of the silver nanoparticles was 10.6 nm with a standard deviation of 5,4 nm.

The UV-Vis absorption spectrum in ***Figure 4.9*** **(B)** confirm the size destitution of the silver nanoparticles. These AgNPs resonate at the 400 nm wavelength band and that was its peak absorbance. This spectrum results shows clearly that the silver nanoparticle that were synthesised were spherical in shape and their cross-sectional area was 1.1 nm^2 and the standard deviation was 0.6 nm^2. These results were shown to be consistent with the HRTEM data.

4.2.1 Energy dispersive X-ray spectroscopic analysis of AgNPs

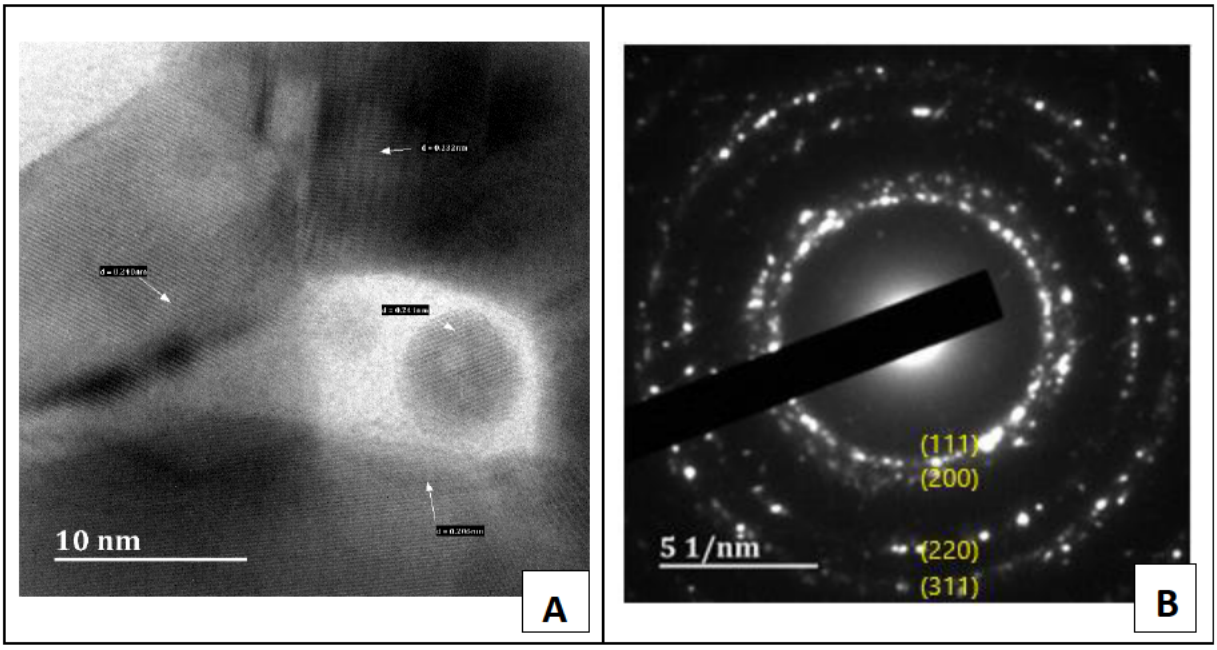

Figure 4.15 (A) HRTEM images showing the d-spacing plane line of the AgNPs grains. (B) SAED pattern of the annealed sample.

The crystal structure of the AgNPs was analysed using the HRTEM. Results were taken for the final selected sample of AgNPs and the image in ***Figure 4.15*** **(A)** showed clear plane lines arranged in different direction as per each grain. Silver nanoparticles had atoms arranged in a unit cell structure of a face centered cubic (FCC) crystal. The AgNPs produced the first four indexed diffracting ring patterns shown in ***Figure 4.15*** **(B)** of (111), (200), (220), (311). These came from the (hkl) planes that give rise to the highlighted lattice d-spacing in ***Figure 4.15*** **(A).** The white arrows highlight the different plane that have lattice fringes of (d) = 0.206nm, 0.232nm, 0.240nm. 0.240nm, per grain and their directions. The clear boundary lines were identified that showed different gains of nanoparticles. The EDS results showed the size of the silver crystallite that was (5-15 nm) with high crystallinity. By basically using the d-spacing of the crystal planes it is shown that the material is polycrystalline in structure. The concentric circle image in the Selected Area Electron Diffraction (SAED), ***Figure 4.15*** **(B)** show that the silver nanoparticles synthesised were polycrystal material.

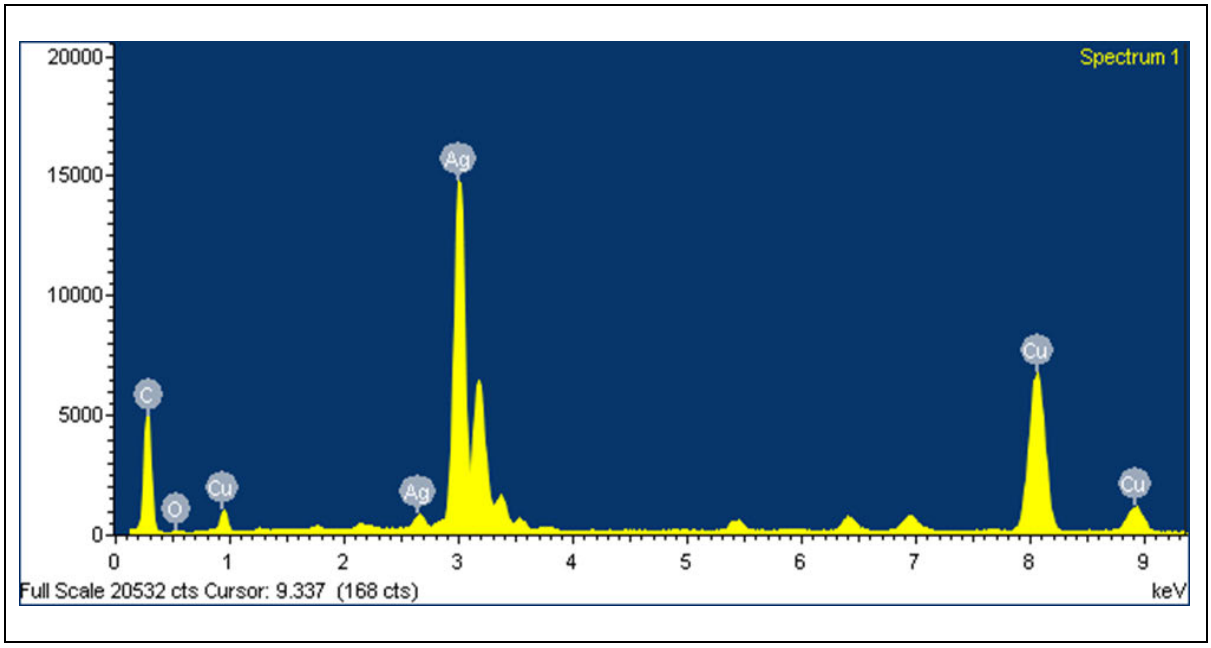

Figure 4.16 Shows the EDS/EDX spectrum of a silver nanoparticle sample

The confirmation of silver nanoparticles formation was done using EDX analysis. The measurement at different areas focused and corresponding peaks as shown in ***Figure 4.16***. AgNPs can be seen in the EDX spectrum, which the quantity of silver was 96% and the measured atomic percentage was 95%. Details of the elemental EDX spectra was measured in atomic and weight percentage were listed in **Table 4.10:**

Table 4.10 EDX weight ratio AgNPS using obtained spectrum focused on the chosen point areas:

(AgNPs) /or (Ag_2O)	Siver (Ag)		Oxygen (O)	
	Weight (%)	Atomic (%)	Weight (%)	Atomic (%)
Spectrum 1	99.91	99.37	0.09	0.63
Spectrum 2	99.78	98.55	0.22	1.45
Sum Spectrum	89.53	87.27	0.00	0.00

The summary of the EDX spectrum results complied on the **Table 4.10.** Showing all the weight percentages and the atomic percentages for silver and oxygen. These results confirm the high purity of the produced silver nanoparticles. The pulsed laser ablation method did produce pristine AgNPs that were over 95% average purity, because no extra chemical reagents or capping agents were used.

4.3 Doxycycline silver nanoparticle results.

The UV-VIS spectroscopy and Raman spectroscopy were used to confirm the synthesis of doxycycline silver nanoparticles in solution. Pristine silver nanoparticles in solution of *sample E* were prepared. This sample was reacted with doxycycline to from doxycycline silver nanoparticle complex *sample E1B*. Characterisation was done on *sample E* and *sample E1B*. The spectrum produced was consistent with the reports from other research papers [40].

4.3.1 Raman spectroscopic analysis of doxycycline silver nanoparticles.

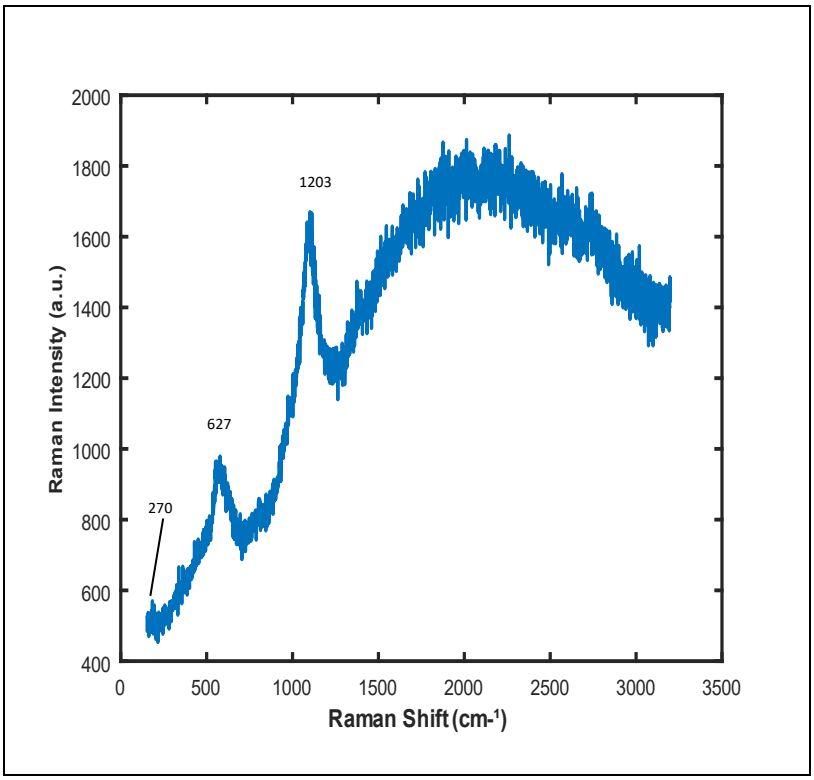

Figure 4.17 The image for the Raman spectrum produced by AgNPS.

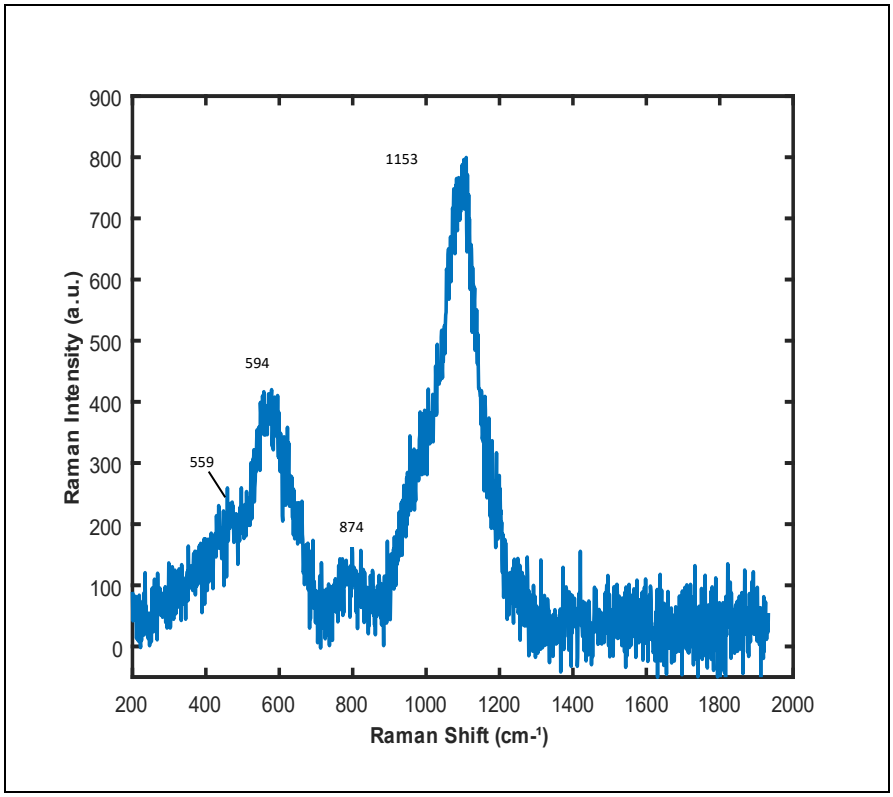

Figure 4.18 the image for the Raman spectrum produced by doxycycline silver nanoparticles.

Figure 4.9 **(A)** shows the image of the synthesised silver nanoparticles in solution. Raman shift for Ag lattice vibrational modes of silver nanoparticles are observed at 270 cm^{-1}. The Raman spectroscopy confirm that we had successfully produced pristine silver nanoparticles in water solution. ***Figure 4.17*** shows the image of the synthetised doxycycline silver nanoparticles in solution. The complex solution formed was yellow in colour. The Raman spectroscopy was consistent with the reported Raman shift for doxycycline silver nanoparticles [109]. Raman peaks were observed at 559, 594. 874 and 1153 cm^{-1} from spectrum. From these the peaks at 559 and 594 cm^{-1} are considered as SERS (surface- enhanced Raman spectroscopy) which is a vibrational spectroscopy technique with sensitivity that provides a fine molecular fingerprint to allow direct identification of target analytes [108]. Hence this feature gives strong indication of DO-AgNPs complex.

4.3.1 UV-VIS absorption spectroscopic analysis of doxycycline-AgNPs.

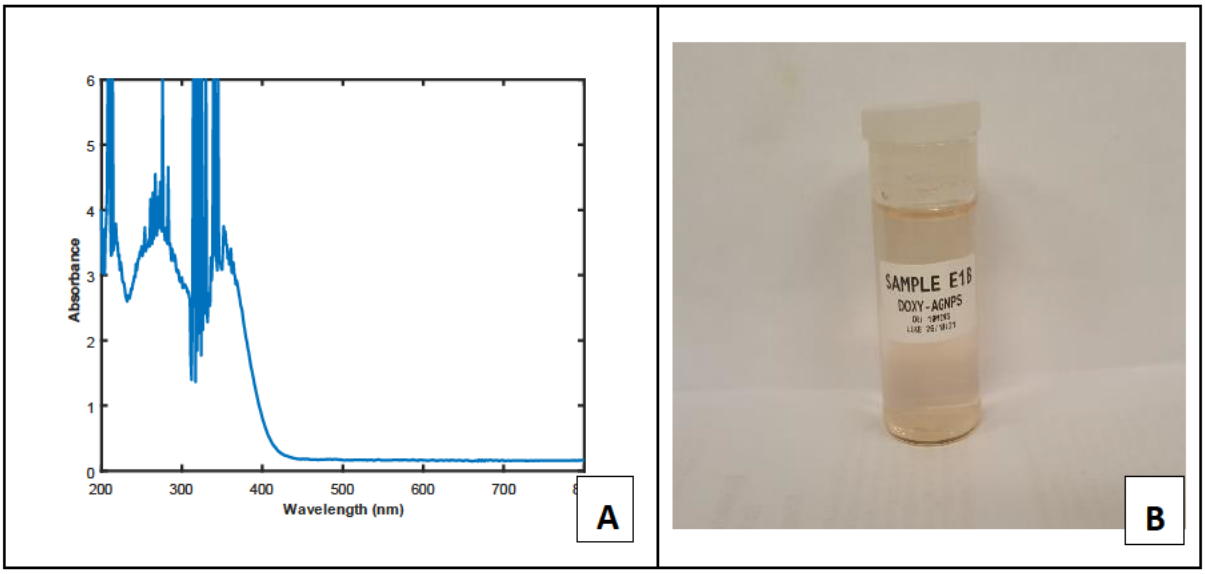

Figure 4.19 **(A)** shows the UV-VIS absorption spectroscopy of synthesised doxycycline-AgNPs **(B)** The image of the produce silver-doxycycline complex in solution *sample E1B*.

The UV-VIS spectrum of doxycycline silver nanoparticles in ***Figure 4.19*** **(A)** shows the absorbance of *sample E1B* and the results were consistent with reports found in the literature review. Doxycycline-AgNPs resonate at 358-370 nm wavelength band [32]. The signal-to-noise ratio was high and the spectrum could be smoothened by diluting the nanoparticle solution. There was little to non-agglomeration of DO-AgNPs since there was no sign of absorbance at the far large wavelength bands. This was due to the doxycycline that can also act as a good Ag-nanoparticle stabilizer. Therefore, nanoparticle dissociation and agglomeration were significantly reduced. The final synthesised doxycycline silver nanoparticle ionophore in solution was successfully produced.

5 CONCLUSIONS AND RECOMMENDATIONS FOR FURTHER RESEARCH

5.1 Conclusion

This research project was set to study the synthesise and optimise the production of doxycycline silver nanoparticles using pulsed laser ablation synthesis in solution. Doxycycline was used as an ionophore as its complex formation with silver nanoparticles was reported to have the best antivirus inhibition activities. To harness the silver nanoparticles' virus replication inhibiting properties which are mainly derived from its physical and surface chemical properties prompt the using of combined 1064 nm and 532 nm pulse laser ablation in water as the preferred approach. This method was chosen because of its simplicity in terms of tuning the properties of silver nanoparticles. Pulsed laser ablation synthesis in solution is one of the best environmentally friendly approaches. Meaning, no toxic precursor, reducing agents, or harmful capping agents are required for AgNPs synthesis. This is an advantage if the AgNPs are to be used in biological organisms.

The outcome of the research was to develop doxycycline silver nanoparticles and all the forementioned procedural steps were critically followed. All the test analysis that was carried out on the samples gave results that were insightful and consistent with the previously reported research of similar kind [40]. Carrying out the experiment for this research allows new inputs and further advancement in scientific research. This research helped to shed light onto topic like water cavitation that have yet to be understood very well. However, its mechanism is very important in the formation of nanoparticles in solution.

Many other drug compounds could have been chosen to be used as the ionophore conjugated for AgNPs, like hydroxychloroquine, quercetin or ivermectin. But reports on SERS 2 covid-19 virus efficacy for hydroxychloroquine and quercetin were not convincingly high to be considered for drug repurpose. However, these drugs can be developed and conjugated with silver nanoparticles using the same method. There is optimism on the efficacy of these drugs against malaria, drug resistant bacteria and cancer diseases. The advantages that doxycycline had was its cost effectiveness, its virus inhibition to covid-19 and its ability to form a stable complex ionophore with AgNPs.

5.2 Revisiting the aims and objectives

This research was set out to synthesis pristine silver nanoparticles in water using pulsed laser ablation. This method was followed and optimised. Distilled water was used as the medium. The silver nanoparticles sizes that range between 9 nm to 12 nm were obtained. The shapes for AgNPs produced was spherical in all samples. A combination of 1064 nm and 532 nm wavelength pulse prove to have enough energy to ablate a silver target and the best ablation time was 25 minutes. Doxycycline was used to graft AgNPs to form ionophore of doxycycline silver nanoparticles. This research was a success.

5.3 Challenges

Challenges that were faced while carrying out this research were more to do with the covid-19 restrictions. This caused long queues, as students had limited time to use the HRTEM spectroscopy and the UV-VIS spectroscopy to analyse their samples. Other challenges were on the unavailability of drugs that could be repurposed as silver ionophores. Most of pharmacies were out of stock of drugs like hydroxychloroquine and ivermectin so we could not use these drugs in this research.

5.4 Future possibilities

Pulsed laser ablation synthesis in solution is an efficient method to synthesise silver nanoparticles. The synthesised doxycycline silver nanoparticles can be used to test their effectiveness in viral replication inhibition. Questions like the required concentration and dosage of do-AgNPs in both laboratory and clinical tests are still yet to be answered. It will be interesting to expand this study by testing other liquid medium apart from distilled water.

5.5 Summary conclusions

In 2020 the world woke up to a deadly pandemic SARS Covid-19 that broke out of Wuhan, China. Many drugs were proposed to help in treating this disease. However few drugs showed potential effectiveness in curing covid-19. This research proposed the use of ionophores conjugated silver nanoparticle as potential drugs that can be effective because of its antiviral activities. Ionophores allow metal ions to enter the selective cell membrane of a cell. Once silver ions enter the cell, they start disrupting the replication of the virus DNA. Hence silver plays an important role as a potential ingredient in drugs that can stop the spread of viruses. Pulsed laser synthesis in solution was method employed in this research to develop relatively smaller sized, spherical nanoparticles.

Silver nanoparticles (AgNPs) developed by pulsed laser ablation in solution enables the preparation of stable silver colloids in pure water without capping or stabilizing agents. This process has proved to produce silver nanoparticles that are more suitable for biomedical applications. These research goes on to conjugate the pristine silver nanoparticles with doxycycline to enhance its antivirus activity. To develop the required size and shape of pristine silver nanoparticles a Nd: YAG, Q-switch combined 1064 nm and 532 nm wavelength pulsed laser was used. The pulsed laser was irradiated onto a silver target placed in a tailored ablation chamber filled with distilled water. Water was the best liquid medium chosen for no contaminates were required in the end products and the water enables the formation of smaller spherical silver nanoparticles. The energy density range incident by the laser ranged between 34.8 $J.cm^{-2}$ and 37.3 $J.cm^{-2}$. The ablation was done for 25 mins to produce the AgNPs.

The silver nanoparticle that was produced had an averaged diameter of 10. 6 nm which has been shown in previous works to be the most effective size for antiviral activities in biological systems. Therefore, by conjugating AgNPs with doxycycline was in effort to enhance its inhibition properties against Covid-19 virus, when used as a drug. The pristine solution of AgNPs was found to be stable in colloidal form for long time that made them easy to work with. The synthesis of doxycycline silver nanoparticle was done successfully reacting monohydrate doxycycline dissolved in water with drops of NaOH as an activator and pristine silver nanoparticles. The produced doxycycline silver nanoparticle in solution was yellowish colour.

The samples of silver nanoparticles collected were characterized by UV-visible absorption, high resolution transmission electron microscopy (HRTEM), and Raman spectroscopic techniques. UV-visible absorption spectrum was used to quickly test the properties of the new synthesised silver nanoparticles and the results was used to quickly optimise the production process. The HRTEM images were analysed and from the data obtained frequency histogram was plotted to clearly display the distribution of sizes and surface area of the nanoparticles formed. The identification of the elements in the nano material composition was done using an Energy dispersive X-ray spectroscopy (EDS or EDX), and the (UV-VIS) was be used to confirm the absorption band gap of AgNPs. The silver nanoparticle that was produced was of high quality, free from toxic reagents and could be used for further medical tests (in-vivo test).

All the results obtained and recorded were consistent with the reported results in the literature review. Finally, the outcome was a synthesise doxycycline silver nanoparticle sample successfully produced using the proposed optimised method of using pulsed laser ablation solution. Therefore, this research project was successfully completed.

APPENDIX A: INFORMATION ON APPENDICES

5.1 Chemometric procedure

Preparations for all reagents and samples were done using stoichiometric quantitative measures stated below:

$$Molarity: \quad M = \frac{moles\ of\ solute}{volume\ of\ solution} \qquad [5.1.1]$$

$$\text{Molarity:} \quad \text{M} = \left(\frac{Mass}{molecular\ mass} \times \frac{1}{volume\ of\ solute}\right) \qquad [5.1.2]$$

$$Molucure\ mass: \quad Mr = C_{22}H_{24}N_2O_8 = 444.4g \qquad [5.1.3]$$

The data results obtained for the analytical instruments was recorded. The MATLAB programme version R2021b from MathWorks U.S. and ImageJ software was used to systematically interrogate the data and visually display the results obtained. The ImageJ software was used to analyse the HRTEM images to extract out the particle size distribution data. The results data obtained was visually represented as tables and graphs for clarity.

REFERENCES

[1] A. Reza Sadrolhosseini, M. Adzir Mahdi, F. Alizadeh, and S. Abdul Rashid, "Laser Ablation Technique for Synthesis of Metal Nanoparticle in Liquid," *Laser Technol. its Appl.*, 2019, doi: 10.5772/intechopen.80374.

[2] M. Tajdidzadeh *et al.*, "Synthesis of silver nanoparticles dispersed in various aqueous media using laser ablation," *Sci. World J.*, vol. 2014, 2014, doi: 10.1155/2014/324921.

[3] S. Dawadi *et al.*, "Current Research on Silver Nanoparticles: Synthesis, Characterization, and Applications," *J. Nanomater.*, vol. 2021, 2021, doi: 10.1155/2021/6687290.

[4] P. N. H. Diem, T. N. M. Phuong, N. Q. Hien, D. T. Quang, T. T. Hoa, and N. D. Cuong, "Silver, Gold, and Silver-Gold Bimetallic Nanoparticle-Decorated Dextran: Facile Synthesis and Versatile Tunability on the Antimicrobial Activity," *J. Nanomater.*, vol. 2020, 2020, doi: 10.1155/2020/7195048.

[5] A. A. Salim, H. Bakhtiar, G. Krishnan, and S. K. Ghoshal, "Nanosecond pulse laser-induced fabrication of gold and silver-integrated cinnamon shell structure: Tunable fluorescence dynamics and morphology," *Opt. Laser Technol.*, vol. 138, no. September 2020, p. 106834, 2021, doi: 10.1016/j.optlastec.2020.106834.

[6] A. C. Burdușel, O. Gherasim, A. M. Grumezescu, L. Mogoantă, A. Ficai, and E. Andronescu, "Biomedical applications of silver nanoparticles: An up-to-date overview," *Nanomaterials*, vol. 8, no. 9, pp. 1–25, 2018, doi: 10.3390/nano8090681.

[7] T. Tsuji, "Preparation of silver nanoparticles by laser ablation in solution," *Appl. Surf. Sci.*, vol. 202, no. 1–2, pp. 80–85, 2002.

[8] P. Wagener, S. Ibrahimkutty, A. Menzel, A. Plech, and S. Barcikowski, "Dynamics of silver nanoparticle formation and agglomeration inside the cavitation bubble after pulsed laser ablation in liquid," *Phys. Chem. Chem. Phys.*, vol. 15, no. 9, pp. 3068–3074, 2013, doi: 10.1039/c2cp42592k.

[9] S. Barcikowski and G. Compagnini, "Advanced nanoparticle generation and excitation by lasers in liquids," *Phys. Chem. Chem. Phys.*, vol. 15, no. 9, pp. 3022–3026, 2013, doi: 10.1039/c2cp90132c.

[10] C. Rehbock, V. Merk, L. Gamrad, R. Streubel, and S. Barcikowski, "Size control of laser-fabricated surfactant-free gold nanoparticles with highly diluted electrolytes and their subsequent bioconjugation," *Phys. Chem. Chem. Phys.*, vol. 15, no. 9, pp. 3057–3067, 2013, doi: 10.1039/c2cp42641b.

[11] R. Intartaglia *et al.*, "Laser synthesis of ligand-free bimetallic nanoparticles for plasmonic applications," *Phys. Chem. Chem. Phys.*, vol. 15, no. 9, pp. 3075–3082, 2013, doi: 10.1039/c2cp42656k.

[12] T. Salminen, M. Honkanen, and T. Niemi, "Coating of gold nanoparticles made by pulsed laser ablation in liquids with silica shells by simultaneous chemical synthesis," *Phys. Chem. Chem. Phys.*, vol. 15, no. 9, pp. 3047–3051, 2013, doi: 10.1039/c2cp42999c.

[13] M. Rai, A. P. Ingle, P. Paralikar, I. Gupta, S. Medici, and C. A. Santos, "Recent advances in use of silver nanoparticles as antimalarial agents," *Int. J. Pharm.*, vol. 526, no. 1–2, pp. 254–270, 2017, doi: 10.1016/j.ijpharm.2017.04.042.

[14] M. E. Povarnitsyn, T. E. Itina, P. R. Levashov, and K. V. Khishchenko, "Mechanisms of nanoparticle formation by ultra-short laser ablation of metals in liquid environment," *Phys. Chem. Chem. Phys.*, vol. 15, no. 9, pp. 3108–3114, 2013, doi: 10.1039/c2cp42650a.

[15] T. Ahmad *et al.*, "Recent advances in combinatorial cancer therapy via multifunctionalized gold nanoparticles," *Nanomedicine*, vol. 15, no. 12, pp. 1221–1237, 2020, doi: 10.2217/nnm-2020-0051.

[16] J. Gao and S. Hu, "Update on use of chloroquine/hydroxychloroquine to treat coronavirus disease 2019 (COVID-19)," *Biosci. Trends*, vol. 14, no. 2, pp. 156–158, 2020, doi: 10.5582/bst.2020.03072.

[17] S. Malawong *et al.*, "Silver nanoparticles enhance antimicrobial efficacy of antibiotics and restore that efficacy against the melioidosis pathogen," *Antibiotics*, vol. 10, no. 7, 2021, doi: 10.3390/antibiotics10070839.

[18] R. K. C. Motol, C. A. Espineli, C. M. V. Tapit, and C. E. Tiangco, "Synthesis and characterization of silver nanoparticles as a potential sensor for volatile organosulfides for visual detection of postharvest storage in garlic," *IOP Conf. Ser. Mater. Sci. Eng.*, vol. 778, no. 1, 2020, doi: 10.1088/1757-899X/778/1/012002.

[19] P. Mathur, S. Jha, S. Ramteke, and N. K. Jain, "Pharmaceutical aspects of silver nanoparticles," *Artif. Cells, Nanomedicine Biotechnol.*, vol. 46, no. sup1, pp. 115–126, 2018, doi: 10.1080/21691401.2017.1414825.

[20] P. P. Fu, Q. Xia, H. M. Hwang, P. C. Ray, and H. Yu, "Mechanisms of nanotoxicity: Generation of reactive oxygen species," *J. Food Drug Anal.*, vol. 22, no. 1, pp. 64–75, 2014, doi: 10.1016/j.jfda.2014.01.005.

[21] C. Brandenberger *et al.*, "Quantitative evaluation of cellular uptake and trafficking of plain and polyethylene glycol-coated gold nanoparticles," *Small*, vol. 6, no. 15, pp. 1669–1678, 2010, doi: 10.1002/smll.201000528.

[22] S. Soneya and K. V. Saritha, "Biofabrication of silver nanoparticles using leaf extract of Rhynchosia beddomei Baker: spectral characterization and their biological activities," *SN Appl. Sci.*, vol. 2, no. 5, pp. 1–14, 2020, doi: 10.1007/s42452-020-2717-0.

[23] J. Huang, W. Song, H. Huang, and Q. Sun, "Pharmacological Therapeutics Targeting RNA-Dependent RNA Polymerase, Proteinase and Spike Protein: From Mechanistic Studies to Clinical Trials for COVID-19," *J. Clin. Med.*, vol. 9, no. 4, p. 1131, 2020, doi: 10.3390/jcm9041131.

[24] M. M. Kemp *et al.*, "Gold and silver nanoparticles conjugated with heparin derivative possess anti-angiogenesis properties," *Nanotechnology*, vol. 20, no. 45, 2009, doi: 10.1088/0957-4484/20/45/455104.

[25] F. Perche *et al.*, "Hydroxychloroquine-conjugated gold nanoparticles for improved siRNA activity," *Biomaterials*, vol. 90, pp. 62–71, 2016, doi: 10.1016/j.biomaterials.2016.02.027.

[26] S. D. Fihn, E. Perencevich, and S. M. Bradley, "Caution Needed on the Use of Chloroquine and Hydroxychloroquine for Coronavirus Disease 2019," *JAMA Netw. open*, vol. 3, no. 4, p. e209035, 2020, doi: 10.1001/jamanetworkopen.2020.9035.

[27] P. D. Kichambare and A. Star, "Nanotechnologies for the Life Sciences," *Nanotechnologies Life Sci.*, vol. 8, 2007, doi: 10.1002/9783527610419.

[28] B. Perito, E. Giorgetti, P. Marsili, and M. Muniz-Miranda, "Antibacterial activity of silver nanoparticles obtained by pulsed laser ablation in pure water and in chloride solution," *Beilstein J. Nanotechnol.*, vol. 7, no. 1, pp. 465–473, 2016, doi: 10.3762/bjnano.7.40.

[29] J. K. Patra *et al.*, "Nano based drug delivery systems: Recent developments and future prospects 10 Technology 1007 Nanotechnology 03 Chemical Sciences 0306 Physical Chemistry (incl. Structural) 03 Chemical Sciences 0303 Macromolecular and Materials Chemistry 11 Medical and He," *J. Nanobiotechnology*, vol. 16, no. 1, pp. 1–33, 2018, doi: 10.1186/s12951-018-0392-8.

[30] P. E. Alexander *et al.*, “COVID-19 coronavirus research has overall low methodological quality thus far: case in point for chloroquine/hydroxychloroquine,” *J. Clin. Epidemiol.*, vol. 123, no. c, pp. 120–126, 2020, doi: 10.1016/j.jclinepi.2020.04.016.

[31] M. C. Sportelli *et al.*, “The pros and cons of the use of laser ablation synthesis for the production of silver nano-antimicrobials,” *Antibiotics*, vol. 7, no. 3, 2018, doi: 10.3390/antibiotics7030067.

[32] H. F. O. Silva *et al.*, “On the synergy between silver nanoparticles and doxycycline towards the inhibition of: Staphylococcus aureus growth,” *RSC Adv.*, vol. 8, no. 42, pp. 23578–23584, 2018, doi: 10.1039/c8ra02176g.

[33] M. G. S. Borba *et al.*, “Effect of High vs Low Doses of Chloroquine Diphosphate as Adjunctive Therapy for Patients Hospitalized With Severe Acute Respiratory Syndrome Coronavirus 2 (SARS-CoV-2) Infection: A Randomized Clinical Trial,” *JAMA Netw. open*, vol. 3, no. 4, p. e208857, 2020, doi: 10.1001/jamanetworkopen.2020.8857.

[34] N. Sharifi, S. Mahernia, and M. Amanlou, “Comparison of different methods in quercetin extraction from leaves of Raphanus sativus L.,” *Pharm. Sci.*, vol. 23, no. 1, pp. 59–65, 2017, doi: 10.15171/PS.2017.09.

[35] M. Ben Haddada, K. Jeannot, and J. Spadavecchia, “Novel Synthesis and Characterization of Doxycycline-Loaded Gold Nanoparticles: The Golden Doxycycline for Antibacterial Applications,” *Part. Part. Syst. Charact.*, vol. 36, no. 2, pp. 1–11, 2019, doi: 10.1002/ppsc.201800395.

[36] J. F. A. De Oliveira, Â. Saito, A. T. Bido, J. Kobarg, H. K. Stassen, and M. B. Cardoso, “Defeating Bacterial Resistance and Preventing Mammalian Cells Toxicity Through Rational Design of Antibiotic-Functionalized Nanoparticles,” *Sci. Rep.*, vol. 7, no. 1, pp. 1–3, 2017, doi: 10.1038/s41598-017-01209-1.

[37] A. M. Fayaz, K. Balaji, M. Girilal, R. Yadav, P. T. Kalaichelvan, and R. Venketesan, “Biogenic synthesis of silver nanoparticles and their synergistic effect with antibiotics: a study against gram-positive and gram-negative bacteria,” *Nanomedicine Nanotechnology, Biol. Med.*, vol. 6, no. 1, pp. 103–109, 2010, doi: 10.1016/j.nano.2009.04.006.

[38] Ó. Benito-román, B. Blanco, M. T. Sanz, and S. Beltrán, “Subcritical water extraction of phenolic compounds from onion skin wastes (Allium cepa cv. horcal): Effect of temperature and solvent properties,” *Antioxidants*, vol. 9, no. 12, pp. 1–20, 2020, doi: 10.3390/antiox9121233.

[39] M. K. Jayaraj, “Synthesis of Silver Nanoparticles by Liquid Phase Pulsed Laser Ablation for Antibacterial Applications,” vol. 13, no. 2, pp. 155–160, 2017.

[40] S. A. R. Kazmi, M. Z. Qureshi, and J. F. Masson, “Drug-Based Gold Nanoparticles Overgrowth for Enhanced SPR Biosensing of Doxycycline,” *Biosensors*, vol. 10, no. 11, pp. 1–14, 2020, doi: 10.3390/bios10110184.

[41] D. A. Giljohann, D. S. Seferos, A. E. Prigodich, P. C. Patel, and C. A. Mirkin, “Gene regulation with polyvalent siRNA-nanoparticle conjugates,” *J. Am. Chem. Soc.*, vol. 131, no. 6, pp. 2072–2073, 2009, doi: 10.1021/ja808719p.

[42] S. Deol, N. Weerasuriya, and Y. S. Shon, “Stability, cytotoxicity and cell uptake of water-soluble dendron-conjugated gold nanoparticles with 3, 12 and 17 nm cores,” *J. Mater. Chem. B*, vol. 3, no. 29, pp. 6071–6080, 2015, doi: 10.1039/c5tb00608b.

[43] E. Ghavidel, A. H. Sari, and D. Dorranian, “Experimental investigation of the effects of different liquid environments on the graphene oxide produced by laser ablation method,” *Opt. Laser Technol.*, vol. 103, no. March, pp. 155–162, 2018, doi: 10.1016/j.optlastec.2018.01.034.

[44] C. Deepa, G. Suresh, P. Devagi, A. Kowsalya, K. Kavitha, and B. Ramesh, “Evaluation of the antibacterial activity of silver nanoparticles, doxycycline, collagen and their amalgamation - An in vitro study,” *Mater. Today Proc.*, vol. 43, pp. 3050–3053, 2021, doi:

10.1016/j.matpr.2021.01.396.

[45] Z. Yan and D. B. Chrisey, “Pulsed laser ablation in liquid for micro-/nanostructure generation,” *J. Photochem. Photobiol. C Photochem. Rev.*, vol. 13, no. 3, pp. 204–223, 2012, doi: 10.1016/j.jphotochemrev.2012.04.004.

[46] R. Pliego-Arreaga, C. Regalado, A. Amaro-Reyes, and B. E. García-Almendárez, “Revista Mexicana de I ngeniería Q uímica,” *Rev. Mex. Ing. Química*, vol. 12, no. 3, pp. 505–511, 2013, [Online]. Available: http://www.redalyc.org/articulo.oa?id=62029966013.

[47] Z. Wang, P. K. Nayak, J. A. Caraveo-Frescas, and H. N. Alshareef, “Recent Developments in p-Type Oxide Semiconductor Materials and Devices,” *Adv. Mater.*, vol. 28, no. 20, pp. 3831–3892, 2016, doi: 10.1002/adma.201503080.

[48] H. Wang *et al.*, “Multifunctional TiO2nanowires-modified nanoparticles bilayer film for 3D dye-sensitized solar cells,” *Optoelectron. Adv. Mater. Rapid Commun.*, vol. 4, no. 8, pp. 1166–1169, 2010, doi: 10.1039/b000000x.

[49] H. Huang, J. Lai, J. Lu, and Z. Li, “Pulsed laser ablation of bulk target and particle products in liquid for nanomaterial fabrication,” *AIP Adv.*, vol. 9, no. 1, 2019, doi: 10.1063/1.5082695.

[50] M. Griot, “Introduction to Laser Technology :Basic laser principles,” pp. 36.2-36.32, 2009.

[51] OP-TEC, *Fundamentals of Light and Lasers*. 2018.

[52] T. Khamliche, S. Khamlich, M. K. Moodley, B. M. Mothudi, M. Henini, and M. Maaza, “Laser fabrication of Cu nanoparticles based nanofluid with enhanced thermal conductivity: Experimental and molecular dynamics studies,” *J. Mol. Liq.*, vol. 323, p. 114975, 2021, doi: 10.1016/j.molliq.2020.114975.

[53] H. Qayyum *et al.*, “Laser synthesis of surfactant-free silver nanoparticles for toxic dyes degradation and SERS applications,” *Opt. Laser Technol.*, vol. 129, no. May 2019, p. 106313, 2020, doi: 10.1016/j.optlastec.2020.106313.

[54] Materion Microelectronics & Services, “Reflectance in ThinFilms,” *Tech. Pap.*, pp. 399–412, 2007, [Online]. Available: https://materion.com/~/media/Files/PDFs/Advanced Materials Group/ME/TechnicalPapers/Reflectance In thin Films_All.pdf.

[55] T. Bruna, F. Maldonado-Bravo, P. Jara, and N. Caro, “Silver nanoparticles and their antibacterial applications,” *Int. J. Mol. Sci.*, vol. 22, no. 13, 2021, doi: 10.3390/ijms22137202.

[56] C. Y. Shih, I. Gnilitskyi, M. V. Shugaev, E. Skoulas, E. Stratakis, and L. V. Zhigilei, “Effect of a liquid environment on single-pulse generation of laser induced periodic surface structures and nanoparticles,” *Nanoscale*, vol. 12, no. 14, pp. 7674–7687, 2020, doi: 10.1039/d0nr00269k.

[57] R. Eason and D. P. Norton, *PULSED LASER APPLICATIONS-LED GROWTH Edited by*. 2007.

[58] R. J. Martín-Palma and J. M. Martínez-Duart, *Nanotechnology for Microelectronics and Photonics: Second Edition*. 2017.

[59] P. K. Gokuldoss, S. Kolla, and J. Eckert, “Additive manufacturing processes: Selective laser melting, electron beam melting and binder jetting-selection guidelines,” *Materials (Basel).*, vol. 10, no. 6, 2017, doi: 10.3390/ma10060672.

[60] K. Antony and N. Arivazhagan, “Studies on energy penetration and marangoni effect during laser melting process,” *J. Eng. Sci. Technol.*, vol. 10, no. 4, pp. 509–525, 2015.

[61] N. M. Bulgakova and A. V. Bulgakov, “Pulsed laser ablation of solids: Transition from normal vaporization to phase explosion,” *Appl. Phys. A Mater. Sci. Process.*, vol. 73, no. 2, pp. 199–208, 2001, doi: 10.1007/s003390000686.

[62] N. T. T. Thuy, L. H. Huy, T. T. Vy, D. T. P. Thuy, N. T. T. Tam, and N. T. M. Lan, “Application of the response surface methodology for green synthesis of silver nanoparticles using a plant

extract of shallot," *Egypt. J. Chem.*, vol. 63, no. 11, pp. 4579–4588, 2020, doi: 10.21608/EJCHEM.2020.25805.2507.

[63] M. K. Moodley, N. J. Coville, B. C. Holloway, and M. Maaza, "Synthesis of single-walled carbon nanotubes by dual laser vaporization," *S. Afr. J. Sci.*, vol. 102, no. 7–8, pp. 364–368, 2006.

[64] X. Yu, J. Li, D. Mu, H. Zhang, Q. Liu, and G. Chen, "Green synthesis and characterizations of silver nanoparticles with enhanced antibacterial properties by secondary metabolites of Bacillus subtilis (SDUM301120)," *Green Chem. Lett. Rev.*, vol. 14, no. 2, pp. 189–202, 2021, doi: 10.1080/17518253.2021.1894244.

[65] P. Paulraj *et al.*, "Solid-State Synthesis of POPD@AgNPs Nanocomposites for Electrochemical Sensors," *J. Nanosci. Nanotechnol.*, vol. 18, no. 6, pp. 3991–3999, 2017, doi: 10.1166/jnn.2018.15219.

[66] L. Schade, S. Franzka, M. Biener, J. Biener, and N. Hartmann, "Surface-enhanced Raman spectroscopy on laser-engineered ruthenium dye-functionalized nanoporous gold," *Appl. Surf. Sci.*, vol. 374, pp. 19–22, 2016, doi: 10.1016/j.apsusc.2015.08.168.

[67] V. Amendola and M. Meneghetti, "What controls the composition and the structure of nanomaterials generated by laser ablation in liquid solution?," *Phys. Chem. Chem. Phys.*, vol. 15, no. 9, pp. 3027–3046, 2013, doi: 10.1039/c2cp42895d.

[68] S. Reich *et al.*, "Pulsed laser ablation in liquids: Impact of the bubble dynamics on particle formation," *J. Colloid Interface Sci.*, vol. 489, pp. 106–113, 2017, doi: 10.1016/j.jcis.2016.08.030.

[69] M. Dell'Aglio, R. Gaudiuso, O. De Pascale, and A. De Giacomo, "Mechanisms and processes of pulsed laser ablation in liquids during nanoparticle production," *Appl. Surf. Sci.*, vol. 348, pp. 4–9, 2015, doi: 10.1016/j.apsusc.2015.01.082.

[70] M. Honda *et al.*, "Nanostructures prepared: Via laser ablation of tin in water," *New J. Chem.*, vol. 41, no. 19, pp. 11308–11316, 2017, doi: 10.1039/c7nj01634d.

[71] L. Li and F. Liou, "Numerical investigation of thermo-mechanical field during selective laser melting process with experimental validation," *Metals (Basel).*, vol. 11, no. 7, 2021, doi: 10.3390/met11071003.

[72] R. B. Sampol, "Preparation of silver nanoparticles by laser ablation and," *October*, vol. 256, no. 5, pp. 252–256, 2006.

[73] "Th Io Th," 2015.

[74] K. M. Tanvir Ahmmed, C. Grambow, and A. M. Kietzig, "Fabrication of micro/nano structures on metals by femtosecond laser micromachining," *Micromachines*, vol. 5, no. 4, pp. 1219–1253, 2014, doi: 10.3390/mi5041219.

[75] W. M. de Azevedo, S. de L. Campello, D. L. da Cunha, L. T. B. de Mendonça, and O. M. M. M. da Costa, "Laser Ablation in Liquid: An Unconventional, Fast, Clean and Straightforward Technique for Material Preparation," *Appl. Laser Ablation - Thin Film Depos. Nanomater. Synth. Surf. Modif.*, 2016, doi: 10.5772/66245.

[76] A. De Giacomo *et al.*, "Cavitation dynamics of laser ablation of bulk and wire-shaped metals in water during nanoparticles production," *Phys. Chem. Chem. Phys.*, vol. 15, no. 9, pp. 3083–3092, 2013, doi: 10.1039/c2cp42649h.

[77] H. Liu, Y. Sun, H. Zhang, J. Wang, and J. Wei, "Hydrodynamic cavitation enhanced biosynthesis of silver nanoparticles at room temperature and its mechanism," *Mater. Lett.*, vol. 236, pp. 387–389, 2019, doi: 10.1016/j.matlet.2018.10.103.

[78] B. Iandolo, B. Seger, I. Chorkendorff, and A. Hellman, "Sunlight-driven water splitting in."

[79] C. E. Brennen, *Cavitation and bubble dynamics*. 2013.

[80] Y. Chivel, "Optical in-process temperature monitoring of selective laser melting," *Phys. Procedia*, vol. 41, pp. 904–910, 2013, doi: 10.1016/j.phpro.2013.03.165.

[81] X. Sun, S. Chen, J. Liu, S. Zhao, and J. Y. Yoon, "Hydrodynamic Cavitation: A Promising Technology for Industrial-Scale Synthesis of Nanomaterials," *Front. Chem.*, vol. 8, no. April, 2020, doi: 10.3389/fchem.2020.00259.

[82] S. I. Kudryashov and V. D. Zvorykin, "Microscale nanosecond laser-induced optical breakdown in water," *Phys. Rev. E - Stat. Nonlinear, Soft Matter Phys.*, vol. 78, no. 3, pp. 1–10, 2008, doi: 10.1103/PhysRevE.78.036404.

[83] H. K. Park, D. Kim, C. P. Grigoropoulos, and A. C. Tam, "Pressure generation and measurement in the rapid vaporization of water on a pulsed-laser-heated surface," *J. Appl. Phys.*, vol. 80, no. 7, pp. 4072–4081, 1996, doi: 10.1063/1.363370.

[84] C. M. Twum-darko and C. Town, "CPUT Copyright Information The dissertation may not be published either in part (in scholarly, scientific or technical journals) or as a whole (as a monograph), unless permission has been obtained from the university," no. November, p. 2015, 2013.

[85] Z. Wu *et al.*, "Plant and biomass extraction and valorisation under hydrodynamic cavitation," *Processes*, vol. 7, no. 12, pp. 1–19, 2019, doi: 10.3390/PR7120965.

[86] S. I. Kudryashov *et al.*, "Nanosecond-laser generation of nanoparticles in liquids: From ablation through bubble dynamics to nanoparticle yield," *Materials (Basel).*, vol. 12, no. 2, 2019, doi: 10.3390/ma12040562.

[87] M. H. Mahdieh and B. Fattahi, "Size properties of colloidal nanoparticles produced by nanosecond pulsed laser ablation and studying the effects of liquid medium and laser fluence," *Appl. Surf. Sci.*, vol. 329, pp. 47–57, 2015, doi: 10.1016/j.apsusc.2014.12.069.

[88] H. Ghasemi-Tabasi, J. Jhabvala, E. Boillat, T. Ivas, R. Drissi-Daoudi, and R. E. Logé, "An effective rule for translating optimal selective laser melting processing parameters from one material to another," *Addit. Manuf.*, vol. 36, no. July, p. 101496, 2020, doi: 10.1016/j.addma.2020.101496.

[89] M. Dell'Aglio *et al.*, "Silver and gold nanoparticles produced by pulsed laser ablation in liquid to investigate their interaction with Ubiquitin," *Appl. Surf. Sci.*, vol. 374, pp. 297–304, 2016, doi: 10.1016/j.apsusc.2015.11.253.

[90] A. Foroozmehr, M. Badrossamay, E. Foroozmehr, and S. Golabi, "Finite Element Simulation of Selective Laser Melting process considering Optical Penetration Depth of laser in powder bed," *Mater. Des.*, vol. 89, pp. 255–263, 2016, doi: 10.1016/j.matdes.2015.10.002.

[91] C. Y. Shih, M. V. Shugaev, C. Wu, and L. V. Zhigilei, "The effect of pulse duration on nanoparticle generation in pulsed laser ablation in liquids: Insights from large-scale atomistic simulations," *Phys. Chem. Chem. Phys.*, vol. 22, no. 13, pp. 7077–7099, 2020, doi: 10.1039/d0cp00608d.

[92] H. Liu *et al.*, "Continuous biosynthesis of silver nanoparticles in a hydrodynamic cavitation device and modeling of the process by numerical simulation strategy," *J. Nanoparticle Res.*, vol. 20, no. 9, 2018, doi: 10.1007/s11051-018-4330-3.

[93] S. M. Hosseini *et al.*, "Doxycycline-encapsulated solid lipid nanoparticles as promising tool against Brucella melitensis enclosed in macrophage: A pharmacodynamics study on J774A.1 cell line," *Antimicrob. Resist. Infect. Control*, vol. 8, no. 1, pp. 1–12, 2019, doi: 10.1186/s13756-019-0504-8.

[94] Y. Junejo and M. Safdar, "Highly effective heterogeneous doxycycline stabilized silver nanocatalyst for the degradation of ibuprofen and paracetamol drugs," *Arab. J. Chem.*, vol. 12,

no. 8, pp. 2823–2832, 2019, doi: 10.1016/j.arabjc.2015.06.014.

[95] N. Kumar, S. Das, A. Jyoti, and S. Kaushik, “Synergistic effect of silver nanoparticles with doxycycline against Klebsiella pneumonia,” *Int. J. Pharm. Pharm. Sci.*, vol. 8, no. 7, pp. 183–186, 2016.

[96] S. C. Singh, R. K. Swarnkar, and R. Gopal, “Zn/ZnO core/shell nanoparticles synthesized by la ser ablation in aqueous environment: Optical and structural characterizations,” *Bull. Mater. Sci.*, vol. 33, no. 1, pp. 21–26, 2010, doi: 10.1007/s12034-010-0003-2.

[97] V. Mohammadkarimi *et al.*, “Synthesis of Silver-Doxycycline Complex Nanoparticles and Their Biological Evaluation on MCF-7 Cell Line of the Breast Cancer,” *J. Chem.*, vol. 2021, 2021, doi: 10.1155/2021/9944214.

[98] M. K. Moodley and N. J. Coville, “Experimental evidence for the early nucleation of single-walled carbon nanotubes,” *Chem. Phys. Lett.*, vol. 498, no. 1–3, pp. 140–144, 2010, doi: 10.1016/j.cplett.2010.08.053.

[99] M. K. Moodley, “Synthesis and Characterization of Single-Walled Carbon Nanotubes by Dual Laser Vaporization,” *Thesis Univ. theWitwatersrand*, no. December, 2010.

[100] G. National and H. Pillars, *No 主*.

[101] H. F. O. Silva *et al.*, “Doxycycline conjugated with polyvinylpyrrolidone-encapsulated silver nanoparticles: a polymer’s malevolent touch against Escherichia coli,” *RSC Adv.*, vol. 5, no. 82, pp. 66886–66893, 2015, doi: 10.1039/c5ra10880b.

[102] T. Tsuji *et al.*, “Preparation and investigation of the formation mechanism of submicron-sized spherical particles of gold using laser ablation and laser irradiation in liquids,” *Phys. Chem. Chem. Phys.*, vol. 15, no. 9, pp. 3099–3107, 2013, doi: 10.1039/c2cp44159d.

[103] R. Lin, J. Zheng, and J. X. Ma, “Transmission electron microscopy,” *PEM Fuel Cell Diagnostic Tools*, pp. 333–350, 2011, doi: 10.31399/asm.tb.mfadr7.t91110461.

[104] R. F. Egerton, “Electron energy-loss spectroscopy in the TEM,” *Reports Prog. Phys.*, vol. 72, no. 1, 2009, doi: 10.1088/0034-4885/72/1/016502.

[105] S. J. Panchu, M. A. Adebisi, E. Manikandan, and M. K. Moodley, “Catalyst-Free Growth of MoS2 Nanorods Synthesized by Dual Pulsed Laser-Assisted Chemical Vapor Deposition and Their Structural, Optical and Electrical Properties,” *J. Electron. Mater.*, vol. 49, no. 3, pp. 1957–1968, 2020, doi: 10.1007/s11664-019-07817-z.

[106] A. Mohammed, <*Bookraman Theory-Abdosalam.Pdf*>. 2011.

[107] Unknown, “8. Raman Scattering,” *Lect. Notes*, pp. 1–6, 1997.

[108] C. Otto, “Fundamentals of Raman Spectroscopy,” *Encycl. Biophys.*, pp. 876–876, 2013, doi: 10.1007/978-3-642-16712-6_100372.

[109] K. Venugopal *et al.*, “The impact of anticancer activity upon Beta vulgaris extract mediated biosynthesized silver nanoparticles (ag-NPs) against human breast (MCF-7), lung (A549) and pharynx (Hep-2) cancer cell lines,” *J. Photochem. Photobiol. B Biol.*, vol. 173, no. February, pp. 99–107, 2017, doi: 10.1016/j.jphotobiol.2017.05.031.